A Model of Instructive Learning in the Avian Midbrain

Dissertation

zur

Erlangung der naturwissenschaftlichen Doktorwürde
(Dr. sc. nat.)

vorgelegt der

Mathematisch-naturwissenschaftlichen Fakultät

der

Universität Zürich

von

Prashanth D'Souza

aus

Indien

Promotionskomitee

Prof. Dr. Richard H. R. Hahnloser (Vorsitz)

Dr. Shih-Chii Liu (Leitung der Dissertation)

Prof. Dr. Rodney J. Douglas

Zürich, 2012

Abstract

Sensory and motor processing in the brain are widely believed to be based on simple computational primitives rooted in cellular and synaptic physiology. However, many gaps remain in our understanding of the connections between neural computations and biophysical properties of neurons. In this thesis, we show that simple interaction of two commonly found biophysical mechanisms throughout the brain – spike-time-dependent synaptic plasticity (STDP) and spike-frequency adaptation (SFA) – in a single neuron together approximate the well-known perceptron learning rule. We performed integrate-and-fire simulations and mathematical analysis to reveal that delayed inputs to a neuron with SFA precisely instructs neural responses to earlier arriving inputs endowed with STDP.

We demonstrate this mechanism on a developmental example of auditory map formation guided by visual inputs from the optic tectum (OT), as it has been observed in the external nucleus of the inferior colliculus (ICX) of barn owls. We found that SFA provides a simple mechanism for generating instructive error responses in ICX neurons elicited by visual OT input. On the assumption that STDP applies to auditory-input synapses, we show that the interplay of SFA and STDP in model ICX neurons precisely transfers the tuning curve from the visual modality onto the auditory modality, demonstrating a useful computation for multimodal and sensory-guided processing. Furthermore, this synergy between SFA and STDP also makes map formation possible even in situations in which informative auditory-visual stimuli are very short in duration and in which auditory noise hinders visually-guided learning.

For a large range of model parameters, the interaction of these common cellular and synaptic properties (SFA and STDP) gives rise to the perceptron rule and represents a robust mechanism for supervised learning in biological systems. Because our learning rule is local – one that makes use only of quantities available at the connection being updated – it is plausible that a biological system could implement this optimization principle. Most importantly, the error signal in our STDP-SFA scenario is implicit, which alleviates the exploratory urge to identify such signals experimentally.

Zusammenfassung

Es wird allgemein angenommen, dass sensorische und motorische Informationsverabreitung im Gehirn auf einfachen Informationsverarbeitungsgrundlagen der zellulären und synaptischen Physiologie beruhen. Es gibt jedoch noch immer viele Lücken in unserem Verständnis des Zusammenhangs zwischen der Informationsverarbeitung und den biophysikalischen Eigenschaften von Neuronen. In dieser Thesis wird gezeigt, wie durch das einfache Zusammenspiel zweier typischer biophysikalischer Mechanismen einzelner Neuronen im Gehirn – Spike-Time-Dependent-Plasticity (STDP) und Spike-Frequency-Adaptation (SFA) – die allgemein bekannte Perzeptron Lernregel approximiert werden kann. Es werden Simulationen von Integrate-And-Fire Neuronen zusammen mit einer mathematischen Analyse dargestellt, mit deren Hilfe erkannt wurde, wie verzögerte Eingangssignale eines Neurons mit SFA dessen Anwort auf andere STDP-abhängige Eingangssignale präzise steuern.

Beispielhaft wird dieser Mechanismus dargestellt anhand der durch visuelle Reize des optischen Tectums (OT) geführten Entwicklung eines auditorischen Ortungssystems, wie es im externen Nukleus des inferioren Kollikulus (ICX) der Schleiereule beobachtet werden kann. Es zeigte sich, dass SFA einen einfachen Mechanismus darstellt, um mithilfe des Eingangssignals aus OT ein instruktives Fehlersignal in ICX zu generieren. Unter der Annahme, dass auditorische Eingangssynapsen STDP unterliegen, zeigen wir, dass das Zusammenspiel von SFA und STDP in ICX Modelneuronen die Antwortkurven von der visuellen Modalität präzise zur auditorischen transferiert, was eine wertvolle Funktion darstellt für multimodale und sensorisch gesteuerte Prozesse. Des weiteren ermöglicht diese Synergie zwischen SFA und STDP die Generierung dieser Abbildung auch in Situationen, in welchen auditorisch-visuell informative Stimuli von kurzer Dauer sind, oder in welchen auditorischer Lärm visuell gesteuertes Lernen verhindert.

Das Zusammenspiel der einfachen zellulären und synaptischen Eigenschaften (SFA und STDP) führt für eine grosse Bandbreite von Modelparametern zur Perzeptron-Lernregel, und stellt somit einen robusten Mechanismus für überwachtes (supervised) Lernen in biologischen Systemen dar. Da die Lernregel lokal ist - sie macht nur Gebrauch von Grössen, welche bei der zu aktualisiertenden Verbindung vorhanden sind - ist es plausibel, dass biologische Systeme diese Lernregel implementieren könnten. Vor allem ist das Fehlersignal

in unserem SFA-STDP Model implizit, nicht explizit, was die experimentelle Suche dieser Signale überflüssig macht.

Publications

Select sections from Chapters 1, 2, 3, 4 & 5 of this thesis have been published as a paper:

- D'Souza P, Liu S-C, Hahnloser RHR (2010) **"Perceptron learning rule derived from spike-frequency adaptation and spike-time-dependent plasticity"** in *PNAS USA*, vol. 107[10], pages 4722–4727.

Contents

List of Figures

Chapter 1

Introduction

Many of the sensory and motor tasks solved by the brain and its subsystems can be captured in simple equations or minimization criteria. For example, minimization of errors made during reconstruction of natural images using sparse priors leads to linear filters reminiscent of simple cells (Karklin & Lewicki, 2005; Olshausen & Field, 1996), minimization of retinal slip or visual error leads to emergence and maintenance of neural integrator networks (Hahnloser, 2003; Robinson, 1989; Xie et al., 2002), and optimality criteria derived from information theory can model the remapping dynamics of receptive fields in the barn owl midbrain (Atwal, 2004).

Despite these advances, only little is known about cellular and physiological properties that could serve as primitives for solving such computational tasks. Among the known primitives are short-term synaptic depression that can give rise to multiplicative gain control (Rothman et al., 2009), spike-frequency adaptation (SFA) that may provide high-pass filtering of sensory inputs (Benda & Herz, 2003; Benda et al., 2005) or spike-timing dependent plasticity (STDP) where relative timing between the presynaptic and postsynaptic spiking determine the direction and the extent of synaptic changes (Bi & Poo, 1998).

In this thesis, we explore biophysical mechanisms and computational primitives for instructive learning. Instructive learning is a computation that allows the brain to adaptively constrain its sensory representations by exploiting intrinsic properties of the physical world. The example we consider in this thesis is that, in the natural world, sound sources and salient visual stimuli often co-localize. For instance, the visual presence of a prey and its vocalizations, or when a dried branch cracks under the footstep of an animal – represent

co-localized auditory-visual stimuli. The brain and sensory systems of many animals have evolved to take advantage of such natural stimuli to adaptively tune their prey or predator detection abilities. This ability is critical especially for situations wherein only one of the bi-modal stimulus is available.

In the barn owl, a highly efficient nocturnal predator, this auditory-visual co-localization is highly evolved, well reflected by registration of auditory and visual maps of space in the inferior colliculus and the optic tectum (OT). The instructive aspect of this registration is that it is actively maintained by plasticity mechanisms: When the visual field of juvenile owls is chronically shifted by prisms, neurons in the external nucleus of the inferior colliculus (ICX) and OT develop a shift in their auditory receptive fields that corresponds to the visual field displacement (Brainard & Knudsen, 1993; Knudsen & Brainard, 1991). Hence, visual inputs to these areas are able to serve instructive roles for auditory spatial tuning.

A cellular computational primitive for instructive learning could be a signal that causes the synaptic strength of a driving afferent to increase when the latter fires below some target rate and decrease in the contrary case. In the computational literature, this scenario corresponds exactly to the perceptron rule, a learning rule for one-layer neural network models (Rosenblatt, 1958; Widrow & Hoff, 1960). This rule guarantees that the firing rate approaches the target rate and is one of the simplest expressions of an almost infinite class of learning algorithms that go under the name of gradient descent algorithms. Although the perceptron rule and gradient descent algorithms have been broadly applied to network models of brain function (Brunel et al., 2004; Fiete et al., 2007; Seriès et al., 2004), to our knowledge they have not been derived from first principles and abundant experimental evidence for their existence is still lacking. One of the most prominent criticisms is that these algorithms depend on the existence of an explicit error signal, for which convincing evidence is scarce in most neural systems.

One candidate cellular computational primitive for instructive learning found in the brain is Hebbian STDP (Markram et al., 1997; Bi & Poo, 1998). In general terms, STDP is the phenomenon of synaptic strengthening when the presynaptic neuron fires an action potential briefly before the postsynaptic neuron and synaptic weakening the reverse case. In spiking-network models, STDP is shown to be capable of inducing network repair and of wiring cross-modal spatial transformations (Song & Abbott, 2001; Brody & Hopfield, 2003;

Davison & Fregnac, 2006; Witten et al., 2008). However, it seems that STDP cannot support arbitrary instructive learning based on gradient-descent error-minimization principles (Legenstein et al., 2005).

In this thesis, we identify a possible scenario for the implementation of the perceptron rule, namely in neurons that display both SFA and STDP. Using simulations and analysis, we study a spike-based network model of auditory map formation in adaptive ICX neurons. The network model is based on the barn owl midbrain organization and on physiological neural responses. We show how SFA in ICX neurons can generate an implicit error signal that is proportional to the mis-match between the auditory and the visual spatial maps. Next, assuming STDP to apply to ICX auditory afferents, we show that synaptic changes that result from the interplay between the error signals and STDP are in excellent agreement with the perceptron learning rule. We also explore other additional benefits that may be conferred to neural systems through the interaction of SFA and STDP.

In this rest of this chapter, we provide the reader with a detailed introduction to the barn owl midbrain auditory localization system, then an introduction the SFA and the STDP mechanisms, current computational studies that employ STDP for map learning and a review of previous work.

1.1 Barn owl auditory localization system

The barn owl is a nocturnal predator which has a remarkable ability to localize sounds in complete darkness. At night, this ability helps it catch mice with nearly flawless precision, just by listening to sounds made by the mice. Central to the barn owl's sound localization system are the precise auditory maps of space found in the owl's midbrain structures - the external nucleus of the inferior colliculus (ICX) and the optic tectum (OT). The dominant auditory localization cue in the horizontal plane (azimuthal) is the interaural time difference (ITD), which results from a difference in the distance that sound travels to reach the near versus far ear (Figure 1.1). The auditory localization system also uses other cues mainly for vertical localization (elevation). These are the interaural level differences (ILD), which is a measure of the difference in sound pressure level between the two ears, and monoaural spectral cues which is amplitude spectrum of the sound at each ear, resulting from the shape of the ear and head.

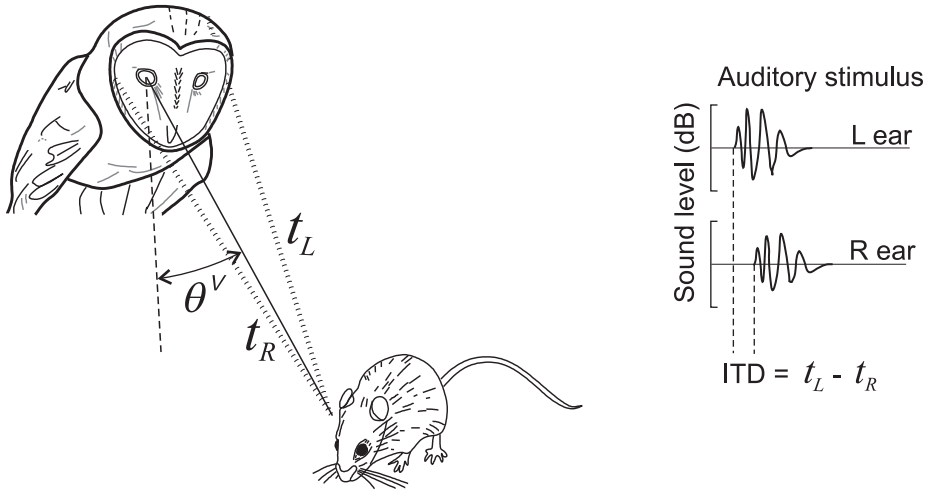

Figure 1.1: Visual and auditory localization in the barn owl. *Left*: Barn owls are able to localize prey in head-centered visual coordinates θ^V (their eyes are essentially immobile in their orbits), and in head-centered auditory (azimuthal) coordinates θ^A based on the interaural time differences (ITD) $t_L - t_R$ of sound waves reaching the left and the right ear. *Right*: The sound waveform arriving at the right ear is delayed and attenuated in this example.

The OT is the center of auditory orientation behaviour – most OT neurons are bimodal (i.e. they respond to both visual and auditory stimuli) and this bimodal map helps the owl to determine the location of its prey using either visual or auditory cues.

1.1.1 Anatomy and functional organization of the barn owl midbrain.

The processing and extraction of sound localization cues in the barn owl midbrain takes place starting at the cochleas. Sound incident on the ears is first processed by the cochleas. The cochlea separates the sound signals into different frequency channels and transduces them into neural impulses (Köppl et al., 1993). This information ascends in two parallel pathways (Sullivan & Konishi, 1984; Carr & Boudreau, 1991; Adolphs, 1993) – one with the timing information and the other with the intensity information – to the central nucleus of the inferior colliculus (ICC). The pathway for timing passes first through the nucleus magnocellularis and then to the nucleus laminaris, at which point the ITD information from binaural inputs is measured and mapped in frequency specific channels. In the second pathway, sound level information is processed through the nucleus angularis and then in the posterior lateral lemniscal nucleus where binaural convergence takes place, and the ILD information is extracted. Cue information from these two pathways (ITD and ILD) merge

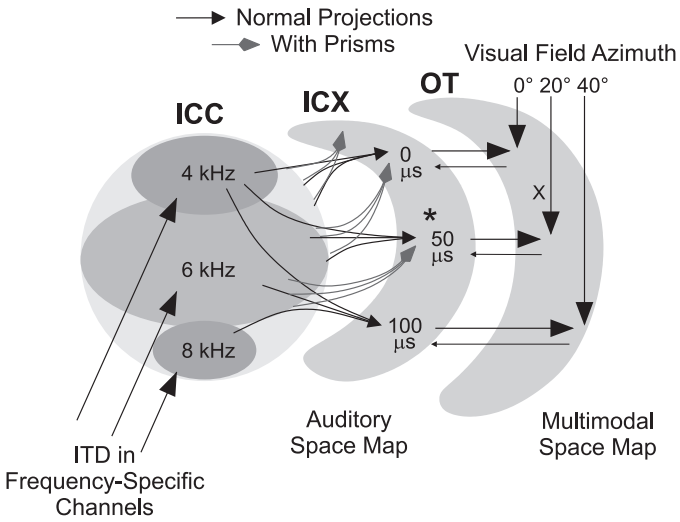

Figure 1.2: Schematic representation of anatomy of the barn owl midbrain auditory localization system (reproduced from Knudsen et al., 2000). Arrows indicate the flow of information. ITD information is initially measured and mapped in frequency-specific channels in the nuclear laminaris (not shown), and then ascends to the ICC. From the ICC, ITD information converges across frequency channels and projects to the ICX resulting in spatially restricted auditory receptive fields and a topographically laid out map of space in ICX. (The numbers 0, 50, 100 μs indicate the best ITDs of the neurons at these locations). The thus created ICX auditory map of space ascends further up and merges with a visual map of space in the optic tectum (OT). Tectal neurons receive visual inputs directly from the retina and indirectly from the forebrain (not shown). The OT also projects topographically back to the ICX (thin right-to-left arrows). The ICC-to-ICX projection is a site of plasticity: in owls raised with prisms, a change in anatomical projection from ICC to the ICX results, bring the ICX auditory spatial map back into registration with the OT visual map.

in the ICC, which is tonotopically organized (Takahashi & Konishi, 1988b,a; Wagner et al., 1987).

The ITD and ILD cues in the ICC are combined across different frequency channels and relayed to the ICX (Knudsen, 1983) where a topographically laid out map of space is created (Knudsen et al., 1977), as shown schematically in Figure 1.2. The ICX neurons are tuned to specific ITDs and ILDs and are completely independent of sound frequency (Takahashi & Konishi, 1986). Next, the ITD and ILD information ascend further up to the OT where a bimodal (auditory and visual) map of space is created. The OT is also topographically organized and receives direct visual inputs from the retina. Neurons in the OT have well defined and mutually aligned auditory-visual spatial receptive fields (Knudsen, 1982). There is also a topographic projection from the OT to the ICX (which we will explain later).

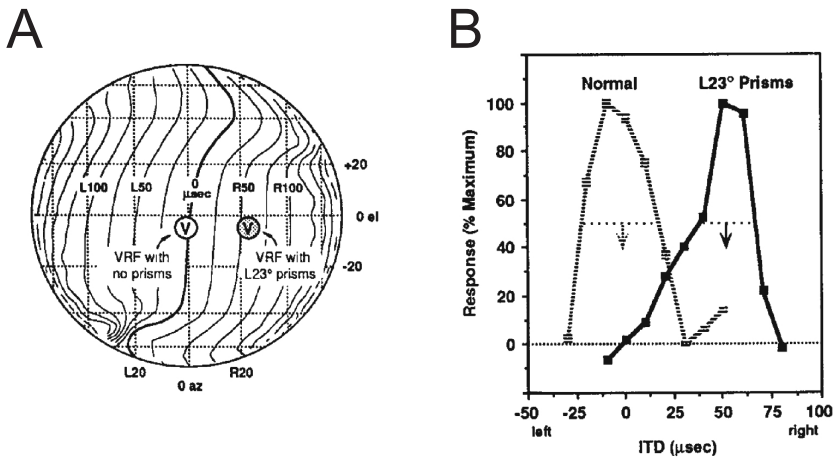

Figure 1.3: Plasticity of auditory tuning in the optic tectum of a juvenile owl resulting from prism rearing (reproduced from Brainard & Knudsen, 1993). (**A**) An example of the horizontal displacement induced by a L23° prism on a visual receptive field (encircled V). The globe represents the space in front of the owl relative to the line of sight. The contour lines indicate the correspondence of ITD values with locations in space (L: left, R: right). (**B**) The normalized ITD tuning of two OT neurons before and after prism rearing. The visual receptive fields of both OT neurons are centered at 0° azimuth. Before prism experience (Normal), the neuron is tuned to 0 μs ITD. After 8 weeks of L23° prism experience, the ITD tuning from a very similar site has shifted to 50 μs right-ear leading. Downward arrows indicate the best ITD for each site.

1.1.2 Behavioral learning and functional plasticity

At birth, the midbrain auditory-visual localization pathway has an innate connectivity pattern which approximately aligns the auditory and the visual modalities in the OT. There is, however, behavioral learning in this system: When a juvenile owl is subjected to sustained lateral displacement of the visual field (e.g. by means of prismatic spectacles, which shifts the visual field in azimuth in the OT by a certain amount), it is observed that after a period of readjustment of about 8 weeks the auditory receptive fields of OT neurons retune themselves by an amount that matches the visual field displacement (Brainard & Knudsen, 1993), illustrated in Figure 1.3. Following-up with this initial finding, a lot of subsequent experiments have been carried out to tease out the exact nature of this functional remapping of the auditory receptive fields. These experiments have revealed that the functional remapping of the auditory space takes place mainly in the ICX (Brainard & Knudsen, 1993; Feldman & Knudsen, 1997). That is, it is the auditory neurons in the ICX whose receptive fields undergo a shift, Figure 1.4.

A similar functional adjustment takes place in ICX neurons' auditory tuning if instead

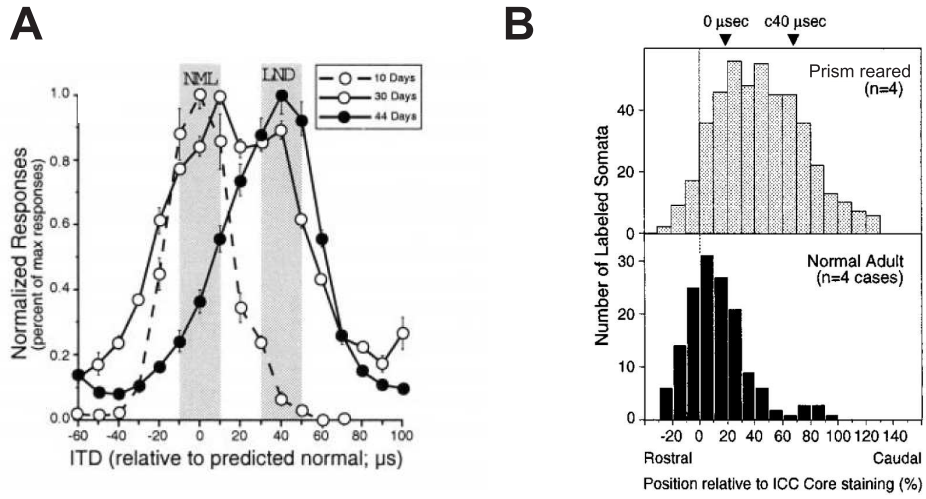

Figure 1.4: The ICX is the site of adaptive auditory plasticity. (**A**) Adjustment of ITD tuning in the ICX of prism wearing owls showing the shift of ITD tuning after different amounts of continuous prism experience (10, 30 and 44 days of experience). Normal and learned ranges of ITD are indicated by gray bars labeled NML and LND, respectively. (Reproduced from Zheng & Knudsen, 2001). (**B**) Remapping of the axonal projection fields from the ICC to ICX after prism experience. Shown is the histogram distributions of labeled ICC cell positions after ICX injections in prism reared owls (top plot) and in normal adults (bottom plot). The distribution for the prism-reared owls contain many more caudally situated neurons than the comparable distribution for normal adults. Triangles, ICC positions corresponding to the normal best ITD for this injection site (0 msec) and to the mean best ITD adopted after prism-rearing (c40 msec). (Reproduced from Feldman & Knudsen, 1997). The change in the projection fields is shown schematically in Figure 1.2 by the gray arrows from ICC to ICX.

of prism experience the auditory experience is altered by plugging one of the owl ears. Such monaural occlusion experiments alters the neural map of ILDs in the ICX to change in an adaptive direction (Joachim & Eric, 1993). Hence, no matter the type of altered experience – whether visual or auditory – it is always the auditory localization system that adaptively adjusts to maintain registry with the visual input.

Associated with the functional changes that take place in the ICX, anatomical evidence using retrograde labeling, show that this remapping of auditory signals takes place in the axonal projection fields from the ICC to the ICX, Figure 1.4 (Feldman & Knudsen, 1997). It remained obscure, however, as to how the OT visual map is able to guide plasticity in the ICX: the ICX was known to be a purely auditory site and attempts at recording any kind of visual signal in the ICX were unsuccessful. A series of experiments then revealed a possible mechanism by which visual information may instruct the remodeling of the auditory pathway in ICX. There exist point-to-point projections from the OT to the ICX (Hyde & Knudsen,

2000; Luksch et al., 2000). A small lesion placed in the OT eliminates adaptive plasticity in the corresponding portion of the auditory space map in the ICX, while the rest of the auditory map continues to shift adaptively in response to experience (Hyde & Knudsen, 2002). A visual instructive signal can be recorded from neurons in the ICX after blocking inhibition in the OT (Gutfreund et al., 2002), suggesting that visual spatial information is gated into the auditory system by an inhibitory mechanism that operates at a higher level in the brain.

1.1.3 Visual instructive signal

The visual instructive responses in ICX neurons elicited by OT input might be the key to the remapping process. Under the effect of inhibition blockade in the OT, Figure 1.5 shows single-unit activity in ICX after presentation of an auditory-only, visual-only or an auditory-visual stimuli. Three interesting observations can be made out of this experimental result. First, the auditory responses are short relative to the stimulus drive, Figure 1.5A. Second, the visual responses are delayed from the auditory responses by about 50-70 ms, Figure 1.5B. Third, and most importantly, the visual responses are only observable when there exists a spatial mismatch between the visual and auditory stimuli, Figure 1.5C. Therefore, the visual responses could be indicative of errors because they are only seen when auditory and visual stimuli are not matched in their spatial directions (Gutfreund et al., 2002).

Mechanistically, the visual error responses are believed to be shaped by spike-frequency adaptation (SFA), in ICX neurons (Gutfreund & Knudsen, 2006). In general terms, SFA is a phenomena of fatigue observed in neurons when driven by a suprathreshold current. ICX visual responses are suppressed in the matching case by SFA elicited by preceding auditory responses, whereas no suppression is seen when preceding auditory responses are absent, Figure 1.5D. Thus shaped error responses in combination with some synaptic plasticity mechanisms may supervise the auditory map formation process in ICX.

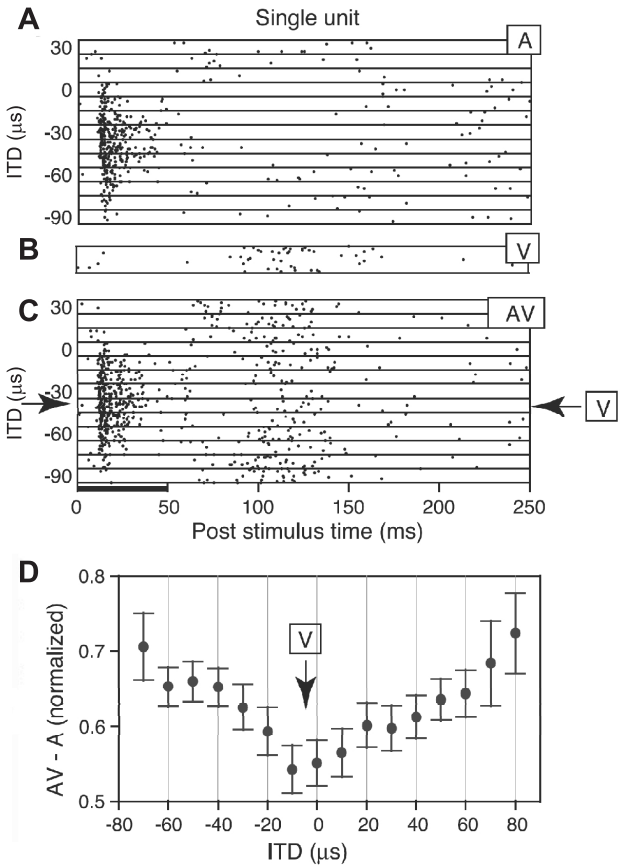

Figure 1.5: Influence of auditory stimuli on visual responses in the ICX under the effect of inhibition blockade in the OT (experimental results, reproduced from Gutfreund et al., 2002). (**A**) Response (spike rasters) of an ICX neuron to an auditory stimulus of 50 ms duration as a function of ITD. The neuron is seen to respond within a few milliseconds of stimulus presentation (**B**) Response (spike rasters) of the same neuron to visual stimulus at the neuron's preferred visual stimulus direction. The onset of the visual responses is seen to be delayed by about 80 ms. (**C**) Responses of the same neuron to simultaneous presentations of auditory and visual stimuli. The visual stimulus is presented in the preferred visual stimulus direction while the auditory stimulus is presented in different spatial directions (reported as ITD's in the y-axis). Visual responses are only elicited when there is a mismatch in the visual and auditory stimulus directions. The arrow indicates the ITD value corresponding with the location of the visual receptive field. (Stimulus duration: 50 ms, indicated by thick solid line on the x-axis.) (**D**) The average ICX visual responses is an approximate linear function of the degree of mis-alignment between the auditory and the visual stimulus. The plots shows the average normalized difference between the response to the auditory-visual stimulus and the response to the auditory stimulus alone (AV-A), for the time window 80 to 140ms after stimulus onset, plotted versus the ITD of the sound relative to the best ITD of the site.

1.2 Spike-frequency adaptation

SFA, a widespread neurobiological phenomenon, is the decrease in the instantaneous firing rate of a neuron during a sustained current injection. It is a characteristic feature of many

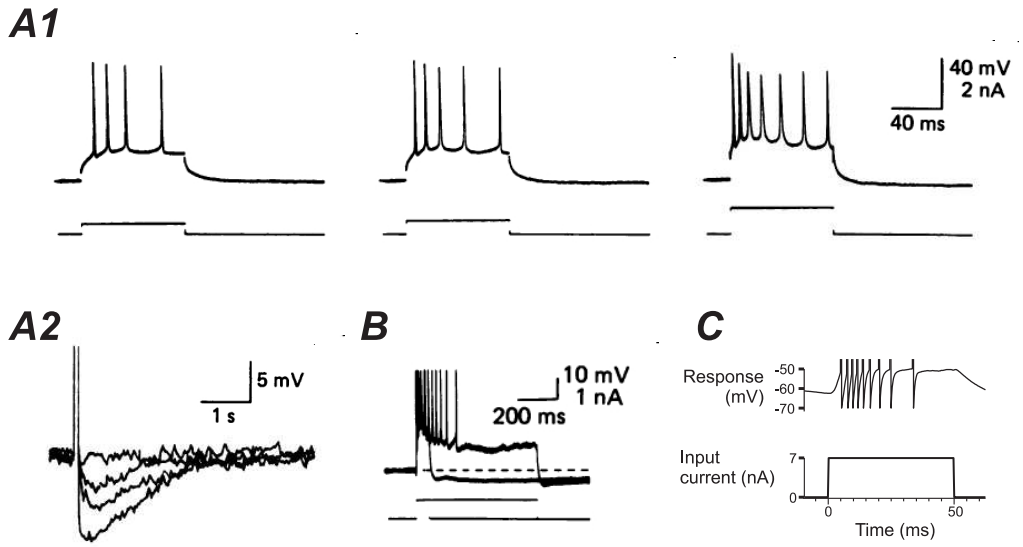

Figure 1.6: Adaptation in the rat hippocampal pyramidal cells (from Madison & Nicoll, 1984) and a computer simulation example of SFA. (**A1**) Responses of a pyramidal cell to depolarizing current pulses passed through the recording electrode. The three plots (from left to right) show the responses to depolarizing currents of increasing amplitudes. Current trace is positioned below the voltage trace. (**A2**) Superimposed tracings of the membrane voltage corresponding to A1 showing the AHP that follows the current pulse. The smallest AHP shown in the superimposed tracings is the response to a stimulus giving a single action potential (not shown). (**B**) Responses of the cell to a long (approximately 600 ms) and a short (approximately 60 ms) depolarizing current are shown superimposed. Action potentials in this record are truncated. The traces A1, A2 and B are reproduced from Madison & Nicoll (1984). (**C**) SFA implemented using an AHP-current in a model neuron simulation. In response to a 50 ms step input current, the spike rate of the conductance-based integrate-and-fire neuron is high at the onset of the step input, but then adapts. (Simulation details are in Chapter 2).

types of neurons, and has been observed in neurons of various systems (Michaelis & Chaplain, 1975; Madison & Nicoll, 1984; Schwindt et al., 1988; Barkai et al., 1994; Ahmed et al., 1998; Kuznetsova et al., 2008). An illustrative example of SFA is presented in Figure 1.6A1 showing *in vitro* responses of a rat CA1 pyramidal cell which was excited by injecting long depolarizing current pulses of increasing amplitudes (from Madison & Nicoll, 1984). The cell responds with an initial rapid action potential discharge rate which then slows, or adapts. That the cell cannot maintain its firing rate to a steady depolarizing input indicates the presence of mechanism(s) which serve to counteract the persistent input drive.

A large variety of cellular mechanisms are known to be responsible for SFA. These mechanisms are most commonly driven by ionic currents. One of the most widespread and principal mechanism is the afterhyperpolarization (AHP) current, which is found to fol-

low current-induced repetitive firing (Madison & Nicoll, 1984). The AHP mechanism is an action-potential-dependent hyperpolarization of the membrane voltage due primarily to Ca^{2+}–activated slow K^+ currents. During repeated firing these currents sum up with successive spikes (Figure 1.6A2) causing the neuron to adapt.

SFA is thought to play many important functions in neural information processing. We will not go into the details of the entire gamut of the functional roles of SFA as these are investigated at length in the literature (see, e.g., Wang, 1998; Fuhrmann et al., 2002; Wang et al., 2003; Benda et al., 2005, and references therein), but here we mention some roles of SFA that may be applicable to and/or advantageous for sensory processing. One example in which SFA may play a role is in 'forward masking', in which the adaptation elicited by an earlier arriving signal reduces the response evoked by a later signal (Smith, 1977; Liu & Wang, 2001; Wang, 1998; see also Meredith et al., 1987). Another functional role of SFA is in pattern adaptation to background disturbances, i.e., SFA can provide a mechanism to reduce redundancy in the processing of natural stimuli by removing temporally constant stimuli while remaining responsive to more rapid changes (Wang, 1998; Wang et al., 2003; Benda et al., 2005; Peron & Gabbiani, 2009).

In this thesis we will use a model AHP-current to implement SFA in our model neurons. An example is shown in Figure 1.6C. As seen in this figure, the simulated AHP-induced adaptation is qualitatively comparable to that in biology. (The simulation and additional details are in Chapter 2).

1.3 Spike-timing dependent synaptic plasticity

Recently, spike-timing dependent synaptic plasticity – a mechanism of activity dependent learning at the cellular level – has emerged as the most studied form of long-term synaptic plasticity both in experimental and in theoretical neuroscience. Increasing experimental evidence have shown that STDP is widespread in diverse brain areas such as hippocampus, retinotectal synapses (e.g. in tadpoles), visual cortex etc., to mention a few (see Dan & Poo, 2004, for a review).

STDP was first observed in synaptic modification data from rat pyramidal neurons in layer 5 of the neocortex (Markram et al., 1997) where it was shown that individual active synaptic connections undergo modification depending on the precise timing of the spikes in

the pre- and postsynaptic neurons. Subsequently, experiments of Bi & Poo (1998) determined the exact functional form of the direction and magnitude of synaptic changes as a function of the pre- and postsynaptic spike timings, shown in Figure 1.7C. The observed modification rule can be summarized as follows: Synapses strengthen when a presynaptic spike is followed by a postsynaptic spike, implying that a causal ordering of events is rewarded. In the reverse case, synapses weaken, implying that a anti-causal ordering of events is punished. The magnitude of this synaptic strength changes is dependent on the time difference between the presynaptic input spike and the postsynaptic firing, and a function called the STDP window function. This function, $W(\Delta t)$, determines the change in the synaptic strength induced by a single pre- and postsynaptic spike pair, as illustrated in Figure 1.7B. Most commonly, a pair of exponential functions shown in Figure 1.7D is taken as the most suitable fit for the experimental data in Figure 1.7C.

In the experiments that study STDP, paradigms to induce synaptic plasticity often are a single pre- and postsynaptic spike-pair. Such single spike pairing is selected for their effectiveness rather than for their physiological relevance, thus providing limited information on how circuits are modified by natural patterns of activity. Naturalistic neuronal activity in vivo is far from regular. So, how well does the STDP learning rule measured with simple spike patterns account for the synaptic changes induced by naturalistic spike trains? When multiple spike pairs fall within the STDP window, the net synaptic strength changes due to individual pre- and postsynaptic spikes can be assumed, to first approximation, to sum up linearly. That is, the synaptic changes due to each pre-post spike pair in the presynaptic and the postsynaptic spike trains add up to give the total change in synaptic strength. Such a linear summation does not exactly apply in biology and experiments show that there can be non-linear interactions between, e.g., spike triplets (Froemke & Dan, 2002; Dan & Poo, 2004; see also Caporale & Dan, 2008). However, owing primarily to the ease and simplicity for analytical and simulation purposes, most computational and simulation studies so far employ a linear summation of synaptic weight changes. We will also employ the linear summation method in this thesis.

The average 'change in EPSC amplitude' in Figure 1.7C does not indicate whether the magnitude of the synaptic efficacy changes is dependent in any manner on the absolute value of the synaptic strength. There are two ways in which this dependency can be assumed.

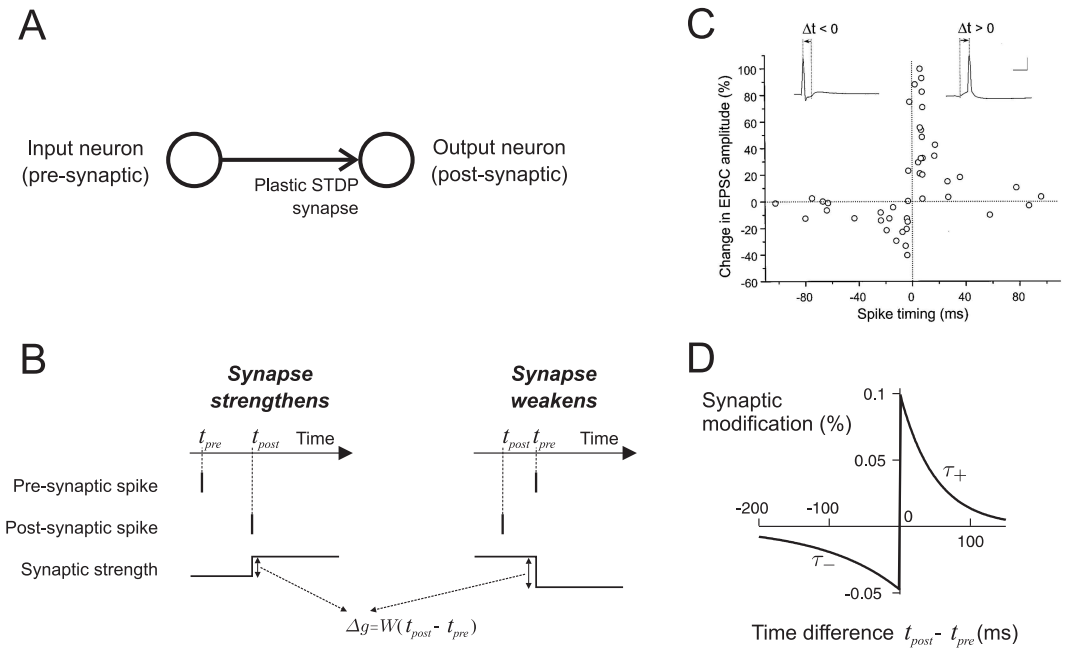

Figure 1.7: Basic workings of the STDP learning rule. (**A**) Schematic of a plastic STDP synapse connecting an input (pre-synaptic) neuron to an output (post-synaptic) neuron. (**B**) The STDP synapse strengthens when the post-synaptic neuron fires an action potential a few milliseconds after the pre-synaptic input arrives (*left*). In the reverse case, the STDP synapse weakens (*right*). The amount of strengthening or weakening Δg (i.e. the magnitude of the step) is determined by the time difference between the pre- and post-synaptic firing (Δt) and a function, $W(\Delta t)$, called the STDP window function. (**C**) Actual synaptic modification data from cultured hippocampal neurons from Bi & Poo (1998) showing the STDP window for induction of synaptic potentiation and depression. Each circle represents the average amount of amount of synaptic strength modification (increase or decrease) from a repeated pairing experiment as a function of time lag (Δt) between pre and postsynaptic spike timing. The smaller the time difference between pre and post synaptic firing, the larger is the synaptic modification. (**D**) Plot of an "analytical" STDP window function with exponential tails that is often used as a approximation of experimental data such as in (C).

The so called "additive" model assumes that the synaptic efficacy changes do not scale with synaptic strength. The "multiplicative" model assumes that the magnitude of the synaptic efficacy changes decreases as either the upper or lower bounds of the synaptic strength are approached. A defining character of these two models, known from computational modeling study, is that the equilibrium synaptic strength distribution in the additive update model tends to be binary (i.e. synaptic strengths are either at 0 or at the maximum value) whereas in the multiplicative update model all synapses are driven to a similar equilibrium value (for more details see Rubin et al., 2001; Gutig et al., 2003). In the system we are attempting to model in this thesis – the ICX auditory tuning and the tuning shift in response to shifted

visual input (see Figures 1.3, 1.5) – are all suggestive of synapses that are either fully active or inactive, which is consistent with the additive STDP update rule rather than the multiplicative one. For this reason, we will exclusively employ the additive update rule in the model presented in this thesis.

An asymmetric STDP window function with decaying tails as shown in Figure 1.7C is only one of a wide range of different window shapes observed experimentally. Many other types of STDP window shapes have been found in brain cells, for example, windows that are temporally symmetric. Generally, it has been found that the window shape is specific to the synapse type and the target cell type (excitatory or inhibitory). A detailed review of these windows is presented in Caporale & Dan (2008). We will employ the asymmetric window with exponential tails (shown in Figure 1.7C,D) in the simulations and analysis in this thesis because in our model all the plastic connections are from excitatory neurons to excitatory neurons and such windows are most common for such connections.

Ever since the time of its experimental discovery and characterization, STDP has been also throughly investigated in computational models of learning. Examples include cortical map development (Song & Abbott, 2001), temporal difference learning (Rao & Sejnowski, 2001; Roberts et al., 2008), cross-modal spatial transformation learning (Davison & Freǵnac, 2006), optimal information transmission (Hennequin et al., 2010), among others. Here we will focus mainly on computational aspects of STDP relevant to instructive learning.

1.4 Instructive learning with STDP

The relevance of STDP for instructive learning comes from the ability of STDP to reinforce temporal correlations present (1) within the activities of the presynaptic input population and (2) between the presynaptic input population and the postsynaptic neuron. In the following we illustrate these concepts by showcasing some computational modeling examples from literature. We first show how STDP affects synapses onto a single postsynaptic neuron, when driven by uncorrelated and correlated inputs. All the synapses we consider here below are excitatory and their strengths are constrained to the interval $[0, g_{\max}]$ where $g_{\max}$ is the maximum synaptic strength. Also, the additive STDP update rule is employed in these simulations.

1.4.1 Uncorrelated inputs

In the first simulation experiment we describe, from Song et al. (2000), a set of 1000 input synapses drive a single postsynaptic neuron. The presynaptic input spike trains are generated in such a manner that they uncorrelated with one another but they all have the same firing rate. The synaptic strengths are initially set to random values (i.e. uniformly distributed in the interval $[0, g_{\max}]$). As the simulation is started, a period of adjustment ensues, after which a steady state is reached. In equilibrium, STDP tends to segregate the synapses into strong and weak groups, creating a bimodal distribution of synaptic strengths, Figure 1.8A. The division of synapses into strong and weak groups is random and a different grouping of synapses is seen each time the experiment is reinitialized.

The bimodal equilibrium distribution of synaptic weights requires, however, a precondition: The net area under the STDP window should be slightly negative (Kempter et al., 1999; Rubin et al., 2001). This implies is that STDP weakens 'chance' input-output correlations, imposing on such inputs a weak tendency to depress. (Commonly, the ratio of the areas under the negative leg ($\Delta t < 0$) and positive leg ($\Delta t \geq 0$) of the STDP window is set to a value around 1.05 to 1.1). Even though the overall bias of STDP is for the synapses to depress, a synapse which drives the postsynaptic neuron to fire "sees" an additional positive correlation between the input and output neuron, as shown by the solid black line in Figure 1.8B in the interval $-20 \leq (t_{\text{pre}} - t_{\text{post}}) \leq 0$. This positive correlation overcomes the negative bias in the update rule and thus sustains the strengths of strong synapses.

1.4.2 Correlated and uncorrelated input groups

In their next simulation experiment (Song et al., 2000), temporal correlations are introduced within the spike trains for inputs 501 through 1000, while the spike trains for inputs 1 through 500 were left uncorrelated as before. In this case, STDP strengthens synapses that are effective at rapidly evoking a postsynaptic action potential, such as groups of presynaptic inputs that fire in a correlated manner. Therefore, after equilibration, synapses in the correlated group ended up stronger than those in the uncorrelated group, Figure 1.8C.

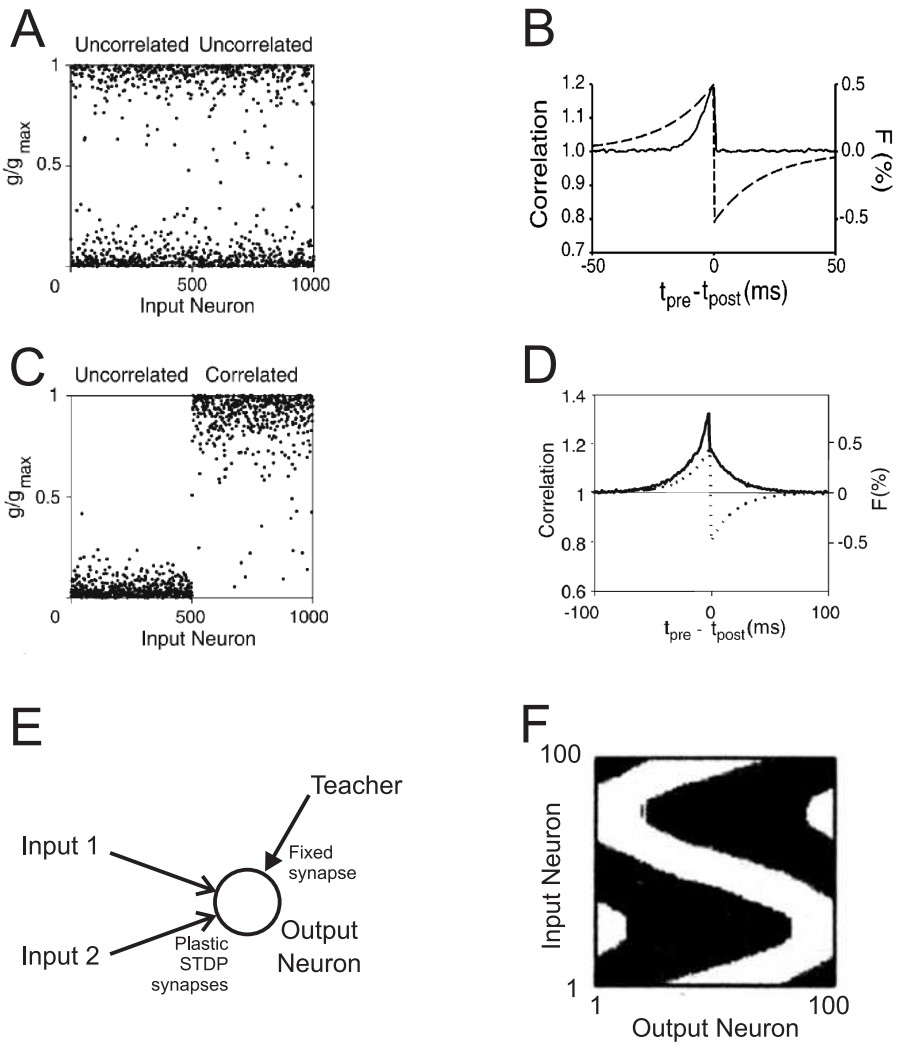

Figure 1.8: Correlation based learning through STDP. (**A**) A single postsynaptic neuron is driven by two afferent groups each containing 500 plastic STDP synapses (input neurons 1 through 500 and 501 through 1000). Shown is the strengths of these synapses (dots) for uncorrelated inputs after STDP has come to an equilibrium. (**B**) Average correlation between presynaptic action potentials of a strong synapse in (A) and the postsynaptic spike train. The solid curves indicate the relative probability of any presynaptic spike occurring at time t_{pre} when a postsynaptic spike occurs at time t_{post}. A correlation of one is the value due solely to chance occurrences of such pairs. The dashed curves show the STDP modification function (termed F in this plot) used in these experiments. (**C**) Equilibrium synaptic strengths when the postsynaptic neuron receives both uncorrelated (input neurons 1 through 500) and correlated (input neurons 501 through 1000) inputs. (**D**) Average correlation between presynaptic action potentials of the correlated group of inputs in (C) and the postsynaptic spike train. (**E**) A conceptual framework of a simple network for correlation based instructive learning through STDP. (**F**) Cross-modal spatial map learned through STDP (reproduced from Davison & Freǵnac, 2006). Shown is the matrix of synaptic weights from the population of 100 input neurons to the population of 100 output neurons, after learning. White corresponds to maximum synaptic strength and black corresponds to zero synaptic strength. The transformation learned in this example is the function $f(\theta) = \sin(\theta)$. [Note: Subplots A,B and D have been reproduced from Song & Abbott (2001), and subplot C from Song et al. (2000)].

The equilibrium distribution of synaptic strengths that arises from STDP depends on the number of pre- and postsynaptic spike pairs that fall into different portions of the STDP window function. The average number of presynaptic action potentials occurring at various times before and after a postsynaptic spike is proportional to the correlation function of the pre- and postsynaptic spike trains. Therefore, an estimate of the overall effect of STDP can be obtained by computing the integral over spike timing differences, Δt, of the product of $W(\Delta t)$ and the average input-output correlation function. In the example of Figure 1.8C, the input-output correlation function is flat for the uncorrelated set of inputs, except for a small excess of presynaptic spikes just before a postsynaptic action potential. The synapses for this input group are therefore weakened by STDP due to the negative total integral of the window function. On the other hand, the correlation function between the correlated input group and the postsynaptic firing has a prominent peak near time difference $\Delta t = 0$, shown in Figure 1.8D. This peak has a large symmetric component that, by itself, would weaken the synapses when $\tau_- = \tau_+$. However, there is also an excess of presynaptic spikes before the postsynaptic response due to the input integration performed by the postsynaptic neuron. The portion of the peak to the left of time differences of 0 in Figure 1.8D is larger than the portion to the right. This excess causes the synaptic strengths of the correlated group of inputs to grow.

1.4.3 Supervised learning with a correlated "activity" pattern

Such synaptic strengthening of correlated inputs provides a direct way to implement a rendition of supervised learning. Consider the conceptual scenario shown in Figure 1.8E, where a postsynaptic neuron is driven by two input groups, 1 and 2, through plastic synapses, and by a "training" input through synapses of fixed strength. Further, let the inputs of each group have within group temporal correlations but the two groups be mutually uncorrelated. In the absence of any training input, the equilibrium state for this network would be that all the synapses from one group would strengthen and those from the other group would weaken, the stronger/weaker group determined purely by chance. Now, if we turn on the training input and make it produce spikes that are temporally correlated with say, input group 1, and run the experiment, it would be this input group that would always strengthen and the other group will always weaken. The reason for this is that the training input primes

the postsynaptic neuron into firing just as input 1 is active, and this correlation drives the synapses from this group to strengthen. This idea forms the basis for the supervised learning simulations from Davison & Fregnac (2006), which shows that any arbitrary input-output transformation can be learned through STDP using a training input that primes the output neurons with the pattern to be learned.

In this simulation study (Davison & Fregnac, 2006), a one-dimensional array of 100 input neurons are connected via plastic STDP synapses to a one-dimensional array of 100 output neurons. The neuron are laid out topographically and the connection is all-to-all. Each of the output neurons additionally receive training inputs from another array of 100 neurons, conveyed through fixed synapses. The network is stimulated by a point-like stimulus object that jumps from one point to another random point in the input space, dwelling for a brief randomly chosen time duration at each point, thus generating a spatiotemporal activity pattern across the inputs. The input neurons that are activated by this stimulus object produce Poissonian spikes. Concurrently, the training neurons are activated in such a way as to impose an appropriate pattern of activity in the output neurons required to implement the desired input-output transformation (for details, see Davison & Fregnac, 2006). As the network is stimulated, the input synapses that are co-activated with the training input strengthen, whereas all other input synapses that are not co-activated with the training input decay to zero, because of the negative total integral of the STDP window. As as result, after a period of adjustment, an equilibrium is reached in which the appropriate input synapses are fully strengthened and whereas all other synapses settle to zero strength, Figure 1.8F. The transformation learned in this example is the function $f(\theta) = \sin(\theta)$.

Note that even though we have termed the co-activated teacher as a 'supervisor', there exist no supervisory system which "knows" if and when the output neuron has learned the target signal. That is why in Davison & Fregnac (2006), the learning process termed as 'unsupervised'. That is, the plasticity is not guided by an explicit error signal that effects changes in the connectivity such that the error becomes minimum when learning is completed.

1.5 Error-correcting learning

In contrast to learning with STDP, in which the teacher signal provides a spatially and temporally correlated 'activity template' for synaptic strengthening, there is a class of supervised learning paradigms called the 'error-correcting' learning. In error correcting learning, an explicit error signal (difference between actual and desired output) drives synaptic weight changes to achieve convergence of the neuron's output to the target value set by the training input (McLaren, 1989; Knudsen, 1994; Schultz & Dickinson, 2000).

One of the simplest form of error driven learning is the single layer perceptron from the artificial neural network theory, for classifying linearly separable patterns, shown schematically in Figure 1.9. In this scheme, the neuron with output, $A(n)$, is driven by a vector of inputs, $\mathbf{a}(n)$, through plastic synapses of strengths $\mathbf{g}(n)$. The index n represents discrete time, or more precisely, the time step of an iterative process involved in adjusting the synaptic weights. The desired (or target) output is not conveyed directly to the neuron, but rather, the output signal is compared to a target value, $v(n)$, using a error computation unit, and consequently an error signal, $e(n)$, is produced:

$$e(n) = v(n) - A(n). \tag{1.1}$$

The error signal $e(n)$ guides an adjustment mechanism that modifies the synaptic weights in such a way that the neuron's output $A(n)$ approaches the target signal $v(n)$. This objective is achieved by minimizing the instantaneous value of the squared error, $\mathcal{E} = e^2(n)$, when the system is presented with a list of training examples. Many mathematical methods are suitable to minimize the instantaneous square error, such as, Newton's method, Gauss-Newton methods to mention a few (for details see, e.g., Haykin, 1994). One of the prominent and simpler technique, both in concept and in implementation, is the method of stochastic gradient descent.

In this method, an instantaneous estimate of the gradient of the squared error, i.e., $\partial\mathcal{E}/\partial\mathbf{g}$, is used to update the synaptic weights in a direction that is opposite to this gradient. Arduous as it may sound, in practice the method does not require the computation of this gradient. We will skip the mathematical steps involved in the derivation of the gradient as these are detailed in e.g. Widrow & Hoff (1960) and Haykin (1994), and simply present

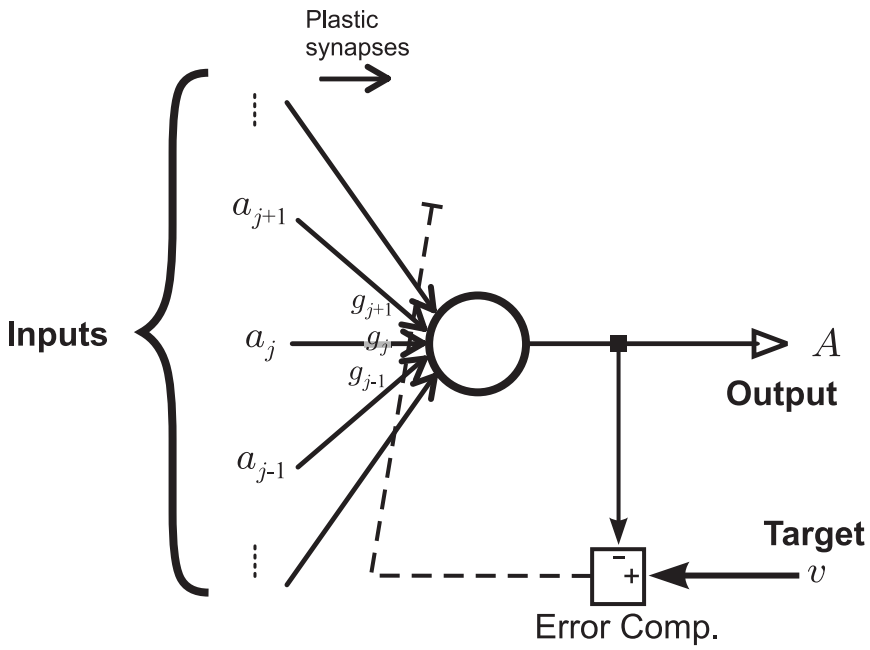

Figure 1.9: A generic, single layer perceptron model for error-correcting learning. The neuron (*circle*) receives an array of inputs with firing rates a_j conveyed via plastic synapses with connection strengths g_j, where j is an index identifying the input. The output of the neuron is the firing rate, A. The target firing rate, v, is conveyed via a separate input. The deviation of the output A from the target v is measured in the error computation unit (*square*). Based on this error, an algorithm adjusts (dashed line) the direction and the magnitude of changes in connectional strength to achieve an objective, which is usually to minimize the squared difference between output A and the desired output v.

the final result: For a neuron with a linear activation function, the synaptic weights update upon presentation of an input and a training sample reduces to:

$$\Delta \mathbf{g}(n) = \eta \left[v(n) - A(n) \right] \mathbf{a}(n), \tag{1.2}$$

where η is a positive constant that determines the rate of learning. This rule is known as the "delta learning rule" or "stochastic gradient descent". The expression within the square brackets on the right-hand-side of Eq. (1.2) is postsynaptic error term $e(n)$, and the last term on the right-hand-side is the presynaptic input, $\mathbf{a}(n)$. Therefore, this rule prescribes synaptic weight changes that are proportional to the postsynaptic error times the presynaptic input. Given a collection of input vectors and associated target values, the repeated application of this synaptic update rule guarantees that the neuron's output, A, converges to the desired output, v.

The implementation of the delta learning-rule, Eq. (1.2), in artificial neural networks is

quite a straightforward business since a computer program would have access to all variables of the system. However, the "implementation" of this rule in biological neuronal networks presents itself with two fundamental requirements: The first is the computation of the aforestated postsynaptic error, and the second is a mechanism to appropriately modify synaptic strengths based on this error and the presynaptic firing rate. Nevertheless, the error computation and weight update is local – the neurons need to use only information in their vicinity, and no global error or other signals are required – and so, the employment of the delta learning-rule by biological systems may be highly plausible. An early example of a way to implement the delta learning-rule in biological neurons is explore in McLaren (1989).

1.6 Review of previous work in modeling the midbrain auditory plasticity

The barn owl's visually guided auditory plasticity has been widely studied and modeled for a number of years now. A wide variety of mechanisms and learning rules have been employed based on experimental evidence available on the organization, connectivity, physiology and synaptic plasticity mechanisms known at the time of those studies. The modeling studies may be broadly classified into two approaches: mechanistic and functional. Among the mechanistic approaches, Gelfand et al. (1988) present a rather simplistic single layer model for adaptive co-registration of the visual and auditory maps in the OT. The bimodal stimuli input (auditory and visual) to their network were simple binary values (1 or 0) conveying the presence or absence of a stimulus at different spatial positions. Synaptic plasticity in this model is not driven by an error signal but rather by a local activity-dependent modification rule based on heterosynaptic interactions and the postsynaptic neuron's membrane voltage. A synapse is strengthened if its presynaptic input is 1 and the postsynaptic voltage is high, and weakened if its presynaptic input is 0 and the postsynaptic voltage is high. The authors show that this simple rule effects competition between the auditory input synapses, such that, a perfectly aligned auditory-visual map in formed in the OT. When presented with a shifted visual map, the auditory map also shifts, and synapses relaying the old auditory map decay to zero.

Rosen et al. (1993) describe a multi-layered feedforward connectionist model* of the midbrain, in which model ICX units receive ITD and ILD information. The ITD information comes from the ICC and ILD information ascending through a series of nuclei starting at the nucleus angularis. The output of the network predicts location of the visual stimulus based on auditory cue inputs (ITD and ILD). The model uses the standard backpropagation algorithm to effect changes to the synaptic weights in all the intermediate layers. However, for synaptic weight changes at the output layer, the authors derive a learning rule that maximizes the cross-entropy between the output units' activations and the probability distribution of the visual cue location. The visual cue location is probabilistic because of the assumption that not all auditory stimuli may be accompanied by matching visual stimuli.

*The elements of the model are 'connectionist' units whose output activations are sigmoidal functions of their weighted inputs.

The authors show that this model is able to accurately reproduce many aspects of experimental findings in the midbrain such as auditory map formation and auditory tuning shift in response prism experience among others.

Prior to the experimental findings of Hyde & Knudsen (2001) and Gutfreund et al. (2002), it was remained obscure if a topographic visual instructive signal from the OT reached the ICX. Therefore, most modeling approaches until this time explored the possibility of an indirect means by which the visual input could guide adaptive adjustments of the ICX auditory tuning. Knudsen (1994) suggested that the visual instructive signal could be a foveation-based, global value signal, derived from a visual assessment of the accuracy of auditory orienting responses to bimodal auditory-visual stimuli. Such a signal would require a diffuse projection system (value system) to the ICX. The value system is activated for salient events and modulates synaptic plasticity. The following two approaches have used such an instructive signal for guiding map formation. Haessly et al. (1995) used a two-dimensional self-organizing feature map, also known as a Kohonen map, to model the auditory spatial map in the ICX. They employed a simple on/off "learn" signal, based on the coincidence of visual attention and auditory input, that turned on and allowed the map to adapt at the visually attended location. Rucci et al. (1997) assumed that auditory synaptic changes depend on the interactions between a pre- and a postsynaptic component reflecting local neural activity and a global modulatory signal that was activated whenever the animal successfully foveated a target. Although both the above approaches were successful in replicating many aspects of ICX auditory map formation in response to normal and shifted visual experience, such a global value signal based mechanism has not been supported by subsequent experiments in barn owls (Hyde & Knudsen, 2001).

Davison & Freǵnac (2006) present a generic framework for learning cross-modal transformations through STDP. They show through their spiking-neuron simulations the realization of any arbitrary transformation from the input space to the output space, with the training input providing the appropriate activity template to the output layer during learning. Their study is not specific to the barn owl auditory system, but they are able to show that model can accommodate latencies in the arrival time of the input and the training modalities, such as seen in barn owls, and also map formation in response to normal and shifted visual experience. Friedel & van Hemmen (2008), present a variant of this model in which they

propose using an inhibitory training input (as against an excitatory one) which is shown to have the effect of improving the quality and speeding up the learning of the map.

The standard instructive learning paradigm assumes that training input is relayed via fixed, non-plastic synapses. Recently, Witten et al. (2008) incorporated plasticity in *both* the auditory input and the visual input synapses. The neurons they used in the simulations were rate based (i.e.n non-spiking). By using a Hebbian weight update rule, they present the surprising result that although the synapses of both the auditory and visual input channels were subject to the same learning rule, the amount of plasticity exhibited by the respective channels was highly asymmetric and depended on the relative strength and width of the afferent receptive fields! The channel with the weaker or broader receptive fields always exhibited most or all of the plasticity.

Among the functional modeling approaches are Kardar & Zee (2002), who modeled the receptive fields of OT neurons by linear filters that sample spatially matched auditory-visual signals and search for filters that maximize the gathered information while subject to the costs of rewiring neurons. Assuming a higher fidelity of visual information, they find that the corresponding receptive fields are robust and unchanged by artificial shifts. The shape of the aural receptive field, however, is controlled by correlations between sight and sound. In response to prismatic glasses, the aural receptive fields shift in the compensating direction, although their shape is modified (i.e. they are no more symmetric) due to the costs of rewiring.

The above line of thought is extended in Atwal (2004), where, by maximizing the mutual information between the stimulus and the neural output, shows how temporal dynamics of ICX auditory receptive field adaptation depended on rewiring costs. In this model, the ability of the aural receptive field to learn is tempered by the parametrized cost of forming extended neural connections and by the rate at which these connections can form. These constraints are shown to result in two qualitatively different types of dynamics depending on the magnitude of the audiovisual misalignment. The reduced costs of neural rewiring, as in the case of young barn owls, reveal two qualitatively different types of receptive field adaptation depending on the magnitude of the audiovisual misalignment. By letting the misalignment increase with time, it is shown that the ability to adapt can be increased even when neural rewiring costs are high, in agreement with experimental findings of the increased

plasticity of the auditory space map in adult barn owls due to incremental learning (Linkenhoker & Knudsen, 2002). In Franosch et al. (2005) presented a supervised learning model of the lateral-line system of the frog *Xenopus*. During the night, the frog relies on its 180 lateral-line organs to localize insects by detecting water waves emanating from insects floundering on the water surface. The plasticity and calibration of the lateral-line system is visually guided. The authors show in their analysis that experimentally observed learning rules like STDP may be derivable from an error minimization principle.

All of these previous models of midbrain auditory plasticity, while being able to explain or reproduce many aspects of the experimental findings in barn owls, are inadequate to varying degrees in their connection to biological realism. Firstly, the none of the models include experimentally observed electrophysiological patterns of activity in the ICC/ICX/OT and are mostly rate based models, with no synaptic integration and latency coding. Secondly, the methods that employ a reinforcement or an error signal lack the explanation for a neuronal or cellular mechanism for computing and conveying such a signal. Thirdly and importantly, most models also do not show how their learning rules for synaptic modification may be mapped to known plasticity mechanisms in the brain such as STDP or other experimentally observed plasticity mechanisms. These inadequacies of the previous models together with new recent experimental results motivates our quest for developing a model that incorporates the latest anatomical and physiological evidence.

1.7 Main results of this thesis

In contrast to the previous models, our model is based closely on the experimentally observed spiking patterns. We study a spike-based network model of auditory map formation in barn owl midbrain. We show how SFA can be one of the simplest biophysical mechanism for computing mis-match error of two modalities; in our case, these are the visual error responses in ICX neurons when auditory responses are not aligned with visual inputs. Next, when we assume STDP to apply to ICX auditory input synapses, we show that the changes in synaptic strength of auditory afferents that result from such SFA generated error responses in combination with STDP leads to the emergence of the delta learning-rule. The consequence is that ICX auditory spatial maps achieve perfect alignment with visual map in OT.

Further, we also show that SFA has many additional benefits for the ICX neuron. We show that the adaptation time constant, by which auditory and visual inputs in ICX interact, reduces sensitivity of the map formation process to uninformative and noisy stimuli. That is, in a noisy auditory environment, SFA amplifies synaptic potentiation associated with visual error responses and makes synaptic modification rather insensitive to responses from uninformative auditory noise. We expect these beneficial effects of adaptation to generalize to other systems where supervised learning plays an important role.

1.7.1 Thesis overview

Like most research, development of the ideas presented in this thesis did not progress in an orderly fashion. However, after having sorted out how the different pieces fit in, I have put together a story that is more didactic and less of the chronological order in which this research was performed. Also, in this thesis, we will focus exclusively on modeling plasticity in the ITD processing pathway, because more is known on the plasticity in the ITD pathway than in the ILD pathway.

In Chapter 2, we consider a single neuron model for instructive coding, in which a conductance based adapting neuron is driven by an auditory and a visual input. We show through spiking-neuron simulation results and analytical derivations (1) how an implicit error signal, which is a measure the auditory-visual misalignment, can be encoded by SFA, and (2) how the delta learning-rule naturally emerges from the interplay between this error signal and STDP.

In Chapter 3, we extend these findings to map formation in a model of the barn owl mid brain. In this model an ICX neuron receives auditory and visual inputs from populations of spatially tuned and topographically laid out neurons. We demonstrate through simulations the formation of ICX auditory receptive fields that are in perfect alignment with OT visual receptive fields. We also present simulation results that show the linearity of receptive field formation and its agreement with the perceptron learning rule.

In Chapter 4, we explore the robustness of map formation with SFA. We show through simulation results that the combination of STDP and SFA is a more robust learning mechanism (in comparison to a model which lacks SFA) when the sensory world is corrupted by noise. We also dwell on the question of map stability in the absence of guiding visual stimuli.

Chapter 5 concludes this thesis with a discussion on our findings, the possible model extensions and the general applicability of our findings in other brain areas. Finally, an appendix containing supplemental information is provided.

Chapter 2

Perceptron learning-rule derived from SFA and STDP

In this chapter, we present a conceptual framework for instructive learning in a single model neuron which is driven by an input signal and a teacher signal. First, we show how spike-frequency adaptation in this neuron can encode an implicit error signal. Next, we show how these error signals when combined with STDP leads to the delta learning-rule. We then present detailed methods for our spiking-neuron simulations. Finally, we provide the detailed analytical derivation of the delta learning-rule in which the conductance-based model equations are simplified using the method of time averaging.

2.1 Network architecture

Our (ICX) model neuron is an adapting conductance-based leaky integrate-and-fire unit in which SFA is modeled by an after-hyperpolarizing potassium conductance (details in the *Methods*, Sec. 2.5). The unit receives excitatory sensory input a from a fast-acting auditory pathway and input v from a slower-acting visual pathway (Figure 2.1). The auditory-input synapses are subject to STDP, whereas the visual-input synapses are fixed.

Our results are based on spiking-neuron simulations; and, to avoid exhaustive parameter testing, we first show analytical results in which we use the method of time averaging to replace spike trains with average firing-rates (Ermentrout, 1994, 1998; Shriki et al., 2003). This approximation is valid as long as neurons operate over a range of firing rates in which

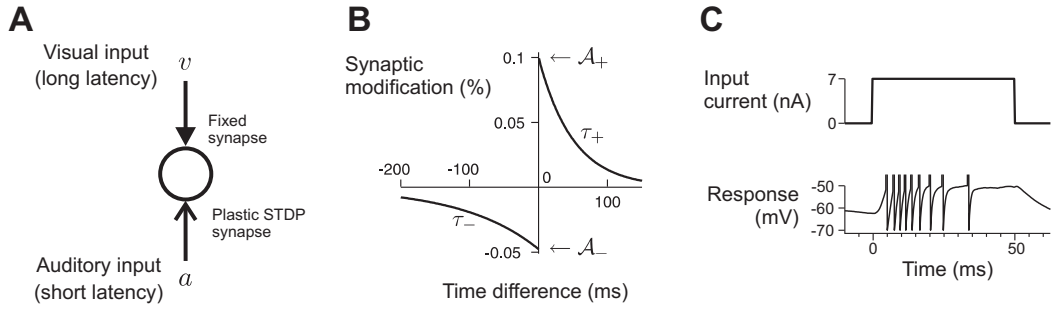

Figure 2.1: A single-neuron model for instructive coding. (**A**) The neuron (*circle*) receives auditory input, a, of short latency and visual input, v, of longer latency. (**B**) The auditory-input synapse is subject to STDP, i.e., it strengthens when the neuron fires action potentials after presynaptic spikes (positive time difference) and weakens in the contrary case. The STDP pairing function shown has exponential tails. τ_+=50 ms, τ_-=110 ms. (**C**) The conductance-based integrate-and-fire neuron exhibits SFA, illustrated by its response to a 50 ms step input. The spike rate in response to the onset of the step input is high, but then quickly adapts.

the slopes of their F-I curves do not change much (details are given later, in Sec. 2.6).

2.2 SFA can encode an implicit error signal

First we examine the effects of SFA on bimodal neural responses. We stimulate the neuron with auditory and visual stimuli that are step functions of duration T. To model the slower visual pathway, visual inputs, v, have a fixed onset lag of $T_{\text{lat}} = 70$ ms, corresponding to estimates in the barn owl from the work of Gutfreund et al. (2002); Gutfreund & Knudsen (2006). When driven by auditory or visual input in isolation, the neuron exhibits a transient response that adapts within a few milliseconds (Figure 2.1C). When both inputs are simultaneously presented, however, the adaptation elicited by early auditory responses persists and leads to suppression of subsequent visual responses, Figure 2.2A.

Mathematically, this interaction of bimodal responses can be expressed in terms of scalars, A and V, representing auditory and visual responses. The auditory response A is the average firing rate of the neuron in the time interval $[0, T]$ and the visual response V is the average firing rate in $[T_{\text{lat}}, T + T_{\text{lat}}]$. For short stimuli $T \leq T_{\text{lat}}$ there is no temporal overlap between auditory and visual responses, allowing us to unambiguously describe our findings in terms of A and V.

Assuming a non-adapted state at stimulus onset, A is purely a function of auditory input current I_A. In contrast, V depends not only on the visual-input current I_V but also on A

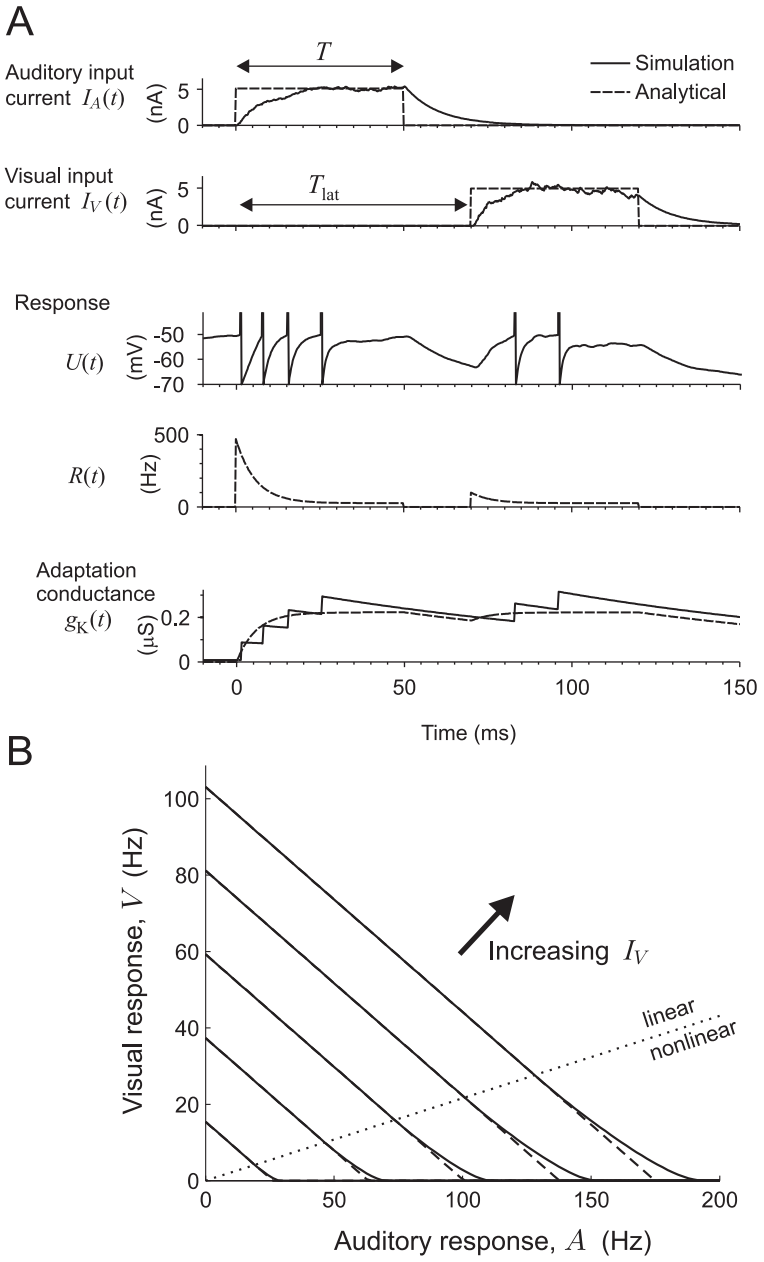

Figure 2.2: Under SFA, visual responses V to a multimodal stimulus report the alignment of preceding auditory responses A. (**A**) *Top*: The auditory and visual input currents I_A and I_V (solid lines) are approximated as step functions of duration T (dashed lines). T_{lat}: visual latency. *Middle*: The firing rate $R(t)$ adapts during the auditory input and leads to reduced firing during the equally strong visual input. $U(t)$: membrane potential. *Bottom*: The fast buildup and slow decay of the adaptation conductance g_K. (**B**) The visual response V is a linear decreasing function of the auditory response A. The different curves correspond to visual input current (I_V) varying from 0.95 nA to 6.35 nA in 1.35 nA increments along the direction of the arrow. This analytical relationship between A and V (Eq. (2.1)) is linear for large I_V. The linear relationship is also a good approximation outside this bound (the bound of the linear range in Eq. (2.2) is indicated by the dotted line and the extrapolation of the linear relationships by the dashed lines).

due to preceding adaptation. Our calculation shows that V is a linear function of both I_V and A:

$$\boxed{V = c_0 + c_1 I_V - c_2 A}, \tag{2.1}$$

where c_0 to c_2 are constants set by cellular and synaptic properties (details in *Analytical Derivation*, Sec. 2.6).

The linear relationship in Eq. (2.1) is exact under the condition that I_V is large enough to override the adaptation current and to drive spike responses in the cell. Expressed in terms of V and A, the range of validity of Eq. (2.1) becomes:

$$V \geq c_3 A, \tag{2.2}$$

where c_3 is a constant that depends on cellular/synaptic parameters (details in *Analytical Derivation*, Sec. 2.6). Note that the condition in Inequality (2.2) is violated whenever A is large or I_V is small, in which case the response V might be either delayed by more than T_{lat} or completely suppressed, implying a non-linear relationship between V, A, and I_V. Nevertheless, even in this nonlinear regime we found the linear relation Eq. (2.1) to be a good approximation of the response behavior of the cell, Figure 2.2B.

In the next section, we show that under the influence of STDP, this antagonism of auditory and visual responses leads to potentiation or depression of auditory input synapses in such a way that converges to a term proportional to I_V (assuming c_0 is small), which is the condition of alignment of auditory responses with visual inputs.

2.3 Interplay between SFA and STDP leads to the delta learning-rule

We endowed auditory synapses with a standard form of Hebbian STDP. According to the STDP rule, the joint occurrence of a presynaptic spike at time t_j and a postsynaptic spike at time t_i leads to a change in synaptic conductance, Δg, that depends solely on the time interval $\Delta t = t_i - t_j$:

$$\Delta g = g_{\max} W(\Delta t), \tag{2.3}$$

where the function $W(\Delta t)$ is the STDP pairing function (Figure 2.1B), and $g_{\max}$ is the upper limit of synaptic conductance. We chose a negative net area under the STDP pairing function, thereby imposing a tendency of the auditory synaptic strength to depress (Song et al., 2000).

To explore the interplay between SFA and STDP, we set the initial synaptic conductance of auditory afferents to zero ($g^A = 0$) and repeatedly stimulated the neuron with step-like auditory and visual inputs of fixed strengths and duration T. The inter-stimulus intervals were long, such that the adaptation conductance decayed to zero between stimulus repetitions. Initially, the neuron responded only to visual inputs but not to auditory inputs ($A = 0$). As the auditory afferents carried spikes just before the visual response, the auditory synapses started to strengthen, because afferent auditory spikes were followed by visually elicited spikes, Figure 2.3A. With further strengthening of the auditory synapses, auditory responses started to appear. Once the neuron displayed robust auditory responses, the visual responses started to decline due to SFA. This decline in turn reduced the amount of synaptic potentiation, as now afferent auditory spikes were followed by fewer postsynaptic spikes. In addition, because adaptation shortened auditory responses relative to the afferent drive, there were many auditory afferent spikes that were not followed by postsynaptic spikes, imparting an additional depressing tendency in the synapse (Figure 2.3B). In combination, there existed a balanced regime in which the synaptic depression induced by transient auditory responses equaled the potentiation induced by delayed visual responses, Figures 2.3C and D. This balanced regime did not depend on the initial synaptic conductance and was also reached when the initial conductance was set to $g_{\max}$ instead of zero.

To calculate the synaptic weight change as a function of all parameters in the model, we replaced the spike trains under the STDP pairing function with the neuron's firing rate function $R(t)$, which represents the time-dependent spike probability (Poisson spike trains). To make these calculations tractable, we assumed that the synaptic strengths are not close to their lower or upper limits and we simply summed over multiple spike pairs inside a given pairing window. Under these conditions, the total conductance change Δg associated with one stimulus presentation becomes the integral

$$\Delta g = g_{\max} \int_{-\infty}^{\infty} W(t')\gamma(t')\mathrm{d}t', \tag{2.4}$$

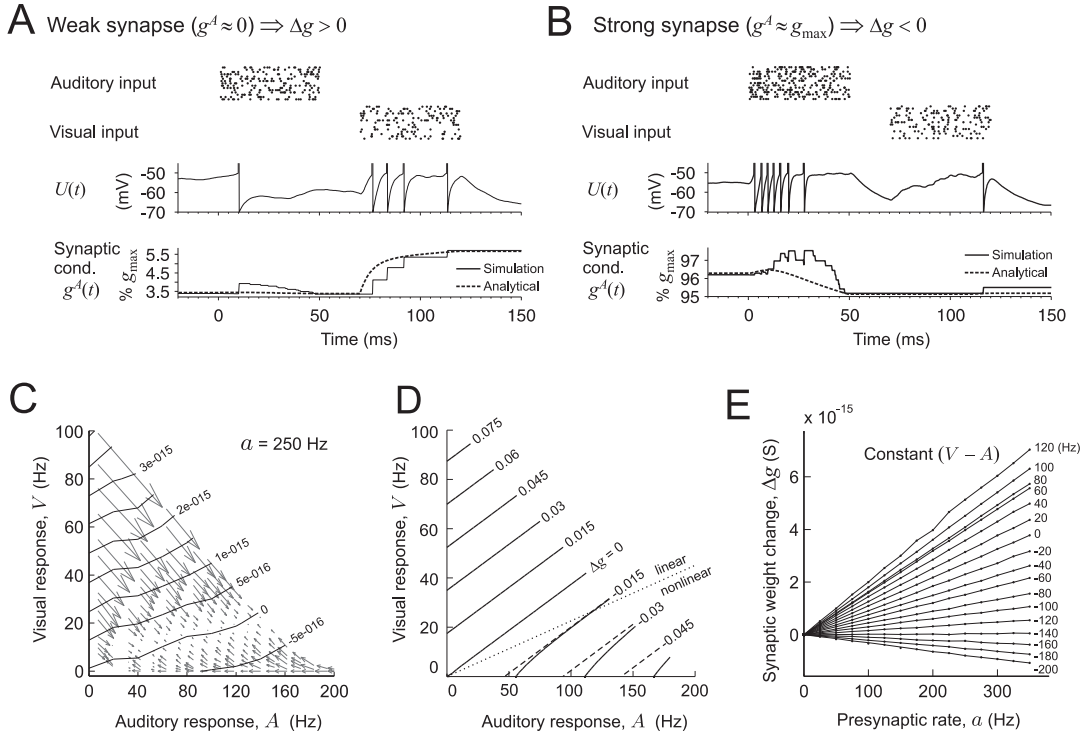

Figure 2.3: The combination of STDP and SFA implements the delta learning rule. (**A**) When afferent synapses are weak, auditory inputs do not elicit auditory responses. As a result, the neuron [with membrane potential $U(t)$] responds strongly to the visual input, thus leading to strengthening of the synaptic conductance g^A of a representative auditory synapse. (**B**) When auditory afferent synapses are strong, the neuron's firing adaptation to auditory inputs results in more post-pre spike pairings, and thus leads to depression of synaptic strength. (**C**) Simulation result of vector field illustrating the interplay between synaptic weight changes and auditory-visual responses. The lengths of the arrows are proportional to the absolute value of Δg (arbitrarily scaled units), and their directions indicate the effects Δg has on auditory responses A and visual responses V. For example, an arrow pointing to the left indicates a negative weight change (depression) with the effect of reducing A; and, an arrow pointing to the lower right indicates a positive weight change (potentiation) that increases A and decreases V. Contour lines of Δg (full lines, in increments of 5×10^{-16} S) are roughly parallel to $bV - A$, where $b = 0.143$ is a constant. Along the contour line '0', potentiation balances depression (equilibrium point). This plot was produced for fixed presynaptic firing rate $a = 250$ Hz and looked qualitatively similar for values of a in the range of 50–350 Hz. (**D**) Contour lines as in (C), but based on numerical evaluation of Eq. (2.3). The bound (Inequality (2.2)) for which the delta rule (Eq. (2.5)) is exact, is indicated by the dotted line. For small V, the extrapolation of the linear relationships in Eq. (2.5) (dashed lines) is a good approximation of the true nonlinear behavior. (**E**) Synaptic weight changes Δg depend linearly on the presynaptic firing rate a (in Hz) for different values of $[V - A]$ (spiking-neuron simulations).

where $\gamma(t') = \int_{-\infty}^{\infty} a(t)R(t+t')\mathrm{d}t$ is the cross-correlation, as a function of the time lag t', between the auditory input rate $a(t)$ and the firing rate $R(t)$.

When we evaluated Δg in Eq. (2.4) for $a(t)$ a step function with peak value a we derived the learning rule:

$$\boxed{\Delta g = g_{\max}(c_4 V - c_5 A)a}, \tag{2.5}$$

where the terms c_4 and c_5 depend on model details and are given by Eq. (2.30) (details in *Analytical Derivation*, Sec. 2.6). We further transformed Eq. (2.5) by replacing V by I_V using Eq. (2.1), to yield:

$$\boxed{\Delta g = g_{\max}(c_6 I_V - c_7 A)a}, \tag{2.6}$$

which is formally equivalent to the delta rule of the perceptron learning theory (see Eq. (1.2)). Namely, the term $(c_6 I_V - c_7 A)$ is the deviation of the auditory response A from the target rate $(c_6/c_7)I_V$ and corresponds to the postsynaptic error, and the term a is the presynaptic firing rate. Hence, mathematically, **STDP and SFA jointly prescribe synaptic weight changes that are proportional to the postsynaptic error times the presynaptic rate**. Because the delta rule corresponds to gradient descent on the square error between the neural response and the target response (Rosenblatt, 1958; Widrow & Hoff, 1960), the effect of **repeated application of the rule is to make auditory responses equal to visual inputs** (with a fixed proportionality factor between them).

Note that Eqs. (2.5) and (2.6) are valid for sufficiently large visual responses V (as specified in Inequality (2.2)). Nevertheless, numerical evaluation of Eq. (2.4) revealed that these equations remained approximately valid even in the full range $V \geq 0$, Figure 2.3D. Also, Eq. (2.5) was in good agreement with weight changes obtained in spiking-neuron simulations, Figures 2.3C and E.

2.4 Perceptron learning-rule without SFA

Under special circumstances, when $\tau_- < \tau_+$, we found that the delta or perceptron rule can also be derived for neurons without SFA. That is, in the absence of SFA ($\Delta_{g_K} \to 0$), the

constant c_5 in Eq. (2.5) simplifies to

$$c_5 = \mathcal{A}_+\tau_+ \left(T\,(B-1) + B\tau_-(e^{-T/\tau_-} - 1) - \tau_+(e^{-T/\tau_+} - 1) \right). \tag{2.7}$$

For $B \approx 1$ and $\tau_- < \tau_+$, this expression for c_5 is positive, and implies that the weight change Δg in Eq. (2.5) is negative for auditory-only inputs. This, in combination with the potentiation afforded by the later arriving visual responses ($c_4 > 0$), preserves the form of the delta learning rule in Eq. (2.5). The condition $\tau_- < \tau_+$ is crucial for this to work, because in the opposite case ($\tau_- > \tau_+$), the constant c_5 in Eq. (2.5) becomes negative, implying positive weight changes for any combination of A and V, and as a consequence the delta learning rule breaks down. However, because $\tau_- < \tau_+$ has not been reported experimentally, it remains to be seen whether this scenario is biologically relevant.

2.5 Methods

2.5.1 ICX neurons

ICX neurons are modeled as leaky integrate-and-fire neurons with the following dynamics

$$C_{\mathrm{m}}\frac{\mathrm{d}U}{\mathrm{d}t} = -I_{\mathrm{L}} + I_{\mathrm{s}} - I_{\mathrm{K}} + I_{\mathrm{b}} \tag{2.8}$$

where U is the membrane potential, $C_{\mathrm{m}} = 0.5$ nF is the membrane capacitance, $I_{\mathrm{L}} = g_{\mathrm{L}}(V - E_{\mathrm{L}})$ is the leakage current, I_{s} is the total excitatory synaptic input current from auditory (ICC) and visual (OT) afferents, I_{K} is a firing-rate adaptation current, and I_{b} is a background input current. When the membrane potential reaches a threshold of E_θ , the neuron produces an action potential, and the membrane potential is reset to E_{L}. There is no refractory period. We used a leakage conductance $g_{\mathrm{L}} = 20$ nS, a resting potential $E_{\mathrm{L}} = -70$ mV and a threshold potential $E_\theta = -50$ mV.

2.5.2 Spike-frequency adaptation

The adaptation current $I_{\mathrm{K}} = g_{\mathrm{K}}(U - E_{\mathrm{K}})$ in Eq. (2.8) models calcium–activated potassium channels, where g_{K} is the potassium conductance and $E_{\mathrm{K}} = -70$ mV is the potassium reversal potential. The conductance g_{K} is a "step-and-decay" function driven by the spike train $\rho(t)$ (sum of delta functions) of the ICX neuron,

$$\frac{\mathrm{d}g_{\mathrm{K}}}{\mathrm{d}t} + \frac{1}{\tau_{\mathrm{K}}}g_{\mathrm{K}} = \Delta_{g_{\mathrm{K}}}\rho(t) \tag{2.9}$$

with increment $\Delta_{g_{\mathrm{K}}} = 80$ nS on every ICX spike, and a decay time constant $\tau_{\mathrm{K}} = 110$ ms (see Figure 2.2A). During repetitive ICX spikes, g_{K} gradually builds up and results in a hyperpolarizing current that causes the firing rate to adapt. The decay time constant was inferred from the work of Gutfreund et al. (2002) and Gutfreund & Knudsen (2006).

2.5.3 Auditory and visual inputs

The synaptic current, I_{s}, in Eq. (2.8) onto the ICX neuron stems from populations of auditory (ICC) and visual (OT) afferents:

$$I_{\rm s} = \sum_j g_j^A s_j^A(t)(U - E_{\rm ex}) + g^V s^V(t)(U - E_{\rm ex}), \tag{2.10}$$

where $s_j^A(t)$ is the synaptic activation of the $j^{\rm th}$ ICC afferent, and $s^V(t)$ is the summed synaptic activation form a pool of OT neurons. The ICC-to-ICX connection strengths g_j^A is modified according to the STDP rule and is constrained to $0 \leq g_j^A \leq g_{\rm max}$. The OT-to-ICX connections are of fixed strength, $g^V = 3$ nS; because they convey inputs from independently firing visual neurons, we represent their synaptic activation variables by the single variable $s^V(t)$ describing the entire pool. All synapses are excitatory with reversal potential $E_{\rm ex} = 0$ mV. Synaptic activations, $s(t)$ are 'step-and-decay' functions. Each time an input spike arrives, $s(t)$ is incremented by 1. Between spikes, $s(t)$ decays exponentially to 0 according to $\tau_{\rm s}{\rm d}s/{\rm d}t = -s$, with a time constant of $\tau_{\rm s} = 10$ ms (Feldman & Knudsen, 1994).

Background input

We included a background current $I_{\rm b} = g_{\rm b}s_{\rm b}(t)(U - E_L)$ in Eq. (2.8) so as to add variability to ICX neuron's spike train. This current models spontaneous vesicle release, with $s_{\rm b}(t)$ corresponding to the synaptic activation of a hypothetical afferent that is driven by Poisson spike trains of summed mean rate 1000 Hz. we used $g_{\rm b} = 1$ nS. These parameter values were chosen so that the ICX neuron spontaneously fired at rates of about 5 Hz. This number was not critical for any of our findings as long as it was not too high and did not cause a state of permanent adaptation in the ICX neuron.

2.5.4 Spike-timing dependent plasticity

The pairing of a presynaptic ICC spike at t_j and a post synaptic ICX spike at t_i separated by a time interval $\Delta t = t_i - t_j$ leads to the modification of the corresponding synaptic conductance by

$$\Delta g_j^A = g_{\rm max} W(\Delta t), \tag{2.11}$$

where the function $W(\Delta t)$ is the STDP pairing function given by $W(\Delta t) = \mathcal{A}_+ e^{-\Delta t/\tau_+}$ for $\Delta t > 0$, and $W(\Delta t) = -\mathcal{A}_- e^{\Delta t/\tau_-}$ for $\Delta t \leq 0$. The halfwidths of the pairing function were set to $\tau_+ = 50$ ms and $\tau_- = 110$ ms, and the amount of potentiation per spike to $\mathcal{A}_+ = 0.001$. The amounts of depression per spike was chosen according to the relation

$B = \mathcal{A}_-\tau_-/\mathcal{A}_+\tau_+ = 1.05$, which implies that the net area under W is negative. Technical details of the implementation of this plasticity rule (and an explanation for the value of $\mathcal{A}_+$) are given in (Song et al., 2000).

The half-widths of the pairing function were chosen to be within the range of the correlation time of auditory and visual inputs. The value for τ_- on the order of 100 ms is typical in cortex (Feldman, 2000; Froemke & Dan, 2002), whereas measured cortical values for τ_+ tend to be smaller than 50 ms (on the order of 20 ms). However, our findings also applied to such small τ_+ values, provided that τ_- was small as well or that auditory stimuli were sufficiently far away from the animal (>10 m) to provide for pre-post spike pairing within τ_+ (see Figure 3.8).

2.5.5 ICX visual and auditory responses

Due to differences in ICX auditory and visual response latencies, we could separately read out auditory and visual responses for simultaneous presentations of nearby auditory and visual stimuli of $T = 50$ ms duration, Figures 3 and 4. ICX auditory responses A were defined by the average firing rate in a window of duration T after stimulus onset:

$$A = \frac{1}{T}\int_0^T \rho(t)\mathrm{d}t. \tag{2.12}$$

Similarly, ICX visual responses V were defined by the average firing rate in the interval $[T_{\mathrm{lat}}, T + T_{\mathrm{lat}}]$ after stimulus onset:

$$V = \frac{1}{T}\int_{T_{\mathrm{lat}}}^{T+T_{\mathrm{lat}}} \rho(t)\mathrm{d}t, \tag{2.13}$$

thereby taking into account the visual response latency, T_{lat}.

2.5.6 Computer simulations

We performed all the simulations with self-written C code that was complied to run under MATLAB (well known as 'MEX'). To numerically solve the differential equation Eq. (2.8) at each time step, we used the Runge-Kutta 4^{th} order method. (The simpler Euler's method turned out to be unstable due to the competing positive excitatory and negative adaptation/inhibiton currents on the right hand side of Eq. (2.8), making the numerical solution

"stiff"). All other differential equations are are simple 'step-and-decay' functions, and we found it sufficient to use the Euler's first order method.

We used a fixed time step of $h = 0.25$ ms for the simulations. This value of h is 40 times smaller than the smallest time constant in the model (i.e., $\tau_s = 10$ ms), and thus is a good rule-of-thumb choice for guaranteeing accurate numerical solutions. (The rule-of-thumb is $h \leq 0.1\tau_{\text{minimum}}$).

The entire source code of the simulations, written in 'C', is provided in the Appendix.

2.6 Analytical derivation of the perceptron learning rule

The perceptron learning rule in Eq. (2.5) is a generic consequence of the interplay between adaptation and STDP and does not depend on model details. In fact, it can be analytically derived by simplifying the conductance-based model equations into rate-based equations using the method of time-averaging and simplifying Poissonian assumptions (Kempter et al., 1999; Drew & Abbott, 2006). For simplicity, we consider only auditory-visual stimuli of duration T smaller than the visual latency ($T \leq T_{\rm lat}$), Figure 2.2A. This means that ICX auditory (A) and visual (V) responses do not temporally overlap and can be unambiguously read out. We first analytically derive the relationship $V = c_0 + c_1 I_V - c_2 A$ in Eq. (2.1) due to SFA, after which we derive the delta learning rule $\Delta g = g_{\max}\,(c_4 V - c_5 A)\,a$ in Eq. (2.5). We assume $E_{\rm K} = E_{\rm L}$.

2.6.1 The derivation of $V = c_0 + c_1 I_V - c_2 A$

The method of time averaging consists of replacing the neuron's spike train, $\rho(t)$, in Eq. (2.9) by the average firing rate $R(\cdot)$, which is a good approximation, provided that the time scale of spike-frequency adaptation ($\tau_{\rm K} = 110$ ms) is much longer than the membrane time constant (given by $C_{\rm m}/g_{\rm L} = 25$ ms). For integrate-and-fire neurons (Eq. (2.8)), this firing rate function $R(\cdot)$ takes the well-known form

$$\rho(t) \leftarrow R(G, I) = \frac{G}{C_{\rm m}} \left[\log\left(1 + \frac{G(E_\theta - E_{\rm L})}{I}\right)\right]^{-1}, \qquad I \geq 0, \tag{2.14}$$

where $G = g_{\rm L} + g_{\rm K}$ is the total conductance; and

$$I = g_{\rm L}(E_{\rm L} - E_\theta) + g_{\rm K}(E_{\rm K} - E_\theta) + I_{\rm s} \tag{2.15}$$

is the total membrane current; and $I_{\rm s} = I_V + I_A$ is the sum of synaptic input currents from the visual and from the auditory inputs (Eq. (2.10)). We approximate this nonlinear expression for the firing rate by the standard threshold-linear function

$$R(I) = \begin{cases} \dfrac{I}{C_{\rm m}(E_\theta - E_{\rm L})}\,, & \text{for } I \geq 0, \\ 0, \qquad \text{otherwise.} \end{cases} \tag{2.16}$$

Note that Eq. (2.16) is a good approximation of Eq. (2.14) for $I \gg G(E_\theta - E_\mathrm{L})$, which can be seen using $\log(1+x) \approx x$ for small x. (Figure B.1 in the Appendix illustrates this approximation).

With this simplification, Eq. (2.9) is a first order linear differential equation in $g_\mathrm{K}(t)$ that can be easily solved in the four cases, shown in Figure 2.4, depending on whether auditory or visual inputs are present. We define $g_0 = g_\mathrm{K}(0)$ as the initial value of $g_\mathrm{K}(t)$ at the onset of the case. In cases II and IV (where no inputs are present), $g_\mathrm{K}(t)$ exponentially decays to zero, that is, $g_\mathrm{K}(t) = g_0 e^{-t/\tau_\mathrm{K}}$, where time t is relative to the onset of the corresponding case. In cases I (where auditory inputs are present) and III (where visual inputs are present) $g_\mathrm{K}(t)$ converges exponentially to a nonzero value:

$$g_\mathrm{K}(t) = \begin{cases} \left(\dfrac{I_\mathrm{s}}{E_\theta - E_\mathrm{L}} - g_\mathrm{L}\right)\dfrac{\tau_\mathrm{eff}}{\tau_1}\left(1 - e^{-\frac{t-t_0}{\tau_\mathrm{eff}}}\right) + g_0 e^{-\frac{t_0}{\tau_\mathrm{K}}} e^{-\frac{t-t_0}{\tau_\mathrm{eff}}}, & \text{for } t \geq t_0 \\ g_0 e^{-t/\tau_\mathrm{K}}, & \text{otherwise.} \end{cases} \tag{2.17}$$

where time t is defined as before. In Eq. (2.17), $\tau_\mathrm{eff} = (1/\tau_1 + 1/\tau_\mathrm{K})^{-1}$ is the effective rise time of the adaptation conductance (5.9 ms in our simulations), with $\tau_1 = C_\mathrm{m}/\Delta_{g_\mathrm{K}}$ (in our simulations, $\tau_1 = 6.25$ ms). And, the variable t_0 arises from the constraint $I \geq 0$ in Eq. (2.16) which can be rewritten as $I_\mathrm{s}/(E_\theta - E_\mathrm{L}) - g_\mathrm{L} \geq g_0 e^{-t_0/\tau_\mathrm{K}}$ using Eq. (2.15), to yield:

$$t_0 := \max\left(0, \tau_\mathrm{K}\left[\log(g_0) - \log\left(\frac{I_\mathrm{s}}{E_\theta - E_\mathrm{L}} - g_\mathrm{L}\right)\right]\right) \tag{2.18}$$

In summary, in Case I, $g_\mathrm{K}(t)$ starts out with initial condition $g_0^I = 0$ and the neuron starts firing immediately at the onset of the stimulus. In Case III, $g_\mathrm{K}(t)$ starts out with nonzero initial value $g_0^{III} > 0$ and the neuron starts firing a delay t_0 after arrival of the visual inputs. As can be seen in Figure 2.4C, t_0 is nonzero if the firing has strongly adapted during the presence of the auditory input (if the initial adaptation conductance g_0^{III} is high).

Having derived expressions for the time evolution of $g_\mathrm{K}(t)$ in the four cases, we can now obtain the expression for the time course of the average firing rate of the neuron. When we substitute the expression for $g_\mathrm{K}(t)$ in Eq. (2.17) into Eqs. (2.15) and (2.16), we can solve for the firing rates R^I and R^{III} in cases I and III

$$R^{I/III}(t) = \begin{cases} \frac{1}{C_{\rm m}}\left[\left(\frac{I_{\rm s}}{E_\theta - E_{\rm L}} - g_{\rm L}\right)\left[\frac{\tau_{\rm eff}}{\tau_{\rm K}} + \frac{\tau_{\rm eff}}{\tau_1}e^{-\frac{t-t_0}{\tau_{\rm eff}}}\right] - g_0 e^{-\frac{t_0}{\tau_{\rm K}}}e^{-\frac{t-t_0}{\tau_{\rm eff}}}\right], & \text{for } t \geq t_0 \\ 0, \quad \text{otherwise} \end{cases} \tag{2.19}$$

and for the firing rates in cases II and IV, $R^{II/IV}(t) = 0$.

For a stimulus duration of T, we have defined the auditory response $A = \langle R^I(t)\rangle$ as the average response in case I,

$$A = \frac{1}{T}\int_0^T R^I(t){\rm d}t \approx \frac{\tilde{I}_A}{C_{\rm m}E_\delta}\left[\frac{\tau_{\rm eff}}{\tau_{\rm K}} + \frac{\tau_{\rm eff}^2}{\tau_1 T}\right] \tag{2.20}$$

where we have defined $\tilde{I}_A = I_A - g_{\rm L}E_\delta$ as the effective synaptic input current from the auditory input synapses and $E_\delta = E_\theta - E_{\rm L}$. We have reached the approximation in Eq. (2.20) by ignoring terms such as $e^{-T/\tau_{\rm eff}}$ since for a stimulus of duration, say $T = 50$ ms, T is much greater than $\tau_{\rm eff}$ (5.9 ms). This assumption ($T \gg \tau_{\rm eff}$) is not crucial for any calculations/estimations performed here. The sole reason for making this assumption is that it simplifies the expressions to follow.

The expression for visual response $V = \langle R^{III}(t)\rangle$ is the average response in case III

$$\begin{aligned} V &= \frac{1}{T}\int_0^{T-t_0} R^{III}(t){\rm d}t = \frac{\tilde{I}_V}{C_{\rm m}E_\delta}\left[\frac{\tau_{\rm eff}}{\tau_{\rm K}T}t - \frac{\tau_{\rm eff}^2}{\tau_1 T}e^{-\frac{t}{\tau_{\rm eff}}}\right] + \frac{g_0^{III}}{C_{\rm m}}\frac{\tau_{\rm eff}}{T}e^{-\frac{t_0}{\tau_{\rm K}}}e^{-\frac{t}{\tau_{\rm eff}}}\Bigg|_0^{T-t_0} \\ &= \frac{\tilde{I}_V}{C_{\rm m}E_\delta}\left[\frac{\tau_{\rm eff}(T-t_0)}{\tau_{\rm K}T} + \frac{\tau_{\rm eff}^2}{\tau_1 T}\right] - \frac{\tilde{I}_V}{C_{\rm m}E_\delta}\frac{\tau_{\rm eff}^2}{\tau_1 T}e^{\frac{-T+t_0}{\tau_{\rm eff}}} - \frac{g_0^{III}}{C_{\rm m}}\frac{\tau_{\rm eff}}{T}e^{-\frac{t_0}{\tau_{\rm K}}}\left(1 - e^{\frac{-T+t_0}{\tau_{\rm eff}}}\right) \end{aligned} \tag{2.21}$$

where $\tilde{I}_V = I_V - g_{\rm L}E_\delta$ is the effective visual input synaptic current, and

$$g_0^{III} = g_0^{II}e^{-\frac{T_{\rm lat}-T}{\tau_{\rm K}}} = \frac{\tau_{\rm eff}}{\tau_1}\frac{\tilde{I}_A}{E_\delta}e^{-\frac{T_{\rm lat}-T}{\tau_{\rm K}}} \tag{2.22}$$

is the initial value of $g_{\rm K}(t)$ in region III. Eq. (2.21) shows that V depends directly on A via g_0^{III} through Eqs. (2.20) and (2.22), but V also depends indirectly on A via t_0 which depends on g_0^{III} in Eq. (2.18). The indirect dependence via t_0 drops out if visual inputs are larger than some threshold value $\tilde{I}_\theta$ set by the adaptation conductance at the onset of the

visual input:

$$\tilde{I}_V \geq \tilde{I}_\theta = g_0^{III} E_\delta = \frac{\tau_{\text{eff}}}{\tau_1} \tilde{I}_A e^{\frac{T - T_{\text{lat}}}{\tau_{\text{K}}}}, \tag{2.23}$$

in which case $t_0 = 0$ according to Eq. (2.18) (see also Figure 2.4B). With only the direct dependence on A remaining, the expression for V in Eq. (2.21) is simplified, yielding a linear relationship between the neuron's auditory and visual responses as a function of visual input current I_V:

$$V = c_0 + c_1 I_V - c_2 A, \quad \text{valid for } \tilde{I}_V \geq \tilde{I}_\theta, \tag{2.24}$$

where the constants c_0–c_2 as given by:

$$c_0 = -\frac{c g_{\text{L}}}{C_{\text{m}}}, \quad c_1 = \frac{c}{C_{\text{m}}(E_\theta - E_{\text{L}})}, \quad \text{and} \quad c_2 = \frac{\tau_{\text{eff}}^2}{c \tau_1 T} e^{-\frac{T_{\text{lat}} - T}{\tau_{\text{K}}}}, \tag{2.25}$$

with $1/\tau_{\text{eff}} = 1/\tau_1 + 1/\tau_{\text{K}}$, $\tau_1 = C_{\text{m}}/\Delta_{g_{\text{K}}}$, and $c = \tau_{\text{eff}}/\tau_{\text{K}} + \tau_{\text{eff}}^2/\tau_1 T$. Note that although we have assumed $T \gg \tau_{\text{eff}}$ to derive Eq. (2.24), a linear relationship between V and A still applies even if this assumption is dropped (not shown).

For a neuron that recovers fast from adaptation ($\tau_{\text{K}} \to 0$), Eq. (2.24) tells us that V becomes independent of A, in agreement with the intuition that for fast adaptation, the neuron should behave as a non-adapting neuron (for $\tau_{\text{K}} \to 0$, the boundary in Eq. (2.27) disappears, $V \geq 0$).

We can also express V in Eq. (2.24) directly in terms of the visual input firing rate, v, instead of the visual input current, I_V, thus expressing the adaptation rule (and the delta learning-rule) entirely in terms of input and output firing rates. (See Eq. (3.1) and Figure 3.2E in Chapter 3). To do this, we realized that for $\tau_{\text{s}} \ll T$ we can simply replace the net synaptic activation, $s^V(t)$, in Eq. (2.10) by a step function; and consequently the visual input current, I_V, in Eq. (2.10) also becomes a step function that is proportional (to first approximation) to the total visual firing rate:

$$I_V = -\langle U \rangle g^V \tau_{\text{s}} N v \tag{2.26}$$

where $\langle U \rangle$ is the average membrane voltage of the neuron and N is the total number of

neurons in the visual input pool. (We assumed the average membrane potential $\langle U \rangle$ in Eq. (2.26) simply to be the midpoint between E_{L} and E_θ).

In summary, the linear relationship in Eq. (2.24) is valid if visual input currents are large, that is, $\tilde{I}_V \geq \tilde{I}_\theta$.

2.6.2 Derivation of $V \geq c_3 A$ as the range of linear behaviour

For $\tilde{I}_V \geq \tilde{I}_\theta$ (Eq. (2.23)), we showed that the neuron immediately responds to the visual input in spite of its adapted state (i.e., $t_0 = 0$), in which case the integral for V in Eq. (2.21) is straightforward to compute and leads to a linear relationship between V and A. We can reformulate the condition $\tilde{I}_V \geq \tilde{I}_\theta$ in terms of V and A using Eqs. (2.20), (2.23) and (2.24), to obtain the Inequality in Eq. (2.2), with the constant c_3 given by:

$$c_3 = \left(\frac{\tau_{\mathrm{eff}}}{\tau_1} - \frac{\tau_{\mathrm{eff}}^2}{c\tau_1 T} \right) e^{-\frac{T_{\mathrm{lat}} - T}{\tau_{\mathrm{K}}}}. \tag{2.27}$$

2.6.3 The linear relationship is a good approximation also for small V

We found that the linear relationship in Eq. (2.24) is also a good approximation for small visual inputs, $\tilde{I}_V < \tilde{I}_\theta$ (or equivalently, $V < c_3 A$). To see this, we compare the intercepts on the x-axis (i.e., $V = 0$) of the exact expression for V in Eq. (2.21) and the linear extrapolation of Eq. (2.24) in Figure 2.2. The relative difference between the intercept of the exact solution [by setting $t_0 = T$ in Eq. (2.21)] and the approximate intercept A_{approx} (linear extrapolation of Eq. (2.24)) satisfies:

$$\frac{A - A_{\mathrm{approx}}}{A} = 1 - \left[\frac{\tau_{\mathrm{eff}}}{\tau_1} + \frac{T}{\tau_{\mathrm{K}}} \right] e^{-\frac{T}{\tau_{\mathrm{K}}}}, \qquad \text{for } V = 0. \tag{2.28}$$

For $T = 50$ ms, this deviation is only 11.2 %.

2.6.4 The derivation of $\Delta g = g_{\max} \left(c_4 V - c_5 A \right) a$

To compute the correlation function $\gamma(t')$ in Eq. (2.4) we assume that $a(t)$ is a step function: $a(t) = a$ for $0 \leq t \leq T$, and $a(t) = 0$ elsewhere. To simplify the calculation, for now we assume large visual inputs $\tilde{I}_V \geq I_\theta$ (Eq. (2.23)), from which it follows that $R(t)$ is given by Eq. (2.19) for $t_0 = 0$. Thus, in the equation for $\gamma(t') = \int_{-\infty}^{\infty} a(t) R(t + t') \mathrm{d}t$, the integrand

is a sum of constants and exponentials in time t, yielding:

$$\gamma(t') = \frac{a}{C_{\rm m}E_\delta}\sum\begin{cases}
\tilde{I}_A\Big[\frac{\tau_{\rm eff}}{\tau_{\rm K}}(T+t') + \frac{\tau_{\rm eff}^2}{\tau_1}\Big(1-e^{-\frac{T+t'}{\tau_{\rm eff}}}\Big)\Big], & \text{for } -T \le t' < 0\\
\tilde{I}_A\Big[\frac{\tau_{\rm eff}}{\tau_{\rm K}}(T-t') + \frac{\tau_{\rm eff}^2}{\tau_1}e^{-\frac{t'}{\tau_{\rm eff}}}\Big], & \text{for } 0 \le t' \le T\\
\tilde{I}_V\Big[\frac{\tau_{\rm eff}}{\tau_{\rm K}}(t'-T_{\rm lat}+T) + \frac{\tau_{\rm eff}^2}{\tau_1}\Big(1-e^{-\frac{t'-T_{\rm lat}+T}{\tau_{\rm eff}}}\Big)\Big] & \\
\quad -\tilde{I}_A e^{-\frac{T_{\rm lat}-T}{\tau_{\rm K}}}\frac{\tau_{\rm eff}^2}{\tau_1}\Big(1-e^{-\frac{t'-T_{\rm lat}+T}{\tau_{\rm eff}}}\Big), & \text{for } T_{\rm lat}-T \le t' < T_{\rm lat}\\
\tilde{I}_V\Big[\frac{\tau_{\rm eff}}{\tau_{\rm K}}(T_{\rm lat}+T-t') + \frac{\tau_{\rm eff}^2}{\tau_1}e^{-\frac{t'-T_{\rm lat}}{\tau_{\rm eff}}}\Big] & \\
\quad -\tilde{I}_A e^{-\frac{T_{\rm lat}-T}{\tau_{\rm K}}}\frac{\tau_{\rm eff}^2}{\tau_1}e^{-\frac{t'-T_{\rm lat}}{\tau_{\rm eff}}}, & \text{for } T_{\rm lat} \le t' \le T_{\rm lat}+T.
\end{cases} \tag{2.29}$$

Because $\gamma(t')$ in Eq. (2.29) is a linear function in both $\tilde{I}_A$ and $\tilde{I}_V$, which by Eqs. (2.20) and (2.24) are linear functions in A and V, we can perform the integral in Eq. (2.4) to arrive at Eq. (2.5), with the constants c_4 and c_5 given by:

$$\begin{aligned}
c_4 =& \mathcal{A}_+\frac{\tau_{\rm eff}\tau_+^2 e^{-\frac{T_{\rm lat}}{\tau_+}}}{c}\left[\frac{4\sinh^2\left(\frac{T}{2\tau_+}\right)}{\tau_{\rm K}} + \frac{\tau_{\rm eff}\left(e^{T/\tau_+}-1\right)}{\tau_1(\tau_+ + \tau_{\rm eff})}\right],\\
c_5 =& -c_2c_4 - \mathcal{A}_+\frac{\tau_{\rm eff}\tau_+}{c}\left[\frac{T(1-B)+\tau_+\left(e^{-T/\tau_+}-1\right)-B\tau_-\left(e^{-T/\tau_-}-1\right)}{\tau_{\rm K}}\right.\\
&\left.+\frac{\tau_{\rm eff}}{\tau_1}\left(\frac{\tau_{\rm eff}-\tau_+e^{-\frac{T_{\rm lat}-T}{\tau_{\rm K}}}e^{-\frac{T_{\rm lat}}{\tau_+}}\left(e^{T/\tau_+}-1\right)}{\tau_+ + \tau_{\rm eff}} - B\left(1-\frac{\tau_-e^{-T/\tau_-}}{\tau_- - \tau_{\rm eff}}\right)\right)\right].
\end{aligned} \tag{2.30}$$

The dependence of synaptic weight changes on the neuron's auditory and visual responses as specified by Eq. (2.4) is illustrated in Figure 2.5.

Detailed plots illustrating the dependence of c_4 and c_5 on various model and stimulation parameters are presented in the Appendix Figures B.4 and B.5. As can be seen is those plots, the delta learning rule is valid for a very wide range of model and stimulation parameters.

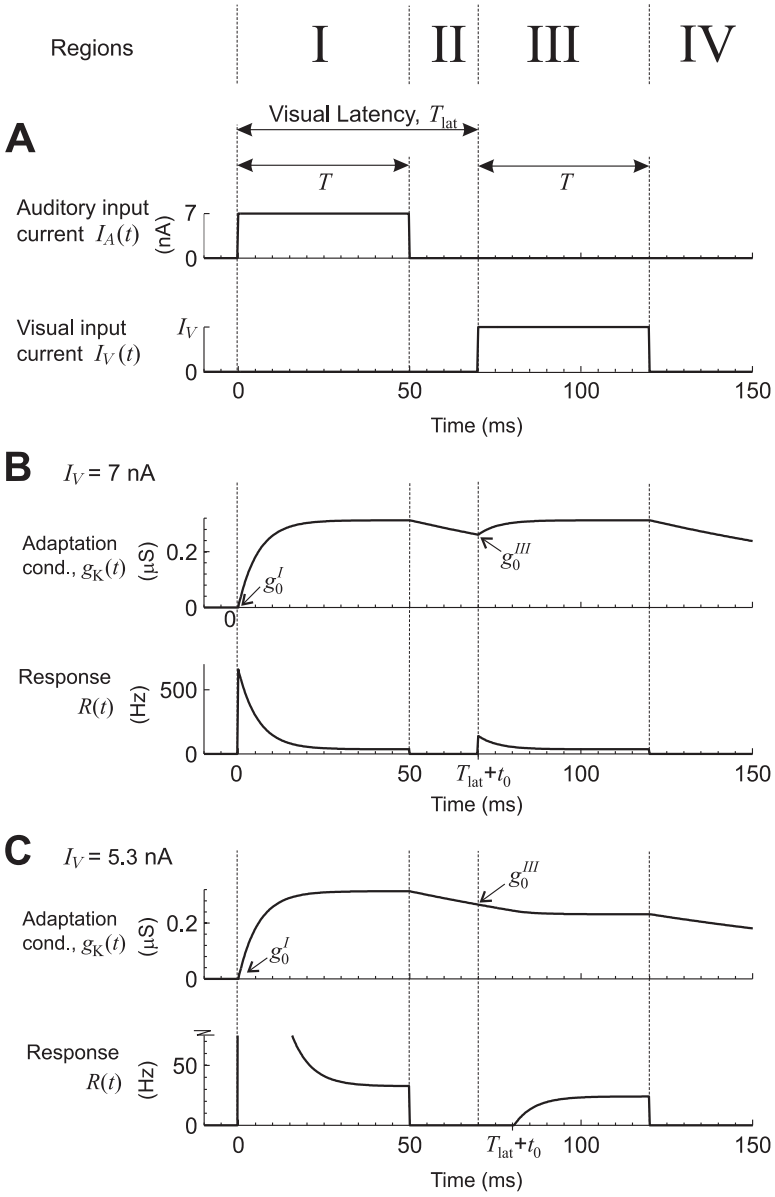

Figure 2.4: Illustrations of time-averaged model equations. Shown are two examples of adaptation currents $g_K(t)$ and the firing rate $R(t)$ of the neuron in response to an auditory-visual input. (**A**) The input currents I_A and I_V from the auditory and the visual inputs are step functions of duration $T = 50$ ms. The visual latency is $T_{lat} = 70$ ms. The four cases I-IV in which we solved the time-averaged model equations are indicated by vertical dashed lines. (**B**) Large visual input, $I_V = 7$ nA. The neuron responds immediately upon the arrival of the visual input, $R^{III}(0) > 0$ (i.e., $t_0 = 0$). (**C**) Small visual input, $I_V = 5.3$ nA. The neuron responds to the visual input with a delay $t_0 \approx 10$ ms). Note: the upper limit of the y-axis of the response plot ($R(t)$) has been clipped for the sake of clarity.

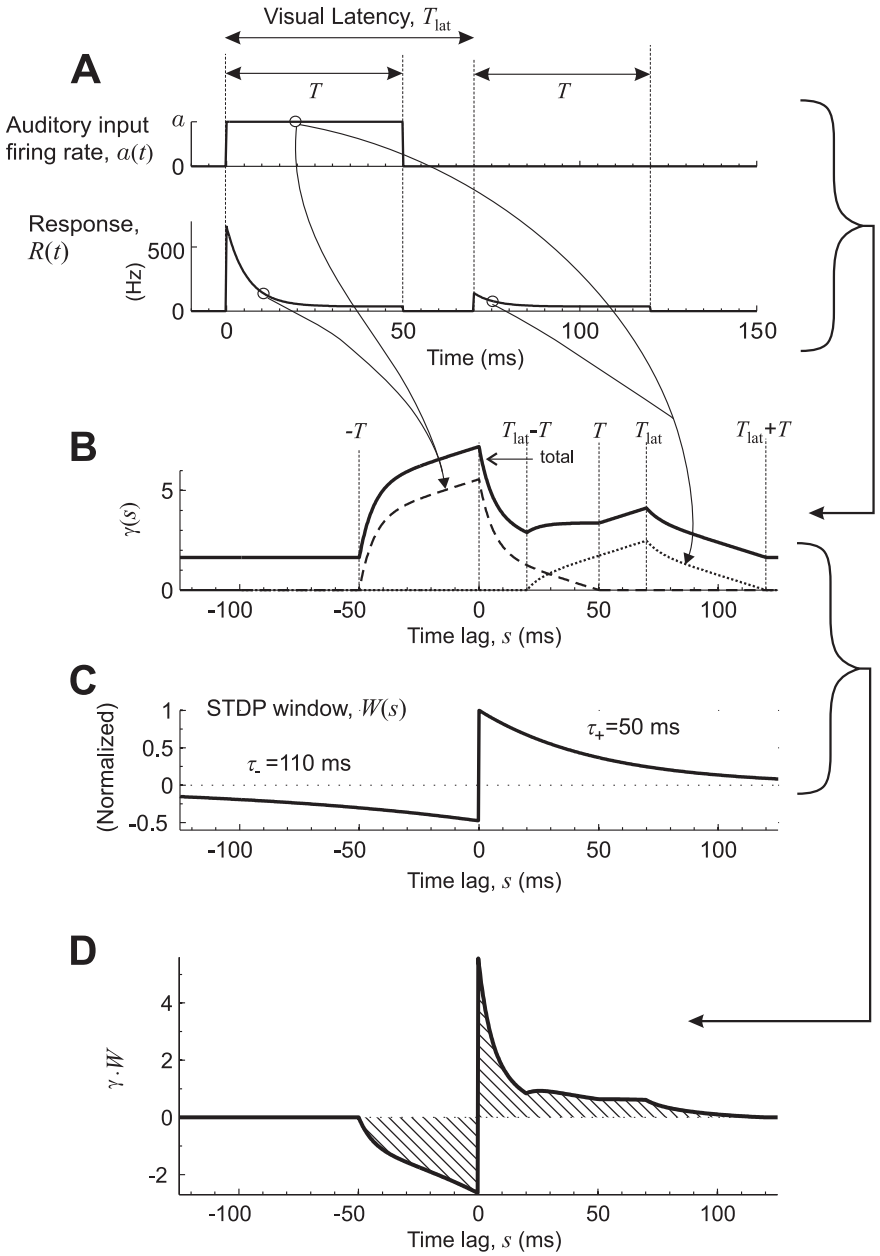

Figure 2.5: Illustration of the steps involved in computing a weight change Δg of an auditory input synapse, Eqs. (2.4), (2.5) and (2.29). (**A**) For an auditory input firing rate that is a step function of duration T and amplitude a (upper panel), the neuron's firing rate response is a combination of exponentials, (lower panel), see also Figure 2.4A, B. (**B**) Plot of the correlation function $\gamma(s)$, Eq. (2.29) (solid line, arbitrary units on y-axis). The contribution to $\gamma(s)$ from the neuron's auditory (visual) response is shown by the dashed (dotted) line. (Note: the solid line has been shifted up by an arbitrary amount for the sake of clarity.) (**C**) The STDP window function $W(s)$. (**D**) The product of the correlation function and the STDP window (arbitrary units on y-axis). The weight change Δg (Eq. (2.4)) equals the net area (shading) under this curve.

Chapter 3

Map formation in the barn owl midbrain

Having derived the perceptron learning rule in a single neuron endowed with SFA and STDP, in this chapter, we extend these results to a model ICX neuron that receives auditory and visual inputs from populations of spatially tuned and topographically laid out neurons. We first consider a normally developed ICX network in an adult barn owl and explore the effects of SFA on ICX auditory and visual responses. Then we consider an unformed ICX network in a juvenile owl and explore auditory map formation in the presence of guiding visual stimuli. We show that in such a network with spatially tuned auditory and visual inputs, the visual tuning from OT is precisely transferred onto auditory response tuning in ICX, in excellent agreement with the delta rule. In a thus-formed ICX map we evaluate map plasticity in response to shifted visual experience. We next discuss simulation results that show how map formation is affected upon varying different model parameters. Finally, we study an extended network in which we introduce ICC-to-ICX feed-forward inhibition and briefly illustrate the effects of such inhibition on map formation.

3.1 Network architecture

We model a single ICX neuron that receives excitatory inputs from populations ("pools") of auditory ICC neurons and visual OT neurons, shown in Figure 3.1. For simplicity, all neurons in a given pool have identical auditory (ICC) and visual (OT) tuning curves. The

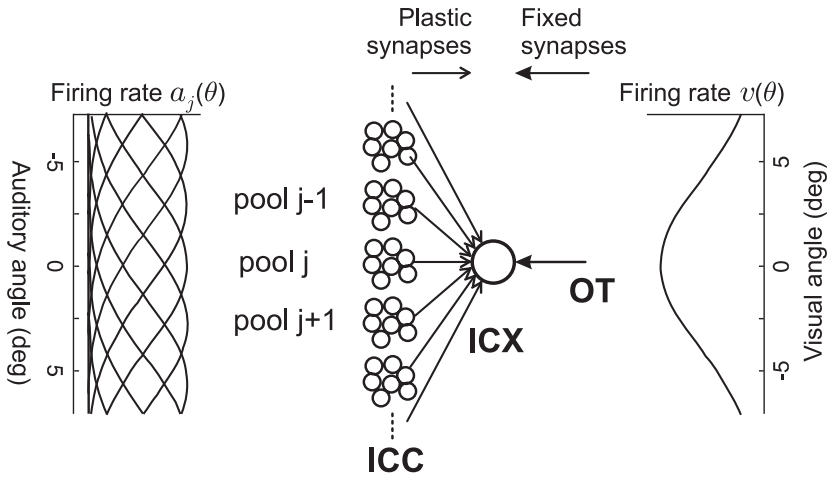

Figure 3.1: Network model for ICX map formation simulations. We model a single ICX neuron receiving auditory inputs from pools of ICC neurons relayed via plastic STDP synapses and visual inputs from pools of OT neurons relayed via synapses of fixed strengths. The auditory ICC and visual OT tuning functions $a_j(\theta)$ and $v(\theta)$ are bell-shaped. (See Methods for details).

pools are laid out topographically such that neurons in neighboring pools have adjacent preferred stimulus directions. ICC and OT neurons are modeled as Poisson spike sources with bell-shaped directional tuning curves depicted in Figure 3.1. We only modeled a single ICX neuron as a placeholder for an entire population, which is a convenient simplification under the assumption of no lateral connections among ICX neurons. To agree with typical auditory and visual response latencies in ICX neurons as observed in the experiments by Gutfreund et al. 2002 (see Figure 1.5), we set the latency of OT inputs to 70 ms. The latency of ICC auditory inputs was set to the sound travel time to reach the ears.

Note that for simplicity we have neglected the frequency dependence of ICC auditory tuning curves. We could incorporate such dependence in ICC and subsequently remove it in ICX by pooling over all sound frequencies as long as preferred ITDs in ICC line up with the preferred ITD of the ICX neuron they innervate.

The ICX neurons in the owl's midbrain do not normally display visual responses because the visual input from OT is believed to be gated by an inhibitory mechanism. However, when the inhibitory network in OT is pharmacologically blocked, visual ICX responses can be unmasked (Gutfreund et al., 2002). In all our simulations, for simplicity, we assumed that ICX neurons are always responsive to OT visual inputs (that is, that the inhibitory gate has been opened for example by the action of attentional mechanisms). We modeled SFA

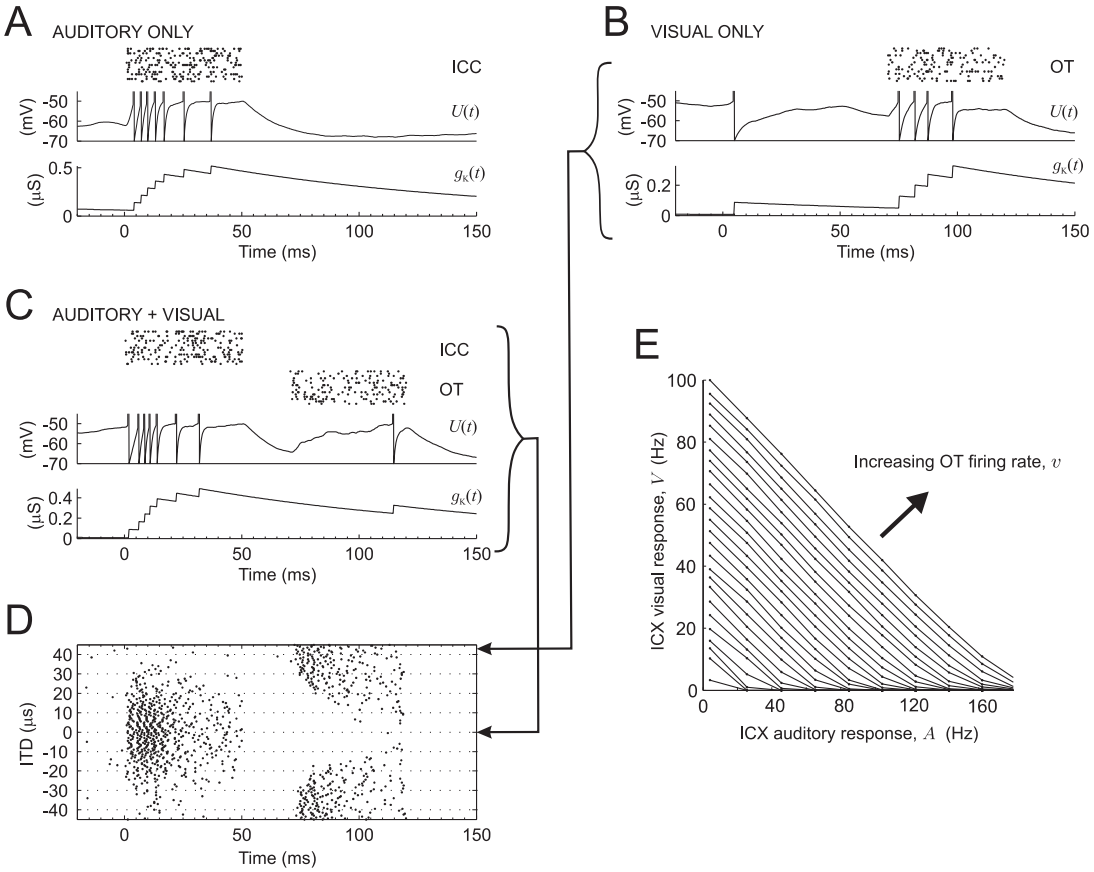

Figure 3.2: SFA and its influence on ICX visual responses. (**A**) ICX responses to a 50 ms auditory stimulus rapidly adapt. $U(t)$ is the membrane voltage and g_{K} the adaptation-related potassium conductance that increases with each ICX spike. The top panel shows a raster plot of auditory input spikes from neurons in the maximally responding ICC pool. (**B**) In response to a 50 ms visual stimulus presented in isolation (from 0 to 50 ms) there is similar firing adaptation in this ICX neuron. Note the large visual response latency in comparison to (A). The top panel shows visual input spikes in the afferent OT pool. (**C**) With simultaneous presentation of auditory and visual inputs (top panels), the ICX neuron responds mainly to the earlier-arriving auditory input but not to the later-occurring visual input. ICX visual responses are suppressed by buildup of g_{a}. (**D**) Spike-raster plot of ICX auditory-visual responses. The visual stimulus is presented in the preferred visual stimulus direction while the auditory stimulus is presented in different spatial directions (reported as ITD's in the y-axis). Visual responses (spike rasters) are only elicited when there is a mismatch in the visual and auditory stimulus directions. The special cases in (B) and (C) are indicated by arrows. (**E**) The ICX visual response, V (average firing rate in the interval 70-120 ms after stimulus onset, see Methods), is a linear decreasing function of the ICX auditory response, A. The different curves correspond to simulation results for mean OT firing rates, v, varying from 0 to 250 Hz in 10 Hz increments along the direction of the arrow.

in ICX neurons in identical terms as in Chapter 2, i.e., by an AHP potassium conductance g_{K} that transiently increases after each ICX spike, and slowly decays back to zero with a recovery time constant of 110 ms. (See Methods for simulation details).

3.2 SFA can generate an error signal

We first describe the effect of SFA on ICX auditory and visual responses in an adult owl, and to do this we preset the ICC-to-ICX synaptic strengths to that shown in Figure 3.3C which represents the equilibrium synaptic projection in a normally formed map. When excited by an auditory or visual input alone, ICX neurons displayed a transient sensory response that adapted within a few tens of milliseconds due to buildup of the adaptation conductance, g_{K}, Figure 3.2A and B. When, however, model ICX neurons are driven by simultaneous auditory and visual stimuli, the adaptation elicited by early auditory responses persists and leads to suppression of subsequent responses to the delayed visual inputs, Figure 3.2C. By keeping the visual stimulus direction fixed and sweeping the auditory stimulus over a directional range much larger than the ICX visual receptive field, suppressive priming of visual ICX responses results, shown in Figure 3.2D, that closely resembles responses found experimentally (Gutfreund et al., 2002) as shown earlier in Figure 1.5C. When we plotted the average auditory against the average visual responses, we found that the relationship between visual and auditory responses in model ICX neurons is approximately linear, Figure 3.2E. The larger the auditory responses A, the smaller are the visual responses V, in good agreement with the following formula, valid for $V > 0$

$$V = c_1' v - c_2' A, \tag{3.1}$$

where v is the average spike rate of OT afferents, and c_1', $c_2' \geq 0$ are fixed parameters that depend on model details. Thus the visual responses, $V(\theta)$, report the mismatch between the OT visual tuning, $v(\theta)$, and the ICX auditory tuning, $A(\theta)$.

3.3 ICC-to-ICX map formation in a juvenile owl

To study the development and plasticity of auditory maps, we ignored the embedding of neurons into physical space and their associated cellular and morphological growth mechanisms. We simply assumed that ICC afferents are highly divergent, allowing ICX neurons to receive auditory inputs from a total azimuthal range of about 60 degrees. We explored the formation of ICC-to-ICX synaptic connections subject to the STDP rule - synapses

potentiated when postsynaptic spikes immediately followed presynaptic spikes, and in the opposite case they depressed. The net area under the STDP pairing function was negative, thereby imposing a weak bias of synaptic strengths to depress (Song et al., 2000). From initial zero connection strengths, ICC-to-ICX synapses evolved by exposing the network to spatially matched auditory-visual stimuli presented at random locations in the environment (see Methods at the end of this chapter for details).

OT-to-ICX synapses were fixed throughout the simulation, and ICX neurons initially responded only to visual inputs, but not to auditory inputs, Figure 3.3A. As some ICC afferents carried spikes just before visual responses in given ICX neurons, these afferents started to strengthen, because presynaptic (ICC) spikes were followed by postsynaptic (ICX) visual responses (cf. Figure 2.3A in Chapter 2). Some ICC-to-ICX synapses potentiated rapidly to form a distinct bell-shaped profile. With further strengthening of these synapses, ICX auditory responses started to appear. Once ICX neurons displayed auditory responses, their visual responses declined due to SFA. This decline in turn reduced the amount of synaptic potentiation, as now presynaptic (ICC) spikes were followed by fewer postsynaptic (ICX) responses. Interestingly, the adaptation imparted an additional depressing tendency in many synapses (cf. Figure 2.3B in Chapter 2), as it shortened ICX auditory responses relative to the ICC drive, thereby leading to many presynaptic (ICC) spikes that were not followed by postsynaptic (ICX) spikes. In combination, there existed a balanced regime, Figure 3.3A bottom panel, where the synaptic depression induced by transient auditory responses equaled the potentiation induced by later visual responses.

In equilibrium, the profile of average synaptic strengths across ICC pools was bell-shaped, Figure 3.3B. Within a given ICC pool, synaptic distributions were unimodal, centered around an average value between 0 and $g_{\max}$. More extensive simulations showed that further stimulus presentations and learning led to divergence of synaptic weights towards their limiting values (see Rubin et al., 2001; Song et al., 2000, for similar findings). The time course over which bimodality of synaptic weights arose was about one thousand times slower than that of convergence of ICX auditory responses. ICX auditory tuning curves $A(\theta)$ were approximately Gaussian shaped and in register with visual tuning curves, Figure 3.3C.

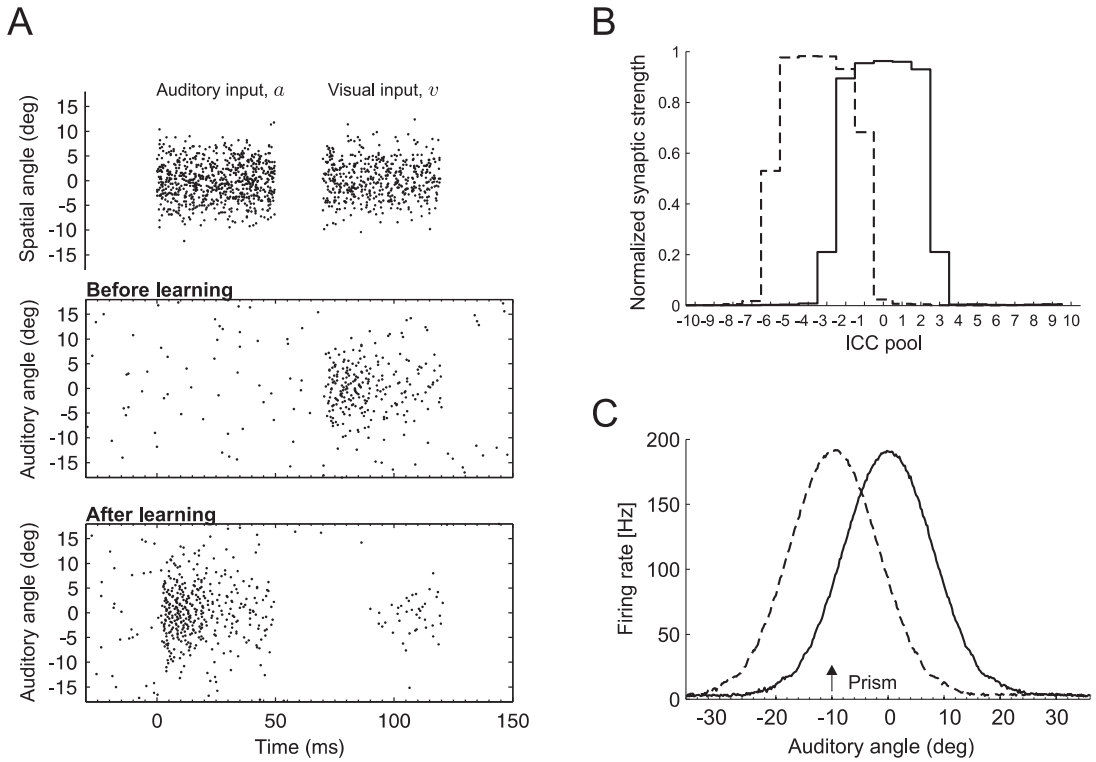

Figure 3.3: Auditory map formation in ICX. (**A**) Spike-raster plot of ICX responses to matched auditory-visual inputs, before and after learning. The auditory-visual stimuli are presented in different spatial directions (degrees, y-axis). Initially, the neuron responds only to visual inputs in a particular direction, and after learning mainly to auditory inputs in the same direction. (**B**) Equilibrium ICC-to-ICX synaptic strength profile (full line) plotted as a function of the ICC pool index and averaged over all synapses in a given pool. When visual inputs are shifted by 10°, the equilibrium profile (dashed line) is centered roughly 4 pools to the left. (**C**) Average ICX auditory receptive field after map formation in ITD coordinates relative to the preferred visual stimulus direction (full line). The average receptive field established after shifted visual experience (dashed line) is offset by an amount that matches the visual offset (indicated by the arrow labeled 'prism'). The final ICX auditory receptive field width is $\sigma^A_{\mathrm{ICX}} \approx 8°$. $\sigma^A = 6°$, $\sigma^V = 4°$.

3.3.1 Response to a shifted visual input

We next explored the network's behavior to shifted visual inputs by displacing the visual spatial map in OT by 10 degrees. In response to this shift, some ICX neurons were activated solely by early auditory inputs (auditory-only), whereas other neurons were activated solely by delayed visual inputs (visual-only). ICC synaptic inputs that matched the spatial preference of visual-only responses started to strengthen by the mechanism just described. Similarly, ICC afferents mediating strong auditory-only responses started to depress due to adaptation. The final synaptic weight profile had a similar, but displaced equilibrium profile

shown in Figure 3.3B, dashed line. Accordingly, the new ICX auditory receptive fields were in registration with the shifted visual inputs, Figure 3.3C, dashed line. (See Figure 1.4 for comparison with experimental results from barn owls).

A closer inspection revealed that during the remapping process, the peaks of ICX auditory tuning curves shifted gradually toward the registered positions, and their shapes were temporarily skewed and widened. For visual shifts exceeding 20 degrees, auditory ICX tuning curves were temporarily bimodal midway through the remapping process, with one peak near the previous preferred direction and a second peak near the new direction, as is seen experimentally in some owls (Brainard & Knudsen, 1995). Overall, we found that mapping and remapping processes were very robust, synaptic weights converged to the same equilibrium profile even from random initial distributions.

3.4 Delta learning-rule

In Chapter 2, we derived the delta learning-rule in a single neuron model driven by auditory and visual inputs that were scalar quantities. Mathematically, this rule prescribes synaptic weight changes proportional to the presynaptic firing rate multiplied by the difference between the postsynaptic rate and a target rate; and the effect of repeated application of the rule is to make postsynaptic rates equal to their target rates. By analogy with this rule, in our ICX map formation model, the postsynaptic rate corresponds to the auditory ICX response, $A(\theta)$, and the target rate to a term proportional to the ICX visual input, $v(\theta)$. Note that there is now an important difference with the model of Chapter 2 in that our ICC and OT inputs are now furnished with a spatial tuning property, and consequently, the ICX responses are also spatially dependent. So does the delta learning-rule still apply in this scenario, given that there would now be spatial and temporal correlations within the ICC firing?

We found that because SFA and STDP act locally at the synapse, the delta learning rule that thus emerges supersedes all heterosynaptic correlations that may exist, and the synaptic change Δg in response to simultaneous presentation of an auditory and a visual stimulus is indeed a linear function of the presynaptic ICC firing rate a, in exact agreement the scalar input scenario of Figure 2.3E. Similarly, for fixed a, Δg is proportional to the postsynaptic firing deviation $c_4'V - c_5'A$, as in Figure 2.3C, where c_4' and c_5' are constants

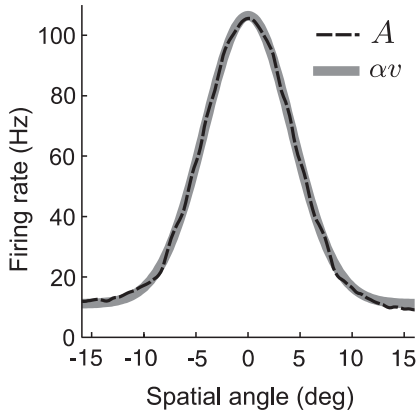

Figure 3.4: Auditory map in ICX matches visual map from OT. Equilibrium ICX auditory response tuning $A(\theta)$ (dashed line) is roughly proportional to OT tuning curves $v(\theta)$ (full line, with a suitable scaling factor α), thereby qualifying OT inputs as perceptron-like teacher signals. For making this plot, map learning was performed with fixed stimulus duration and latency, $\sigma^V = 5°$, $\sigma^A = 4°$ (see Methods for details).

that depend on model parameters (derived analytically in Chapter 2). In short notation, we have that

$$\Delta g \propto (c_4' V - c_5' A)\, a \tag{3.2}$$

According to this equation, the proportionality $A \propto V$ applies in equilibrium ($\Delta g = 0$). By inserting this relation into Eq. (3.1), it follows that equilibrium auditory responses are proportional to OT visual inputs, i.e., $A(\theta) \propto v(\theta)$. A test of this proportionality shows excellent agreement, Figure 3.4. Thus, the OT visual inputs serve as targets to which ICX auditory responses must converge over time. The error-minimization achieved by the delta learning-rule is remarkably linear as we demonstrate next.

3.4.1 Linearity of the receptive field formation

In Figure 3.3C, the equilibrium auditory responses in ICX were more broadly tuned than visual responses, because we assumed that auditory receptive fields in ICC are wider than visual receptive fields in OT,a result that qualitatively agrees well with the ICX and OT receptive field widths measured in barn owls (Knudsen, 1982). However, when we increased the width σ^V of OT receptive fields beyond that of ICC receptive-fields, we found a proportional scaling of ICX auditory response widths σ^A_{ICX}, Figure 3.5. Hence, not only the centers of ICX auditory receptive fields could be instructed by visual inputs, but also their widths. Furthermore, by varying the peak and baseline OT firing rates, we observed an approximately proportional change in the peak and baseline of equilibrium ICX auditory responses, Figure 3.6. However, peak equilibrium ICX responses were reduced when baseline firing rates in ICC were much higher than in OT, Figure 3.7.

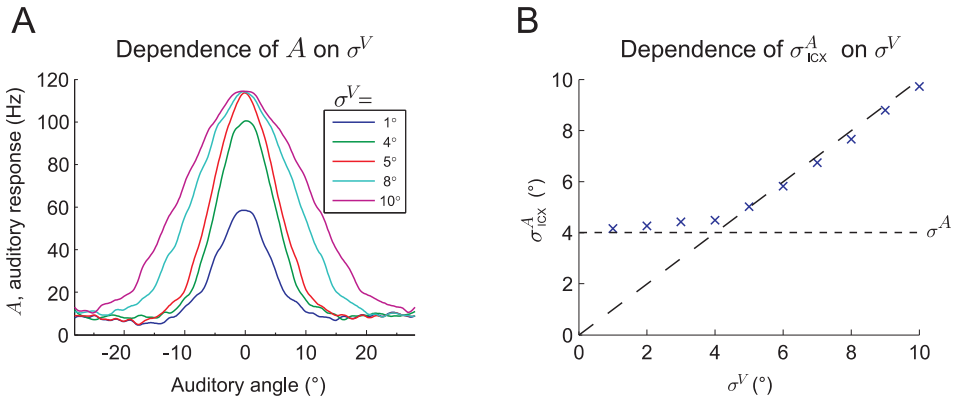

Figure 3.5: The equilibrium auditory response tuning depends on the width, σ^V, of visual inputs. (**A**) Auditory response tuning $A(\theta)$, for different values of σ^V. (**B**) The width σ^A_{ICX} of the equilibrium auditory response tuning closely follows σ^V for $\sigma^V \geq 4°$. For $\sigma^V < 4°$, σ^A_{ICX} remains roughly constant at 4°. This lower bound of σ^A_{ICX} corresponds to the tuning width of the auditory input $\sigma^A = 4°$ (dashed horizontal line): the auditory response is a weighted sum of excitatory auditory inputs, and can therefore be only as narrow as the auditory input tuning width. For these plots we used $a_{\text{peak}} = 300$ Hz, $v_{\text{peak}} = 200$ Hz, $a_{\text{base}}, v_{\text{base}} = 0$ Hz.

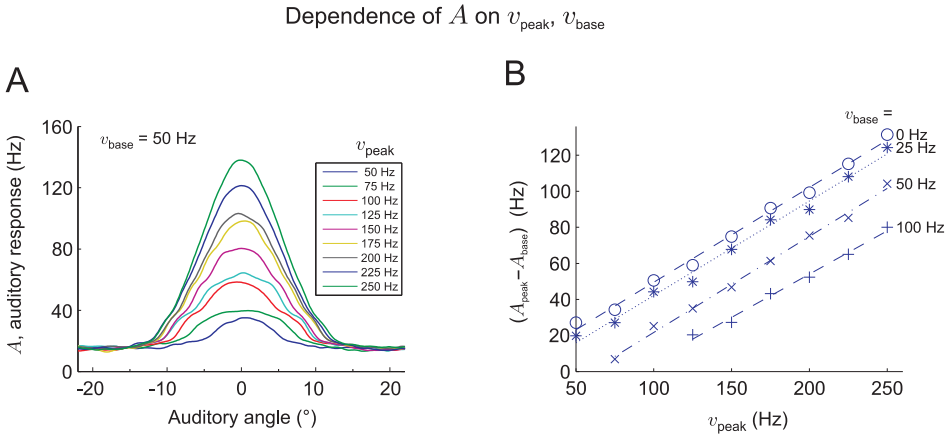

Figure 3.6: Influence of peak and baseline firing rates of the visual input (v_{peak} and v_{base}) on the equilibrium auditory response tuning. (**A**) Auditory response tuning $A(\theta)$ for different visual input peak firing rates v_{peak} (50-250 Hz). The peak of the auditory response A_{peak} increases linearly with increasing v_{peak}, whereas the response baseline remains constant. $v_{\text{base}} = 50$ Hz. (**B**) The auditory response amplitude $A_{\text{peak}} - A_{\text{base}}$ is roughly a linear function of v_{peak}. The different markers are for four different values of v_{base}. The straight lines are linear fits. The linear fits are mutually parallel, and they are equally spaced for a fixed increment of v_{base} ($v_{\text{base}} = 0$, 50, 100 Hz), in agreement with the delta rule (see Eq. (2.5)). For these plots we used $\sigma^V = 5°$, $a_{\text{peak}} = 300$ Hz, $a_{\text{base}} = 0$ Hz.

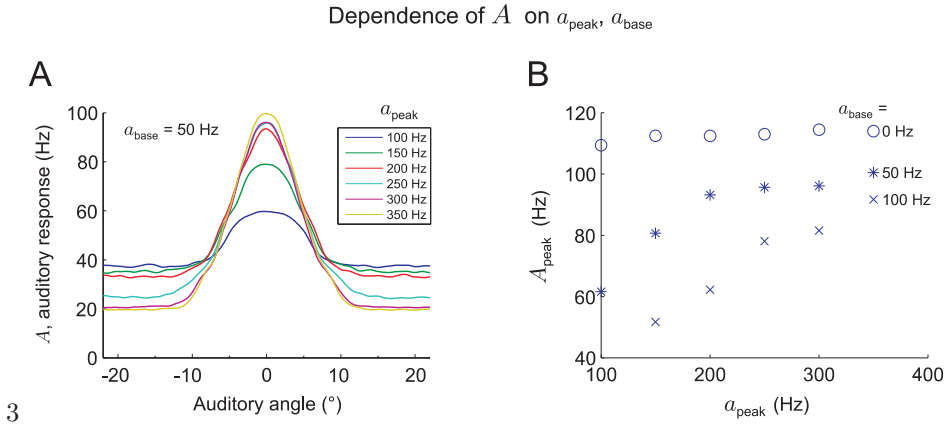

Figure 3.7: Influence of peak and baseline firing rates of the auditory input (a_{peak} and a_{base}) on auditory response tuning curves. (**A**) Peak auditory responses A_{peak} increase in parallel with a_{peak}, but at the same time baseline auditory responses decrease. The reason for this non-intuitive behavior is that the neuron's auditory responses cannot match both the peak and the baseline of the visual input, because by construction the auditory responses must be proportional to auditory inputs. $a_{\text{base}} = 50$ Hz, $v_{\text{base}} = 0$ Hz. (**B**) When auditory and visual input baseline firing rates are matched ($a_{\text{base}} = v_{\text{base}} = 0$ Hz), then the neurons' peak auditory firing rates A_{peak} are independent of a_{peak} (auditory responses perfectly match visual inputs). However, when there is mismatch between visual and auditory input baseline firing ($a_{\text{base}} = 50$ Hz and 100 Hz), synaptic weights do not grow as much, with the result that A_{peak} undershoots its target value. For these plots we used $\sigma^V = 5°$, $v_{\text{peak}} = 200$ Hz, $v_{\text{base}} = 0$ Hz.

3.4.2 Effect of varying stimulus durations and latencies

In the natural world, the stimulus durations and latencies are continuously distributed. So would the delta learning-rule still be valid in such a case? In our derivation of Chapter 2, we assumed for mathematical simplicity a fixed stimulus duration T, an auditory latency of 0 ms (distance to auditory-visual stimulus $r = 0$) and non-overlapping ICX auditory and visual responses ($T \leq T_{\text{lat}}$). However, the constants c_4' and c_5' (and implicitly c_1' and c_2') which determine the equilibrium point of the network, are also functions of the stimulus duration and latencies, for example, shown in Figure 3.8 where the stimulus duration is varied. In a distributed stimulus ensemble, the network settles at an equilibrium point that is determined by the mean value of the corresponding distributions of constants c_4' and c_5'. We found map formation in the network to be quite robust with distributed stimulus ensembles also when the stimulus ensemble included a small range of incompatible durations and latencies (where the delta rule breaks down due to unrestrained potentiation).

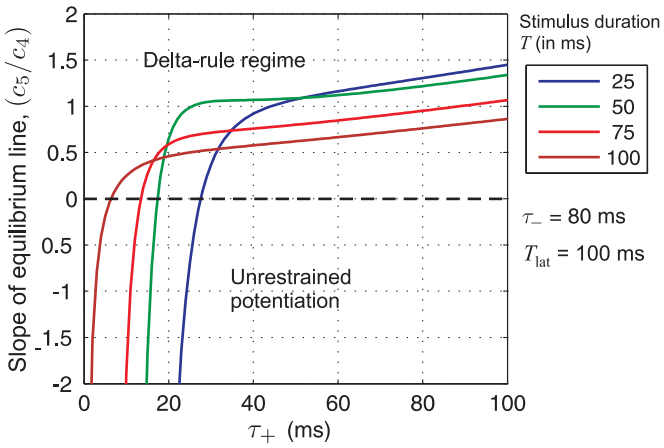

Figure 3.8: The perceptron learning rule is robust to variations in model parameters. Here we vary the length τ_+ of the STDP pairing window and the stimulus duration, T. Shown in the plots is the slope (c_5/c_4) of the equilibrium curve in Figure 2.3 for four different values of stimulus durations, T (solid lines). The perceptron learning rule holds true whenever the slope is positive (i.e. in the region above the dashed line), which is the case for $\tau_+ > 20$ ms and for even very short auditory stimulus durations. See Appendix B for a detailed characterization of the dependencies of c_1 through c_5 on the model and stimulus parameters, and more plots like this one.

3.4.3 Effect of synaptic strength saturation

The equilibrium point dictated by Eq. (3.2) assumes that the weight changes are not constrained in any manner. But it is possible that with a certain setting of model parameters and stimulus ensemble, the upper bound on synaptic strengths, $g_{\max}$, prevents the network from reaching the equilibrium point of Eq. (3.2). In such a case, increasing the number of neurons-per-pool in ICC results in a monotonic increase in the peak ICX auditory tuning, reflecting a loosened constraint on summed synaptic strengths by $g_{\max}$. However, with more than a certain number of neurons in a pool, the network reaches a state of dynamic equilibrium of Eq. (3.2), and the equilibrium ICX auditory tuning becomes independent of the number of neurons-per-pool, Figure 3.9.

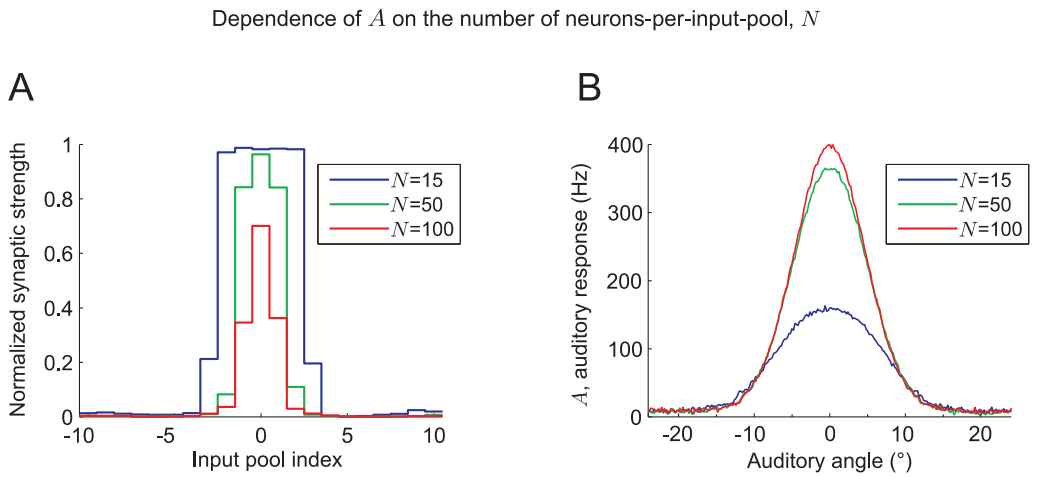

Figure 3.9: Saturation of synaptic strengths constrains the amplitude but not the width of auditory response tuning. (**A**) Normalized ICC-to-ICX synaptic strengths for three different numbers of neurons-per-pool N in ICC (N=15, 50, 100). For N=15 and 50, all synapses from the central ICC pools (pools -2 to 2 in the case of N=15, and pool 0 in the case of N=50) reach the upper bound $g_{\max}$. For N=100 the network achieves a dynamic equilibrium governed by the interplay between SFA and STDP. In this case, the mean synaptic strengths stabilizes at values below the upper bound $g_{\max}$. (**B**) ICX auditory response $A(\theta)$ for three different values of N. With increasing N, the amplitude of $A(\theta)$ increases, but not its width. Amplitude saturation is reached for $N \geq 70$. For these plots we used $\sigma^V = 5°$, $a_{\text{peak}} = 300$ Hz, $v_{\text{peak}} = 200$ Hz, $v_{\text{base}} = a_{\text{base}} = 0$ Hz, and varying stimulus durations $T \in [15, 100]$ ms, locations $\theta \in [-40°, 40°]$ and distances $r \in [0, 25]$ m, with these values drawn from uniform distributions in the given ranges.

3.5 A network with feed-forward inhibition

Anatomical and physiological experiments have long established the presence of an inhibitory network at the ICX. In its basic role, this GABAergic inhibition is known to shape the horizontal dimension of the auditory receptive fields. That is, inhibition sharpens ITD selectivity in the ICC and ICX, contributes to the elimination of phase ambiguity in the ICX, and controls response magnitude and temporal characteristics in the ICC and ICX (Fujita & Konishi, 1991). In a more advanced role, inhibition also contributes importantly to functional plasticity – in adult barn owls that are subjected to shifted visual experience, GABAergic inhibition initially masks and possibly opposes adaptive excitatory plasticity, thereby preserving the established functional properties of the network. By the end of the learning process, however, GABAergic inhibition eliminates normal responses so that ICX tuning curves shift fully, enabling the selective expression of the learned ITD map (Zheng & Knudsen, 1999, 2001; Knudsen, 2002).

In this thesis, we do not seek to model and evaluate any of the above intricate anatomical and functional details of inhibition in the ICX. But we explored what effects inhibition would have on the map formation process and specifically on the delta learning-rule in our model.

To answer these questions, we performed simulations in which we included feed-forward inhibition from the ICC to the ICX, as shown in Figure 3.10, in a simplified representation of the connectivity observed in the barn owl midbrain (Fujita & Konishi, 1991; Knudsen, 2002). The inhibition was relayed via synapses of fixed strengths and the inhibitory synaptic projection was set to be somewhat broad relative to the visual input tuning width (thus set mainly to avoid ambiguous interactions between the auditory and visual responses). The inhibitory synaptic strengths were set to values comparable to the ICC-to-ICX excitatory synaptic strengths. Shown in Figure 3.11 is an example of the inhibitory and excitatory synaptic conductances and the ICX response with inhibition included. We set the time constant of the inhibitory synapses to 80 ms, a value that is comparable to the slow component of GABAergic inhibitory synapses. The precise value of this time constant was not crucial to our findings as long as it was greater than 50 ms.

Starting from an initial zero or randomly distributed ICC-to-ICX excitatory synapses, we simulated the network with matched auditory-visual stimuli. After a period of adjustment, a precise auditory map was formed in the ICX in about the same amount of simulation time

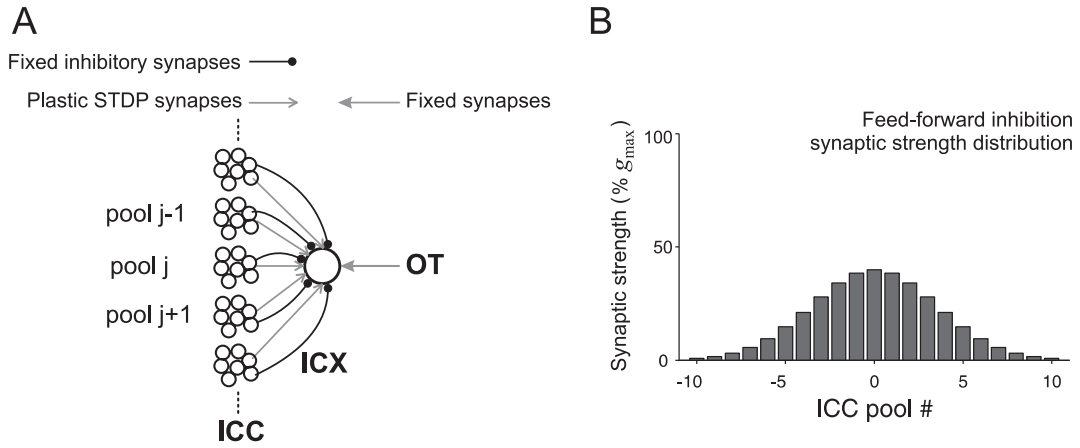

Figure 3.10: Network model for ICX map formation simulations with auditory feed-forward inhibition included. (**A**) The feed-forward inhibition is from the ICC to the ICX and is relayed through fixed inhibitory synapses. The excitatory connections are as usual - the ICX neuron receives auditory inputs from the ICC neurons and visual inputs from the OT neurons. (**B**) The connectivity profile (distribution) of the feed-forward inhibitory synapses from the ICC to the ICX.

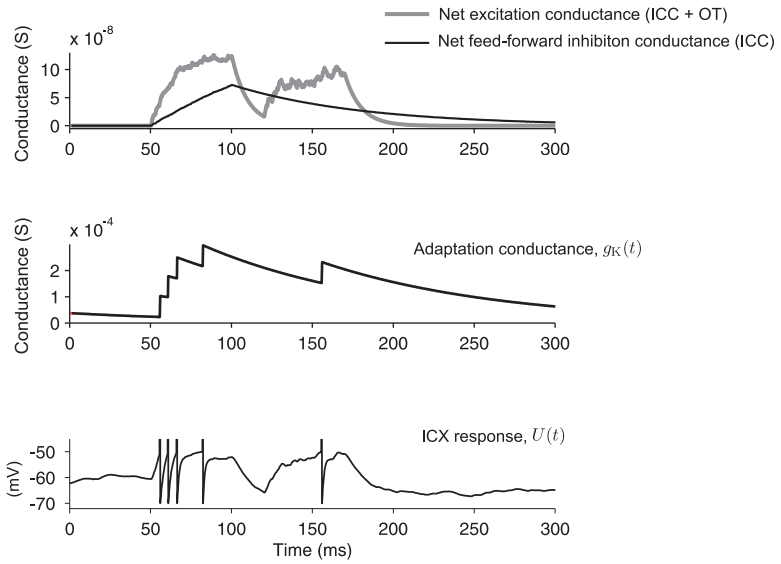

Figure 3.11: Illustration of ICX responses with feed-forward inhibition for the network shown in Figure 3.10. The *top* panel shows the net excitatory synaptic conductance (gray line) and the net feed-forward inhibition synaptic conductance (black line) in response to a 50 ms auditory-visual stimulus. The *middle* panel shows the adaptation conductance, $g_K(t)$. The *bottom* panel shows the ICX response, shown by the membrane voltage, $U(t)$.

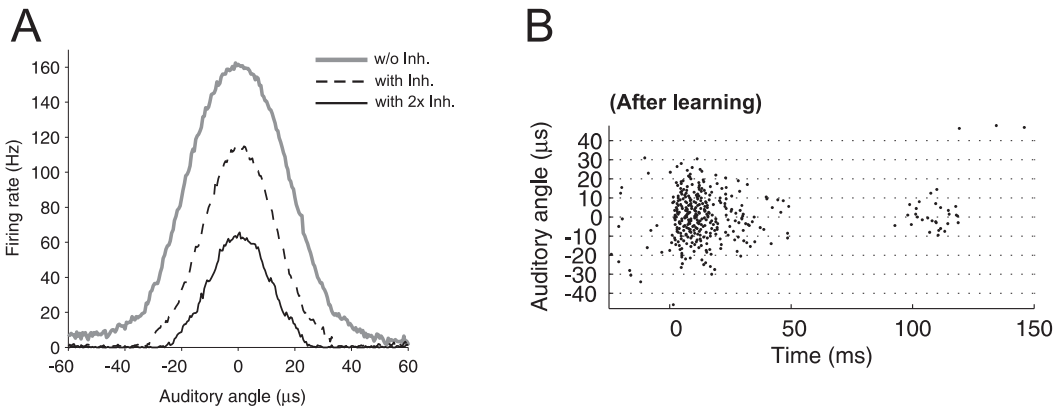

Figure 3.12: ICX auditory response tuning after learning with auditory feed-forward inhibition. (**A**) Equilibrium ICX auditory response tuning $A(\theta)$ with varying amounts of inhibition. The tuning curve amplitude is reduced (dashed line) when compared with learning without feed-forward inhibition (gray line). Doubling the conductances of the inhibitory synapses resulted in a further reduction in the tuning curve amplitude (solid line), and this reduction is approximately linear as seen by the roughly equal differences in the peaks of the tuning curves. $\sigma^A, \sigma^V = 4°$. (**B**) Spike-raster plot of ICX responses to matched auditory-visual inputs after learning. The auditory-visual stimuli of 50 ms duration are presented in different spatial directions (ITDs, y-axis).

it takes for a network without inhibition to learn. The main effect with inhibition included was a reduction in the tuning curve amplitude of the learned map. We found that increasing or decreasing the inhibitory synaptic strengths resulted in an approximately proportional change in the tuning curve amplitude, Figure 3.12.

3.5.1 Delta learning-rule with inhibition

The reason why inhibition reduces the equilibrium ICX auditory responses is not immediately apparent: Intuitively speaking, because the inhibition is relayed through fixed synapses and its time constant is long compared to T_{lat}, the main effect of feed-forward inhibition should be to reduce slightly the overall ICX activity (both auditory and visual). This would leave unchanged the relative timing and the ratio of the ICX auditory and visual responses, implying that the equilibrium point for the network should be approximately the same as without inhibition. But in simulations, we found that the equilibrium point for the network with inhibition, shown in Figure 3.13A is different from that of the network without inhibition (shown in Figure 2.3C).

The reason for this different equilibrium curve lies in the fact that the inhibition induced hyperpolarization of the ICX neuron has the effect of always delaying the ICX visual re-

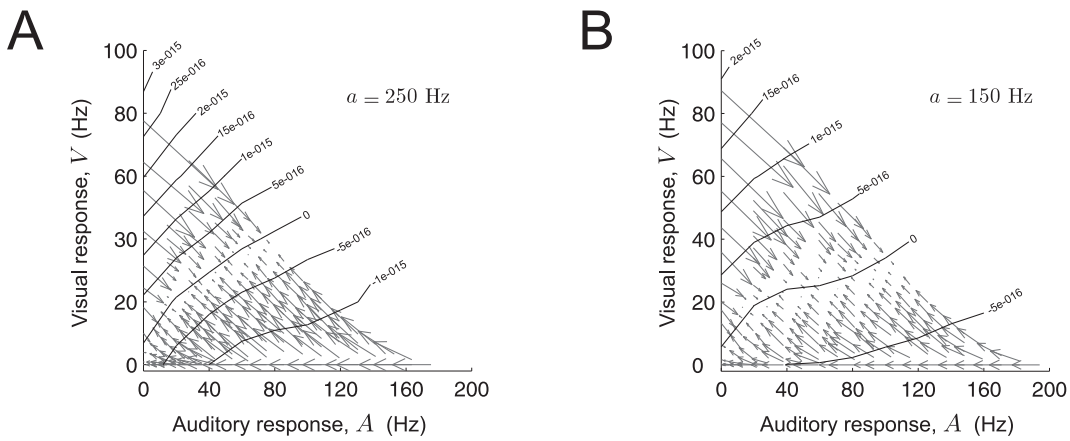

Figure 3.13: The delta learning-rule is obeyed even with auditory feed-forward inhibition. (**A**) Simulation result of the vector field (as in Figure 2.3C) illustrating the interplay between synaptic weight changes and auditory-visual responses. This plot is made using the same simulation parameters as in Figure 2.3C plus the feed-forward inhibition. The equilibrium point is along the contour line '0' where potentiation balances depression. Presynaptic firing rate, $a = 250$ Hz. (**B**) Same as (A) but with presynaptic firing rate, $a = 150$ Hz. The equilibrium point (along the contour line '0') is slightly different from that in (A).

sponses by more than T_{lat}. This delay reduces the average amount of synaptic potentiation, and thereby a reduction in the amplitude of the equilibrium ICX auditory responses. Additionally, because the magnitude of the inhibitory currents is proportional to the presynaptic (ICC) firing rates, a slightly different equilibrium point is reached for different presynaptic firing rates, Figure 3.13A and B. Also, the competing interactions of SFA and inhibition results in the equilibrium curve becoming nonlinear as seen in the plots.

3.6 Methods

3.6.1 Note on parameter choice

In the simulations and analysis presented in this chapter, we tried to constrain model parameters by existing data found in literature on barn owl physiology and on STDP. When we could not find data/estimates of a parameter value, we adhered to the constraint that simulated ICX rates should match those of experimentally recorded ICX responses by Gutfreund et al. (2002) (Figure 1.5C). A listing of all the parameter values used in our model/simulations is given in Table A.1 in the *Appendix*.

3.6.2 Model of the barn owl midbrain

We simulated an ICX neuron receiving excitatory inputs from pools of auditory ICC neurons and visual OT neurons (Figure 3.1). Although no reports of STDP in ICX neurons exist in the literature, here we assumed STDP applies to the ICC-ICX connections.

The model ICX neuron received auditory inputs from 21 contiguous ICC pools and for simplicity, visual input from one OT pool only. The number of neurons per pool was set to 15, but our results were not sensitive to this number, as long as it was larger than about 10. All neurons in pool j shared the same preferred stimulus direction θ_j. The pools are laid out topographically such that neurons in neighboring pools have adjacent preferred stimulus directions. In response to a stimulus at azimuth θ, neurons in pool j produced Poisson spike trains with mean rate given by

$$f_j(\theta) = f_{\text{base}} + (f_{\text{peak}} - f_{\text{base}})e^{-(\theta-\theta_j)^2/2\sigma}, \tag{3.3}$$

where f_{base} is the baseline firing rate, f_{peak} is the peak firing rate, σ is the width of the Gaussian tuning function (see Figure 3.1). For neurons in ICC pools, mean rates are denoted by $a(\theta)$, and for neurons in OT pools by $v(\theta)$. In the case of normal viewing, auditory and visual stimulus azimuths are aligned, $\theta = \theta^V = \theta^A$, and in the case of a visual shift, they are misaligned according to $\theta^V = \theta^A + \theta_{\text{shift}}$ (Figure 1.5). The preferred stimulus directions θ_j of the contiguous ICC pools are spaced apart by $\Delta\theta = 2.8^\circ$ (equals 7 μs in ITD coordinates).

The firing rates and spatial tuning widths of input ICC and OT neurons in our simulations are within the range of physiologically recorded data from these neurons (Wagner et al., 2002; Knudsen, 1982). For simulation results in Figures 3.2D, 3.3, and 3.4 we used the following parameters for ICC (a) and OT (v) neurons: $a_{\text{peak}} = 300$ Hz, $v_{\text{peak}} = 200$ Hz, and $a_{\text{base}}, v_{\text{base}} = 0$ Hz. For simulations in Figures 3.2D and 3.3 the ICC tuning width $\sigma^A = 4^\circ$ and the OT tuning width $\sigma^V = 6^\circ$, and for simulations in Figure 3.4, $\sigma^A = 4^\circ$ and $\sigma^V = 5^\circ$. For simulations in Figure 3.2E, and Figures 2.3C and E (in Chap. 2), spatial tuning of ICC and OT inputs is neglected; auditory inputs $a = a_{\text{peak}} = a_{\text{base}}$ vary from 0 to 350 Hz, and visual inputs $v = v_{\text{peak}} = v_{\text{base}}$ vary from 0 to 250 Hz.

To model ICX responses in adult owls, we manually set connection profiles of OT and ICC afferents to the shapes depicted in Figure 3.3B, solid line.

3.6.3 Stimulus duration and response latency

For ICX map formation simulations in Figure 3.3 and 3.9, we set the latency of the visual input $T_{\text{lat}} = 70$ ms from the onset of the visual stimulus (see, for example, Gutfreund et al., 2002). The latency of auditory input varied according to the distance r of the sound source to the ears. The latency of auditory inputs is thus set by r/c where $c \approx 340$ m/s is the speed of sound in air (we ignored the signal propagation time from the hair cells to ICC because it is on the order of a few ms). For example, a sound source positioned 10 m away from the owl results in an auditory latency of $(10/340) \approx 30$ ms. Auditory and visual stimuli were presented simultaneously, either at matching or offset spatial locations. The distance r and duration T of stimuli were random variables with uniform distributions in the intervals 0-25 m and 15-100 ms, respectively. The range of the former parameter implies that auditory ICX responses almost always preceded ICX visual responses. The interval between consecutive stimulus presentations was set to 500 ms.

For simulations results showing the linearity of receptive field formation in Figures 3.5, 3.6 and 3.7 we held the durations and distances of stimuli constant. The auditory stimulus duration was set to 70 ms, the visual stimulus duration to 50 ms, the distance to 0 m. Our results were insensitive to these and similar differential changes of auditory and visual stimulus durations, and neither to the fact that T and r were held fixed. The delta rule is obeyed even when these stimulus parameters are random variables drawn from the distributions specified in the previous paragraph.

3.6.4 Note on ITD units

Throughout this thesis we specify auditory spatial tuning, which is physically based on interaural time differences, interchangeably in either micro seconds (μs) or in spatial degrees. For barn-owl-sized heads, one spatial degree ($^\circ$) corresponds to an ITD of 2.5 μs. This is calculated as follows: with an estimated ear separation of $d = 8$ cm and the speed of sound in air of $c = 340$ m/s, it follows that the maximum ITD (corresponding to a 90 angle of incidence w.r.t to the rostro-caudal axis) is d/c. Therefore the ITD per degree of spatial angle is given by $\frac{d/c}{90} \approx 2.5$ μs.

Chapter 4

Robustness and stability of map formation with SFA

In this chapter, we first explore whether there exist cooperative behaviors of SFA and ICX synaptic plasticity when the sensory world is corrupted by noisy stimuli. We show that a neuron, in which SFA is included, is better able to cope when learning in a noisy environment. Next, we demonstrate in simulations how, as a consequence of the delta learning-rule, our network is able to make compensatory readjustments when a subset of the auditory inputs are lesioned and plasticity is switched off in these. We discuss next how our network would be able to maintain the stability of learned synaptic weights when visual inputs are absent (e.g. at night). Finally, we explore whether SFA in combination with other forms of synaptic plasticity, e.g. a non activity-dependent synaptic depression, can give rise to the delta learning-rule.

4.1 Adaptation imparts selectivity to map formation

SFA has typically not been considered in models of neural map formation, because supervised learning is possible without adaptation (Davison & Freǵnac, 2006; Friedel & van Hemmen, 2008). So, what benefits could barn owls draw upon for evolution to have included SFA in ICX neurons? We hypothesized that the adaptation observed in ICX neurons may confer an advantage for map formation under *real-world* visual-auditory stimulus conditions, that is, in the presence of uninformative visual or auditory stimuli (such as noise). To test this

idea, we compared simulation results in model ICX neurons in which SFA was included or excluded, which we describe in the following.

4.1.1 SFA de-emphasizes auditory-only stimuli

We first explored the effects of variable auditory stimulus durations on the map formation process. We simulated a single ICX neuron driven by sparse inputs from a single pool of auditory afferents ('sparse' meaning that there is a long dead time between consecutive stimuli). Independently of whether SFA was included in the simulations or not, ICC synapses potentiated when auditory stimuli were very short, Figure 4.1A. However, for intermediate stimulus durations on the order of 50 ms, synapses tended to depress when SFA was present and to potentiate when SFA was absent. The reason for this difference was that adaptation reduced the number of ICX response spikes after the initial burst, leading to excess of post-pre pairings, and thus to synaptic depression. For much longer stimuli, synapses always depressed as the number of pre-post and post-pre pairings tended to balance, which implies, by the negative area under the pairing function, that more synapses entered a depressed state.

When we simultaneously applied auditory and visual stimuli (Figure 4.1B) we found that in both the SFA and no-SFA cases synapses tended to potentiate, provided that the visual input was simultaneous or immediately followed the auditory input. If the visual stimulus was applied much before or after the auditory stimulus, it had no effect on plasticity on ICC-to-ICX synapses due to the absence of presynaptic spikes.

4.1.2 SFA makes map formation robust in noisy environments

We imagined that the reduced sensitivity of synaptic potentiation to auditory-only stimuli in adapting ICX neurons could be relevant in situations of high auditory background noise. We therefore studied map formation in a network that receives two types of input stimuli - 'broad' and 'tuned'. Broad stimuli had durations of 500 ms and represented spatially broad and long-duration sounds such as leaves rustling in the wind. Such stimuli do not contain any valuable information for map formation because they contain no or only very little directional information that can be associated with a visual stimulus (in our model, broad stimuli activated all presynaptic auditory afferents, Figure 4.2A). Tuned stimuli were

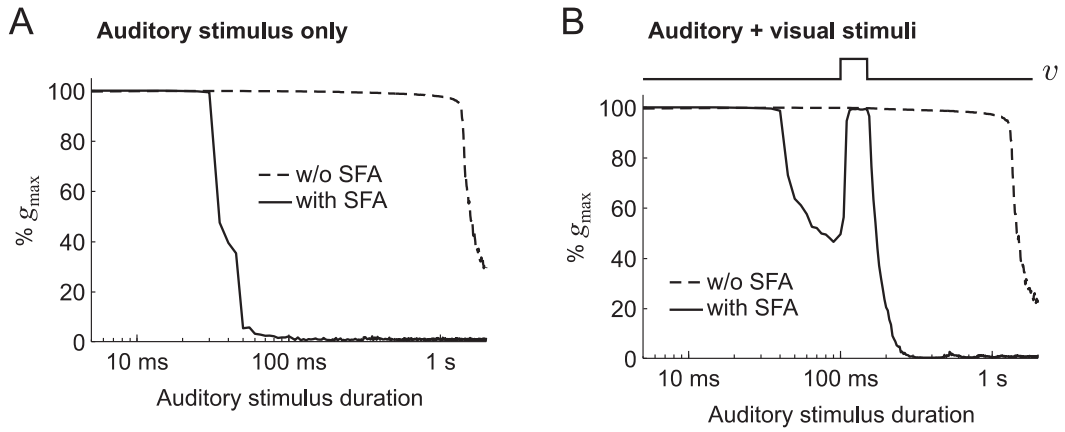

Figure 4.1: SFA de-emphasizes auditory-only stimuli. (**A**) Auditory-only stimuli: For auditory stimuli shorter than $T_{\text{auditory}} = 50$ ms, ICC synapses potentiate. For intermediate stimulus durations ($T_{\text{auditory}} = 50$-1800 ms), synapses depress when adaptation is present (solid line), but still potentiate when adaptation is absent (dashed line). Shown is the average synaptic strength in equilibrium, normalized to $g_{\max}$. (**B**) Auditory + visual stimuli: With adaptation, synaptic potentiation (instructive learning) is seen (solid line) when auditory stimuli larger than 50 ms temporally overlap with visual stimuli v (shown on top). Without adaptation, visual inputs have no instructive function in this range of auditory stimuli (dashed line). Hence, adaptation reduces the range of auditory stimulus durations in which sparse stimuli lead to undesired potentiation. $T_{\text{lat}} = 100$ ms. $\tau_{-} = 110$ ms.

brief (75 ms), they represented co-localized auditory-visual targets and therefore provided valuable information for map formation (see Methods at the end of this chapter). The network, and presumably the owl, should desirably ignore the broad stimuli and learn the spatial map based on the tuned bimodal stimuli only.

When we stimulated our network by randomly interleaving broad and tuned stimuli, we found that the network without SFA was not able to form a functional ICX map, because synapses potentiated for both broad and tuned stimuli. However, the network with SFA did form a visually registered ICX map, as synapses tended to be highly strengthened by the tuned stimuli and moderately depressed by the broad stimuli (see insets in Figure 4.2B).

We used a maximum likelihood read-out to assess the spatial encoding accuracy of the auditory maps with and without SFA (see Methods at the end of this Chapter). For the network including SFA, the encoding of auditory stimulus direction was unbiased and the read-out error (the variance of the maximum likelihood estimate of stimulus direction) was a monotonic function of the noise level (percentage of broad stimuli), and thus map formation was quite robust even under noisy conditions, Figure 4.2B. Robustness was also seen with regard to stimulus durations, as our simulation results were unchanged for broad stimulus

durations in the range 60-1500 ms and tuned stimuli durations in the range 20-120 ms.

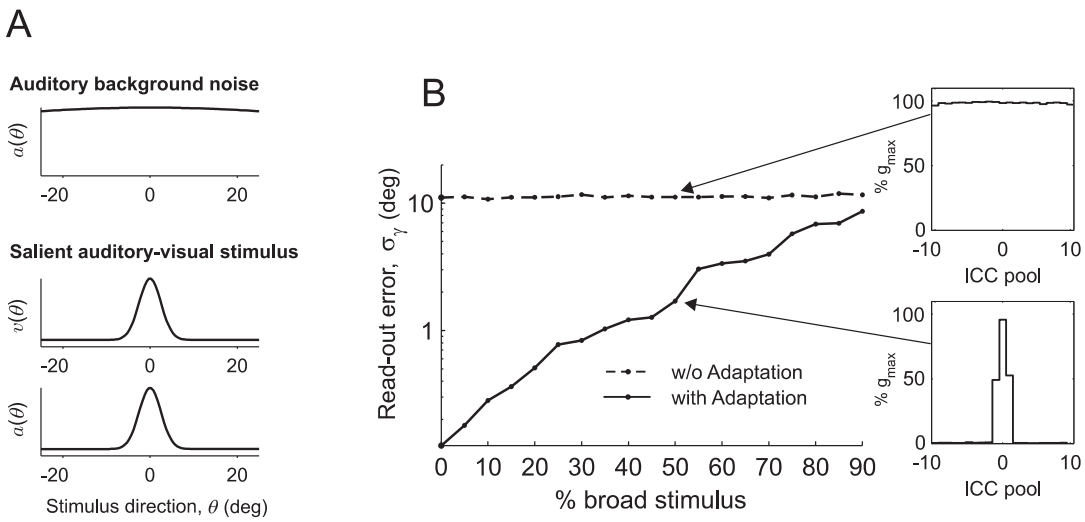

Figure 4.2: Robust map formation with spike-frequency adaptation. (**A**) Map formation in the presence of broad auditory stimuli (500 ms duration, *Top*) and tuned auditory-visual stimuli (simultaneous presentation, 75 ms duration, visual latency 70 ms, *Bottom*). (**B**) Read-out error of auditory stimulus direction in equilibrium (standard deviation σ_γ of maximum-likelihood read-out) as a function of the percentage of 'broad' stimuli used during the map formation process. For all relative presentation rates of the broad stimulus, the network with adaptation performs better than the network without adaptation. *Insets:* Learned synaptic connection strengths of a representative ICX neuron with and without adaptation, as a function of ICC pool number.

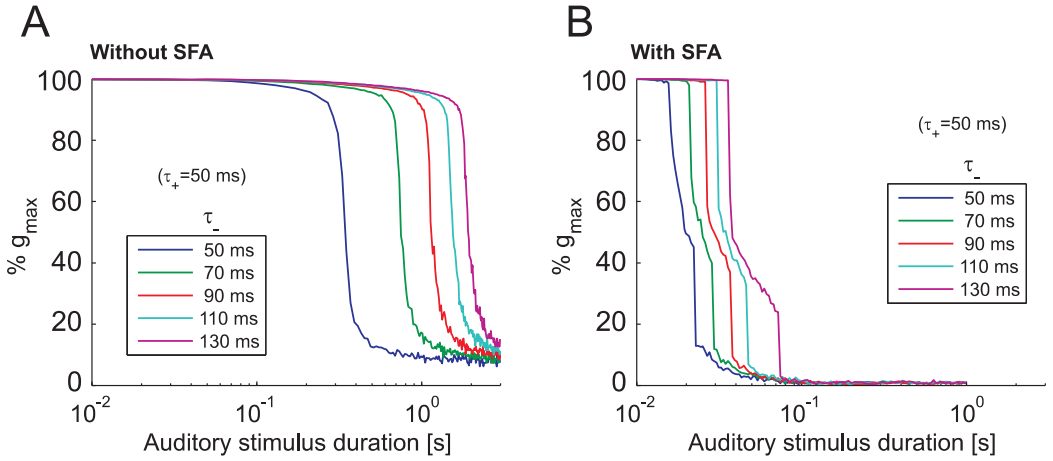

Figure 4.3: SFA reduces extreme sensitivity of synaptic plasticity to variation in τ_- of the STDP window. Shown is the average equilibrium synaptic strength as in Figure 4.1 without SFA (**A**) and with SFA (**B**). The 'knee-point' auditory stimulus duration (where the network switches from potentiation to depression) advances as τ_- increases for both the cases of without adaptation (A) and with adaptation (B). However, in the case with adaptation, the sensitivity of the knee-point to τ_- is lower by more than an order of magnitude.

4.1.3 SFA makes learning immune to STDP window variations

In Figure 4.1A the 'knee-point' stimulus duration at which the network switched from a state of net potentiation to that of net depression depended strongly on τ_- and on the STDP area ratio $\mathcal{A}_-\tau_-/\mathcal{A}_+\tau_+$. Increasing τ_- advanced the knee-point to longer durations in an approximately linear fashion in both the SFA and no-SFA cases, Figure 4.3. However, in the case with SFA, the knee-point was an order of magnitude less sensitive to τ_- variations as compared to the case without SFA.

SFA also reduces the extreme sensitivity of synaptic plasticity to the balance, $\mathcal{A}_-\tau_-/\mathcal{A}_+\tau_+$, of the STDP window, Figure 4.4. Therefore, with SFA included, the range of stimuli for which there is the undesirable effect of unrestrained potentiation for short and sparse stimuli is reduced.

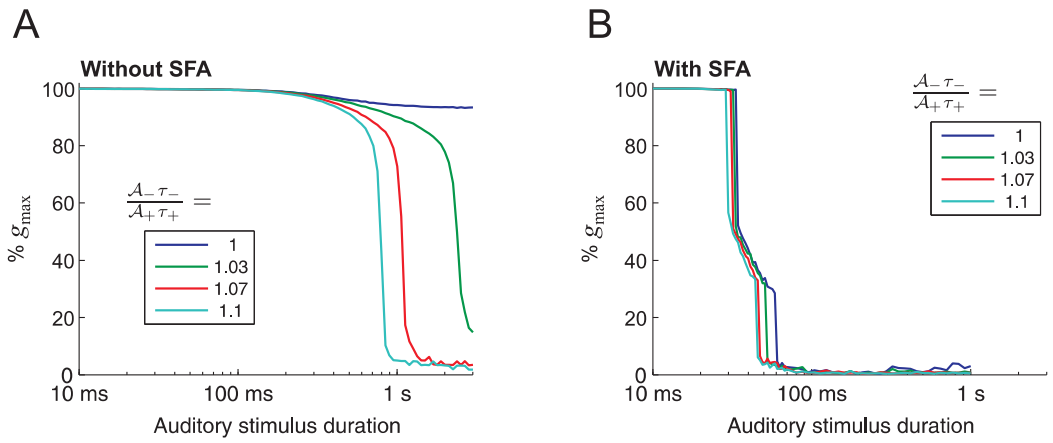

Figure 4.4: SFA reduces extreme sensitivity of synaptic plasticity to the balance of the STDP window. Shown is the average equilibrium synaptic strength, (**A**) without SFA and (**B**) with SFA . Without SFA, the relationship between the equilibrium synaptic strength and stimulus duration depends strongly on the STDP area ratio $\mathcal{A}_-\tau_-/\mathcal{A}_+\tau_+$. By contrast, only a minimal dependence is seen with SFA.

4.2 Conservation of net synaptic input and stabilization of firing rates

A general problem besetting most Hebbian-like learning-rules is one of stability: In Hebbian learning, where synaptic plasticity is driven by correlations between pre- and postsynaptic activity, an uncontrolled synaptic strengthening may happen because the potentiation

of synapses increases the likelihood that they will be further strengthened. To control such runaway synaptic strengthening, many network models use some kind of normalization techniques where, e.g., postsynaptic activity modifies the relative strength of inputs while conserving total synaptic weights or overall neuronal activity. By contrast, in most network models that incorporate STDP it is found that explicit normalization is not required for stability. More precisely, in network models using STDP, if the integral over the learning window is negative, a form of subtractive normalization of the synaptic weights (summed over all presynaptic inputs converging on a postsynaptic neuron) takes effect and an intrinsic stabilization of the output firing rate is reached (Song et al., 2000; Kempter et al., 2001; Davison & Fregnac, 2006).

We found that such a conservation of net synaptic input and an intrinsic stabilization of the output firing rates also applied to our STDP-plus-SFA model. To demonstrate this, we performed simulations in which we disabled plasticity of a subset of synapses in a fully formed map and evaluated if the network was able to adjust and arrive at the same equilibrium state as before.

Starting from a normally formed equilibrium ICC-to-ICX synaptic strengths distribution, shown in Figure 3.3B, we disabled plasticity in all synapses from the ICC pool '-1' and clamped the weights of this subset of synapses to 0. When we now stimulated our network in the usual manner with auditory-visual stimuli, we found that the network made compensatory readjustments in the remaining plastic synapses and was able to re-learn the map. Not only did the output firing rates (ICX auditory receptive field) converged back to normal values, the net presynaptic input was also approximately conserved. We tested this readjustment ability for different values of the non-plastic subset in a range from 0 to twice their strengths under normal map formation, and in all cases the network correctly readjusted, Figure 4.5.

The results from the above experiment does not come across as a surprise given that, in our network, the delta learning-rule is in operation and its sole effect is in minimizing the square error between OT visual input and ICX auditory responses. Therefore, when the network experiences imbalances due to the fixed subset of synapses from ICC pool '-1', the synapses from adjacent ICC pools, whose receptive fields overlap with ICC pool '-1', strengthen or weaken in an appropriate manner so as to minimize the visual error responses.

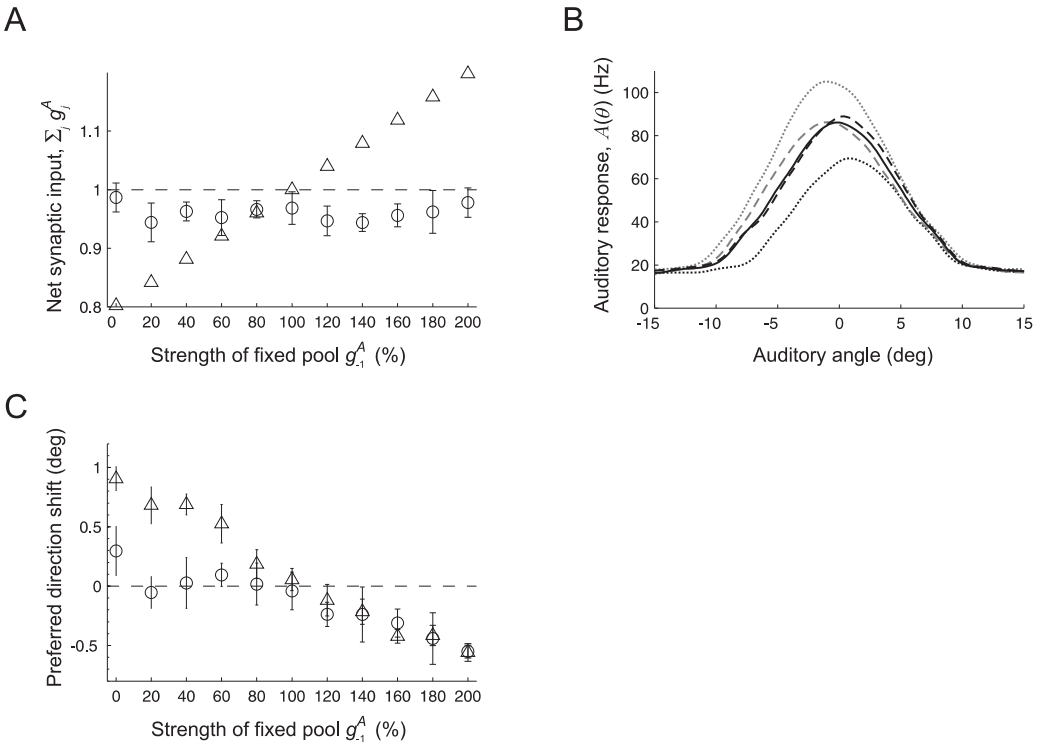

Figure 4.5: Conservation of net synaptic input and stabilization of firing rates. (**A**) All ICC-to-ICX synapses are plastic except for synapses from pool $j{=}{-}1$ whose strengths g_{-1}^A are fixed. The plot shows the net ICC-to-ICX synaptic conductance ($\sum_j g_j^A$) as a function of the conductance of the fixed pool (g_{-1}^A). The axes are normalized to the final established distribution in Figure 3.3B: The x-axis is normalized to the g_{-1}^A value and y-axis is normalized to the total synaptic conductance of the distribution in Figure 3.3B. *Circles*: Net synaptic conductances after the system has reached equilibrium. *Triangles*: Net synaptic conductances at the start of the simulation. (**B**) ICX auditory receptive fields, $A(\theta)$, at the start of the simulation (dotted curves) and after the system has reached equilibrium (dashed curves). For clarity, only two curves corresponding to a g_{-1}^A of 0% and 200% are shown. For reference, the normally developed receptive field is also shown (solid curve). (**C**) Shift in preferred ITD (θ_i) of the ICX neuron (i.e. the mean value of the receptive field curves). *Circles*: Preferred direction after the system has reached equilibrium. *Triangles*: Preferred direction at the start of the simulation.

4.3 Stability of learned synaptic weights when visual inputs are absent

So far in this thesis, we showed how vision is able to guide plasticity and maintain auditory spatial maps in the ICX under various situations. But what happens if the visual input is completely withdrawn in a network with a fully formed ICX auditory map (e.g. at night)? In such a case, synaptic weights in our model slowly decay down to zero, in agreement with the perceptron learning rule. On the other hand, synaptic plasticity mechanisms without SFA (STDP only) can be stable in the absence of instructive (visual) inputs, when (auditory) inputs are non-sparse (Song & Abbott, 2001; Davison & Fregnac, 2006). Indeed, in simulations of STDP without SFA, we found that synaptic conductances remained stable for dense auditory inputs*, in such a way that neurons locked in their stable firing modes (stable auditory map). The stability came at a price, however, in that the synaptic connection profile was not sensitive to shifted visual inputs (i.e., the network is hysteretic, see Sec. 4.4).

By contrast, neurons with SFA and STDP are unstable when visual input is absent, because they obey the perceptron learning rule (the perceptron learning rule depresses synapses and erases the auditory map when visual inputs are absent). Note that any network model can either satisfy stability or the perceptron learning rule, but not both. The benefit of the lack of stability is that a network with SFA remains responsive to visual inputs (no hysteresis) and thereby is able to maintain a highly accurate alignment of auditory and visual maps.

Nevertheless, map stability during the absence of instructive (visual) signals is a highly desirable feature. So, how can our model cope when visual inputs are lacking or not correlated with auditory inputs? We now describe two biologically plausible mechanisms that can robustly maintain the stability of learned synaptic strengths with absent visual inputs.

4.3.1 Stability through inter-areal feedback loops

We postulate that a mechanism to counteract undesirable synaptic decay during the absence of visual instructive inputs could arise from the existence of an additional source of delayed input to ICX neurons, with function similar to the delayed visual inputs. For example, an

*'Dense' meaning there is no dead time between consecutive stimuli, i.e., the stimulus object jumps from one point in space to another without ever disappearing between jumps.

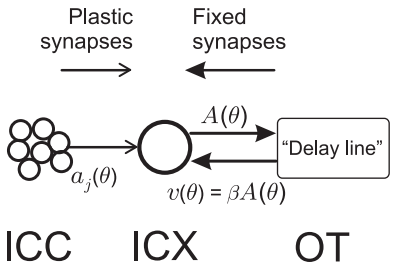

Figure 4.6: A plausible realization of inter-areal (OT-ICX) delayed feedback loops that can be a basis for map stability in the absence of visual stimulus. Ascending pathways convey the auditory spatial map in ICX, $A(\theta)$, to the OT. (For simplicity, we have assumed the ICX-to-OT connection strength to be equal to 1). An hypothetical delay-line in the OT delays this auditory signal by roughly $T_{\rm lat}$ and feeds this signal back to the ICX via the preexisting OT-ICX projections. The delayed feedback signal $v(\theta) = \beta A(\theta)$ has the same tuning as the preceding auditory ICX auditory responses and is scaled by a feedback factor β.

hypothetical feedback loop between the ICX and OT could act as a delay line, Figure 4.6, and give rise to delayed auditory inputs with similar tuning as the preceding ICX auditory responses thereby maintaining the ICC-to-ICX synaptic stability.

An important question that arises, then, is the stability of the network overall. Any solution that relies on positive feedback to maintain memory suffers from a severe tuning problem: The amount of positive feedback must exactly balance the intrinsic decay tendencies of the learned map. Too much feedback leads to runaway growth of neural activity, while too little leads to decay. In the scenario shown in Figure 4.6, the role of the visual input $v(\theta)$ is taken over by the delayed auditory feedback $\beta A(\theta)$, where β is the feedback factor. To keep the map stable, the net drift of synaptic weights should be zero. That is, β should chosen such that average weight change Δg in Eq. (2.5) is 0. This value for β can be calculated analytically via Eqs. (2.1), (2.5) and (2.26), and assuming fixed stimulus duration and latency, and neglecting c_0, we get: $\beta \approx -(c_2 + c_5/c_4)/(c_1 \langle U \rangle g^V \tau_{\rm s} N)$.

In our simulation experiments to test map stability (described later, in Sec. 4.3.3), we found after some juggling a value of $\beta = 1.45$ to be the required feedback factor. Values of β below this number tended to slowly increase the rate of map erasure, whereas values above this number tended towards causing runaway instability of the map.

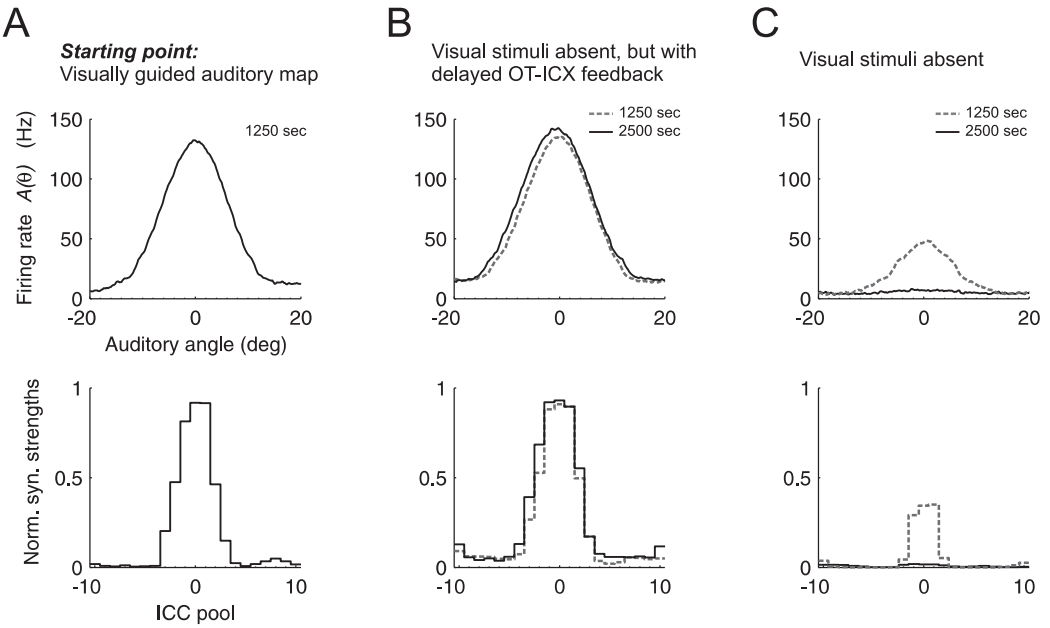

Figure 4.7: Simulation results showing map stability achieved by employing the delayed OT-ICX feedback loop mechanism. (**A**) The starting point for these simulations is a stable and fully formed visually guided ICX auditory map, 1250 seconds of simulation time after starting from random initial synaptic strengths. Shown is the ICX auditory RF (*above*) and the ICC-ICX connection profile (*below*) (**B**) When the visual stimulus is switched off and the delayed OT-ICX feedback loop made active, the map remains stable for long periods (1250 and 2500 seconds of simulation time). (**C**) In comparison, without any stability mechanism, the ICX auditory synapses go into a continuous state of decline, and the map is erased in about 2500 seconds of simulation time. Feedback factor $\beta = 1.45$ for the simulations in (B).

4.3.2 Stability through balanced potentiation and depression

Another way to allow a network with SFA to be stable is based on the fact that the drift of synaptic weights during absence of visual inputs strongly depends on the duration of auditory inputs. Whereas short auditory stimuli lead to synaptic potentiation (because presynaptic ICC activity is shortly followed by postsynaptic ICX activity), long auditory stimuli lead to synaptic depression (because adaptation shortens the postsynaptic response but not the presynaptic input, leading to many presynaptic spikes not followed by postsynaptic spikes), see Figure 4.1A. If the network were thus set-up in such a way that the 'critical' auditory stimulus duration ('knee' in Figure 4.1A) equals the average auditory stimulus duration (by choosing suitable τ_K, etc.), there would be equal amounts of potentiation and depression on average, thereby canceling any bias in the drift of synaptic weights.

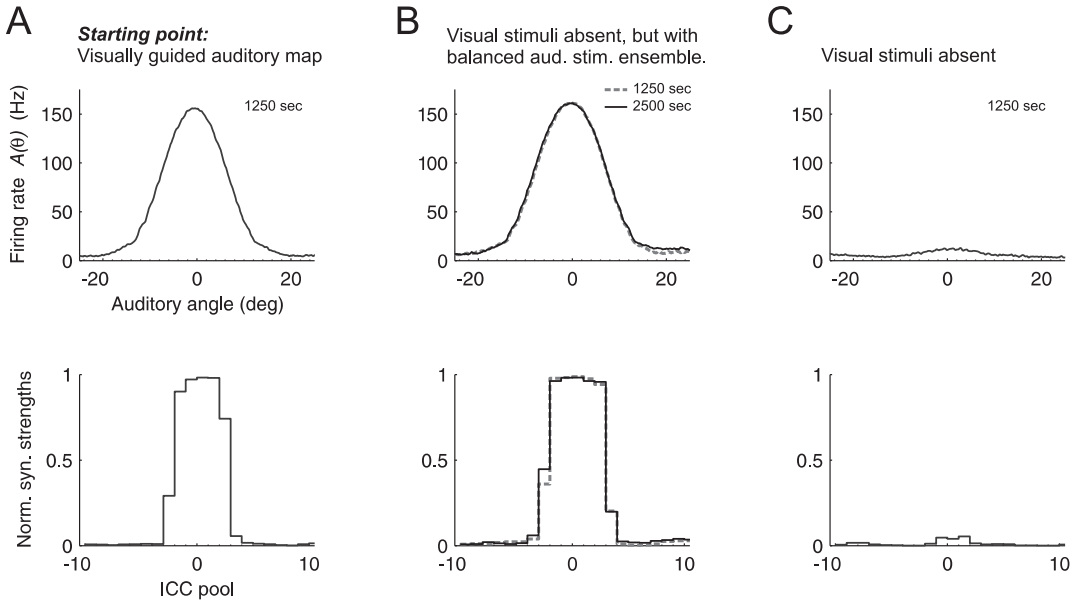

Figure 4.8: Simulation results of map stability achieved through balanced potentiation and depression. (**A**) The starting point for these simulations is a fully formed ICX auditory map that is visually guided, 1250 seconds of simulation time after starting from random initial synaptic strengths. For map formation, auditory-visual stimulus durations were drawn from a uniform distribution of [15-100] ms. Shown is the ICX auditory RF (*above*) and the ICC-ICX connection profile (*below*) (**B**) When the visual stimulus is switched off and the distribution of the auditory stimuli duration is reduced to the range 15-50 ms, the map remains stable for long periods (1250 and 2500 seconds of simulation time) when compared to the time scale required for map formation in (A). (**C**) For comparison, with visual stimulus is switched off, stimulating with an auditory only stimulus ensemble of duration distribution 15-100 ms [used originally for map formation in (A)] results in the ICX auditory synapses going into a continuous state of decline, and the map is erased after about 1250 seconds of simulation time.

4.3.3 Map stability simulations

We performed simulations to test the above two mechanisms for map stability. Starting out with a fully developed ICX auditory map (formed with auditory-visual stimuli), we deprived the network of visual input and we examined the pace of map erasure with and without the stability mechanisms.

Without any stability mechanisms, the initial fully formed map (which takes 1250 seconds of simulation time to form) was erased in about 1250 seconds. That is, the time scale for formation and erasure are similar. With either of the stability mechanisms in place, we found that the ICX auditory map remained stable and accurate for long time scales of up to and beyond 2500 seconds, which is twice the time scale that it takes a map to form with visual inputs, Figure 4.7 and Figure 4.8. Over extended time periods, however, the map

progressively drifted away and became imprecise. Nevertheless, the time scale of passive map drift was much longer than the time scale of active (visually guided) map formation. Therefore, a temporary elimination of visual inputs (e.g. at night) would only result in a small deterioration of the map (assuming a night rich in auditory stimuli), and the network can quickly re-calibrate the auditory map when exposed to auditory-visual stimuli during daytime.

4.3.4 Concluding remarks

For completeness, we would like to remind the reader that stability of networks without SFA (STDP only, as in e.g. Davison & Fregnac (2006)) applies only in the case of dense auditory input. In the sparse case, such networks are in fact more unstable than networks with SFA, as shown by the unrestrained potentiation in Figure 4.1A, B.

Finally, note that stability to visual-only inputs (during silence) is trivial because plasticity of ICC-to-ICX synapses is contingent on ICC firing.

4.4 Hysteresis in STDP-only learning

We now describe a simple example that illustrates how a network without SFA (STDP only) is insensitive to shifted visual inputs (i.e. the network is hysteretic). For this purpose, we performed simulations of cross-modal spatial learning in a network from Davison & Fregnac (2006), which has essentially the same architecture as ours. First, we stimulated the network with a 'training' input[†] peak firing rate of 45 Hz. in this case, a correctly formed auditory map was learned after a initial period of adjustment. When we turned-off the training input and continued to provided auditory input, the map was indefinitely stable without any change or degradation whatsoever on the learned auditory map. However, when this fully formed network was now presented with a spatially shifted training input with a peak firing rate of 45 Hz, we found that the auditory map failed to re-align with the now shifted training input. The only way to make this re-alignment possible was to increase the training input's peak firing rate to > 60 Hz. Thus even though this network is able to learn an initial map with a peak training input rate of 45 Hz, this network is unable to shift in response to a shifted training input unless the training input peak firing rate is raised by $\approx 30\%$. That is,

[†]The 'training' input in this model corresponds to the visual input in our network.

the network exhibits hystersis in terms of its sensitivity to training input firing rates. The details of this simulation are provided in Appendix C and Figure C.1.

4.5 Learning with a non temporally-specific synaptic depression

The defining cellular mechanisms that serve as primitives for the emergence of the delta learning-rule in our network have been (1) SFA in the ICX, which provides a mechanism to compute the visual error signal, and (2) STDP which potentiates the auditory input synapses that are active just before the visual error responses are elicited. Also, because SFA shortens the ICX auditory responses relative to the ICC drive, strong synapses are additionally depressed due to the excess of the post-pre spiking pairings (see Figures 2.3B and 2.5). While the potentiation to later visual responses requires a temporally specific LTP window, we now investigate whether the depressive part of STDP is really needed or not – i.e., do we need temporal specificity of LTD for the delta learning-rule to work?

We explored the answer to this question by modifying the learning rule in our network simulations to incorporate a temporally non-specific (not activity dependent) "flat" depression. The learning rule for synaptic depression was thus modified as follows: Every time a presynaptic spike arrived, the strength of the synapse was decreased by a fixed amount of $\Delta g = g_{\max}\mathcal{A}_-$ regardless of the postsynaptic activity. The value of $\mathcal{A}_-$ in this expression is set independently of $\mathcal{A}_+\tau_+$, and this value is set such that in the absence of visual inputs all the auditory inputs synapses gradually decay down to zero irrespective of their initial strengths.

We stimulated the network as usual with matched auditory-visual stimuli and examined whether SFA in combination with potentiation based on the LTP window of STDP and a flat depression is enough to provide the balance for map learning. We found that a stable ICX auditory map can form only if the OT input peak firing rate, v_{peak}, is above a certain threshold value that depended on the value of $\mathcal{A}_-$. Below this threshold no map auditory map was formed and all auditory input synapses settled near zero, Figure 4.9A. Above this threshold, small increments of v_{peak} resulted in steep increments in the peak of the learned auditory map A_{peak}, Figure 4.9B. Also, the width of the learned ICX auditory RF was

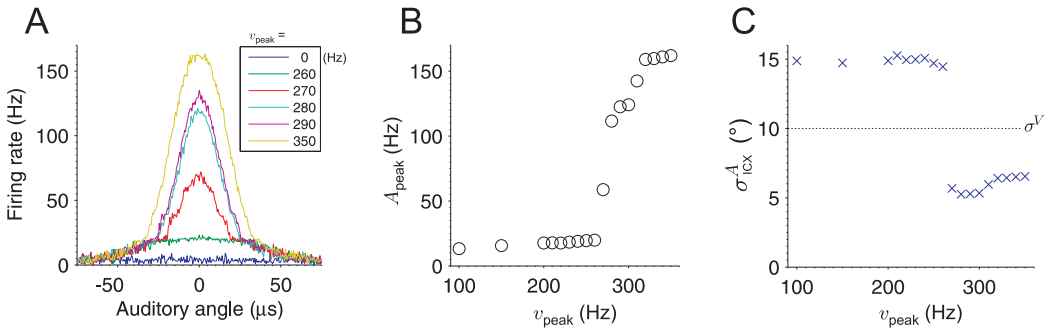

Figure 4.9: With a flat LTD window, the delta learning-rule is obeyed only in a narrow range of stimulus parameters. Shown is the influence of visual input peak firing rates on the equilibrium auditory response tuning. (**A**) Auditory response tuning, $A(\theta)$, for different visual input peak firing rates, v_{peak} (0-350 Hz). (**B**) The auditory response peak, A_{peak}, plotted as a function of v_{peak}. When $v_{\text{peak}} < 260$ Hz, no viable auditory map is learned. However, for $v_{\text{peak}} > 260$ Hz, A_{peak} steeply increases in a roughly linear manner until $A_{\text{peak}} \approx 165$ Hz, after which, synaptic saturation prevents further increase of the auditory response. (**C**) The auditory response width, σ^A_{ICX}, plotted as a function of v_{peak}. The auditory response width is approximately constant at $\sigma^A_{\text{ICX}} \approx 6.5°$ for $v_{\text{peak}} > 260$ Hz even though the visual input width in these simulations is set to $\sigma^V = 10°$. For these plots we used a flat LTD window with $A_- = 0.0053$ per presynaptic spike. The LTP pairing window was as usual with $\tau_+ = 50$ ms and $A_+ = 0.0025$. Other parameters are $a_{\text{peak}} = 300$ Hz, $a_{\text{base}} = 0$ Hz, $v_{\text{base}} = 0$ Hz and we used fixed stimulus durations of $T = 70$ ms and a visual latency of $T_{\text{lat}} = 70$ ms.

narrower than the visual input tuning width, Figure 4.9C.

The foregoing simulation results can be analyzed by looking at how a flat LTD window modifies the synaptic weight change rule of Eq. (2.5). With a flat LTD, this weight change rule can be written as:

$$\Delta g = g_{\max}(c_4 V + [c_8 A - c_9])a \tag{4.1}$$

where the original term $-c_5 A$ which describes the synaptic depression that is proportional to the auditory firing rate A (which, in turn, is proportional to the strength of the synapse) is replaced by the term $[c_8 A - c9]$. Here, the positive term $c_8 A$ represents the net potentiation due to pre-post spike pairings of the presynaptic ICC input and the postsynaptic auditory response (corresponding to the dashed line from $s = 0$ to T in Figure 2.5B), and the negative term $-c_9$ represents the constant depression term (not linked to A) of the flat LTD. Next, by replacing V in Eq. (4.1) above by I_V (using Eq. (2.1)), we arrive at the learning equation:

$$\Delta g = g_{\max}(c_1 c_4 I_V - c_2 c_4 A + c_8 A - c_9)a$$

or, after rearranging terms,

$$\Delta g = g_{\max}([c_1 c_4 I_V - c_9] - [c_2 c_4 - c_8]A)a. \tag{4.2}$$

Therefore, in equilibrium (i.e., $\Delta g = 0$), the auditory response, A, converges to the term $(c_1 c_4 I_V - c_9)/(c_2 c_4 - c_8)$, valid for $A > 0$. The expression $(c_1 c_4 I_V - c_9)$ implies that the visual input RF is clipped by a certain amount c_9. This is the reason why below a certain value of v_{peak} there is no auditory map formed. Above this value of v_{peak}, a stable auditory map forms. However, because of the clipping, the width of the visual input RF relayed to the ICX is reduced by some amount explaining the reason for the reduced width of the learned ICX auditory RFs.

The value of c_9 which dictates the flat LTD of all synapses cannot be made too small either. This is because in Eq. (4.1) if $c_9 < c_8 A$, synapses that are already strong will be able to remain strong simply by driven the postsynaptic neuron to fire and thus be able to perpetually sustain their strong strengths. That is, they will not depress if there is no visual input, and the delta learning-rule breaks down. Changing c_9 has the effect of moving the threshold point in Figure 4.9B to the left or to the right.

The term $(c_2 c_4 - c_8)$ in Eq. (4.2) indicates that the original term c_5 is reduced by an amount c_8, which has the consequence that amplitude of the equilibrium auditory responses become very sensitive to the amplitude of the visual input, resulting in the steep increase of A_{peak} after the threshold point (Figure 4.9A,B). Once synaptic saturation is reached, A_{peak} cannot increase any further to match the value dictated by the delta learning-rule.

So, in summary, our tests show that even though robust map formation is possible with a non temporally-specific LTD, the delta learning-rule – that is, a linear scaling of the learned auditory tuning amplitude and widths w.r.t the visual input – is confined to a narrow range of model and stimulus parameters.

4.6 Methods

All the simulations in this chapter are nearly identical to the map formation simulations described in Chapter 3. Specific modifications and parameters are as given below.

For the subplots in Figure 4.1A and B, we used $a_{\text{peak}} = v_{\text{peak}} = 100$ Hz for the case

with SFA, and $a_{\text{peak}} = v_{\text{peak}} = 30$ Hz and $a_{\text{base}} = 3$ Hz for the case without SFA. The 'broad' stimuli in Figure 4.2B were defined by $\sigma^A = \infty$, $v_{\text{peak}} = 0$ (i.e., no visual input), and $a_{\text{peak}} = 40$ Hz for the case with SFA and $a_{\text{peak}} = 10$ Hz for the case without SFA. Note that because the ICX neuron's firing rate can be very high when SFA is absent, we set lower peak input firing rates in the case without SFA so that the postsynaptic firing rate is roughly similar to that when SFA is included.

For the map stability experiments described in Sec. 4.3.1 and Figure 4.7, we used fixed stimulus duration of $T = 50$ ms and latency of $T_{\text{lat}} = 70$ ms (see Appendix D.0.1 for the simulation program source code). For the map stability experiments described in Sec. 4.3.2 and Figure 4.8, we used a fixed latency of $T_{\text{lat}} = 70$ ms and the stimulus durations were uniformly distributed in the range specified in the caption of Figure 4.8. The fact that we set some of the stimulus parameters to fixed values was not critical for our results and map stability was also achieved when both the above stimulus parameters were distributed. The sole reason for holding some of the stimulus parameters fixed was to illustrate the main neuronal and network quantities that contributed to the stability of the maps.

4.6.1 Population read-out

In Figure 4.2B, we used maximum likelihood estimation to read out the auditory stimulus location from ICX responses (see Seung & Sompolinsky, 1993). Accordingly, the estimate γ of stimulus location was given by $\gamma = \arg\max_\theta \sum_i \ln \mathrm{P}\left(A_i|\theta\right)$, where A_i is the auditory response of the i^{th} ICX neuron when the model network was presented with a stimulus at location θ. For this experiment we used 17 ICX neurons which were laid out topographically. We assumed that responses A_i obeyed a Gaussian distribution $\mathrm{P}\left(A_i|\theta\right)$ of fixed standard deviation of 10 Hz for the case with SFA and 20Hz when adaptation was absent (measured values). As a function of θ, the means $\langle \mathrm{P}\left(A_i|\theta\right)\rangle$ were given by a Gaussian function with nonzero baseline (see Figure 3.3D). The 'arg max' was computed numerically using the `fminsearch` function in MATLAB. The standard deviation of γ in Figure 4.2B was evaluated for 500 repeated stimulus presentations chosen randomly in a 50° spatial field. We did not use the more common method of population vector decoding because our network lacked periodic boundary conditions and the population vector would have introduced a large bias towards the center of the visual field.

Chapter 5

Discussion

In this thesis, we have endeavored to understand how simple cellular and biophysical mechanisms can serve as primitives for solving complex computational tasks performed by the brain. The example we consider is instructive learning in the barn owl midbrain sound localization pathway in which a visual spatial map from the OT guides and calibrates the formation of an auditory spatial map in the ICX. By studying a computational model of this network, we show how the interaction of two simple biophysical mechanisms – SFA and STDP – jointly leads to the emergence of the delta learning rule, showcasing an example of how theoretical principles of learning can be realized in neural systems.

We show that SFA can be viewed as a mechanism for instructive error signaling in sensory neurons when these are driven by sparse multimodal inputs in a slow and a fast pathway. SFA trades off between slow ("late arriving") responses of one modality and fast ("early arriving") responses of another modality in an approximately linear fashion. The consequence is that the late sensory responses can be viewed as instructive or error signals that convey the need to respond to the earlier arriving inputs.

When we incorporated STDP into the early-input synapses, we found that synaptic changes were well described by the delta learning rule (Rosenblatt, 1958; Widrow & Hoff, 1960). Our implementation does not rely on an explicit neural representation of the error term; the error is implicitly computed through the interplay of SFA and STDP.

Finally, in our extended model of an ICX neuron that received auditory inputs from pools of spatially tuned and topographically laid out ICC neurons, we found that, in equilibrium, visual tuning from the OT was precisely transferred onto auditory response tuning in ICX,

in excellent agreement with the delta learning rule.

In the following we discuss the neurophysiological relevance of our findings and the broader computational implications of SFA and STDP.

5.1 Linear responses and transient stimuli

Our work suggests that SFA in ICX neurons has a wide ranging impact on auditory processing and map formation in the barn owl. On a very basic level, SFA shortens ICX responses and emphasizes fast and brief auditory stimuli, in agreement with previous reports that SFA has high-pass filtering properties useful for separating transient communication signals from background oscillations (Benda & Herz, 2003; Benda et al., 2005). Moreover, SFA is also known to have linearizing effects, for example on spike-frequency curves as a function of injected electrical current (F-I curves) (Ermentrout, 1998). Though in our analytical derivations we have studied a simpler neuron model where F-I curves are intrinsically close to linear (Figure B.1A), there was an effect of negative-feedback linearization also in our work as shown by the excellent quantitative agreement of our analytical derivations with our simulation model (in which, the F-I curves are highly nonlinear) (Figures 2.2B, 3.2E and B.1B). The result of this linearization is that in our model, the ICX visual responses are precisely proportional to the error in the auditory-visual mis-match.

The factor of this proportionality was also quite insensitive to SFA parameters as long as the adaptation time-constant was much longer than T_{lat} (Figures B.3), in line with the theoretical findings by Ermentrout (1998) showing that the particular form of SFA (in our case AHP-currents) is not crucial for the linearization effect to take place; the only requirements are that the adaptation is slow and the unadapted F-I curve is highly nonlinear at the threshold point.

5.2 Spike-frequency adaptation and learning

In our simulations and analytical derivation, we assumed sparseness of auditory and visual inputs (long dead time between consecutive inputs). In this regime, SFA helps to reduce a known instability of STDP (unrestrained potentiation) that arises from very brief auditory-only inputs: For short transient stimuli, STDP alone tends to induce unbounded synaptic

strengthening in response to whatever excitatory input drives the cell (Figure 4.2B). SFA prevents this from happening by shortening stimulus responses, thereby leading to fewer pre-post spike pairings and to lessened potentiation (Figures 2.3C and 4.2A). That is, SFA reduces the detrimental potentiation induced by auditory-only stimuli. We believe this is one key advantage conferred by SFA.

In our model, visual ICX responses influence plasticity of ICC synapses. Because visual inputs are delayed with respect to auditory inputs, their main effect is to induce potentiation. Bimodal stimuli providing spatial information in both visual and auditory domains are rare in natural environments; it makes sense to think that circuits in the midbrain have evolved to incorporate SFA in their attempts to maximize the dependence of map registration processes on these rare transient events where informative co-localized inputs are present. Thus, irrespective of the auditory environment of the animal, be it noisy or silent, and irrespective of background firing rates of synaptic afferents, with SFA, bimodal stimuli are highly effective in guiding map formation (Figure 4.2C).

In summary, sensory map formation can benefit from SFA which effectively narrows down the stimulus ensemble that induces synaptic potentiation to an ensemble where delayed top-down inputs instruct the formation of bottom-up connections.

5.3 Inhibitory and excitatory connections in ICX

Simplifications in our barn owl midbrain map formation model were the omission of inhibitory and lateral excitatory connections in ICX and the differential functional expression of N-methyl-D-aspartate (NMDA) receptor currents in the ICX during learning. In experimental studies of prism-induced auditory remapping, it was found that 'old' ICC synapses in ICX do not disappear, but that inhibition masks the responses they used to mediate - thanks to this latent stability of synaptic contacts, functional synaptic connections can re-emerge quickly after prism removal (Zheng & Knudsen, 1999, 2001; DeBello et al., 2001). Thus, inhibition may help to store traces of old memories, thereby biasing map plasticity towards stimuli experienced in the past. Inhibition may also be important to overcome some limitations in our model such as the fast narrowing of auditory tuning curves in ICX (Wagner, 1990; Fujita & Konishi, 1991). Preliminary simulations in which we included feedforward inhibitory connections of fixed strength onto ICX neurons indicate that visually-guided au-

ditory maps can form in the presence of inhibition (Figures 3.12 and 3.13), suggesting that these and other computational advantages of inhibition may be well reproduced. For example, the inclusion of inhibition in an ICX model was shown to result in an auditory space map that shifts adaptively and dynamically in response to stimulus motion in agreement with the experimental findings of the predictive nature of OT auditory receptive fields when the owls are presented with moving sounds (Witten et al., 2006).

Neuropharmacological studies reveal that the NMDA receptor currents, is crucial in the expression of newly learned responses. Early in the learning process (that is, after a few weeks into a sustained prism experience), NMDA receptor currents are found to play a preferential role (to the extent of 50% of the receptor currents) in the expression of learned responses. However, with extended periods of prism experience (and also late in normal development), the differential NMDA receptor-mediated component of these responses disappears (Feldman & Knudsen, 1998b), suggesting a maturation of these glutamatergic synapses, switching from NMDA receptors to that of mainly the α-amino-3-hydroxy-5-methyl-4-isoxazoleproprionate (AMPA) receptors (Feldman & Knudsen, 1998a). In our work we did not distinguish between such NMDA and non-NMDA receptors at the synapses. Our work is based on the premise that synaptic contacts are already present and only their efficacies are modified in an experience dependent manner (our synapses, with an activation time of 10 ms, are matched to non-NMDA receptors in this respect). An advantage that ICC-to-ICX NMDA receptor based synapses might provide in learning a shifted visual map is that that they would transmit information to the postsynaptic ICX neuron only when it was depolarized by the visual instructive signal. Otherwise, the synapses would remain ineffective and so would not disrupt the established pattern of information processing (Knudsen, 2002).

The degree to which lateral excitatory connections in ICX exist and contribute to map formation is currently not known. In general lateral excitation is believed to serve the purpose of increasing the robustness and accuracy of encoded stimulus attributes (Pouget et al., 1998). Hypothetical synergistic interaction between adaptation and lateral connections might be limited, though. In model networks it was found that coexistence of SFA and excitatory connections may lead to spontaneous generation of neuronal rhythms (Ermentrout et al., 2001; Fuhrmann et al., 2002). When rhythms have a spatial, wave-like attribute,

they may have a role in the formation and maintenance of topographic maps, for example, in the retina and the cortex (Prechtl et al., 1997; Diamond et al., 1999; Wong et al., 1993). It is thus possible that adaptation may contribute to ICX activity waves, if these were to be found in early development.

5.4 Robustness to parameter variation

Synaptic changes onto adapting neurons in our model are well described by the delta learning rule (Rosenblatt, 1958; Widrow & Hoff, 1960). This learning rule implements error minimization along the direction of steepest descent. In our case, the error is the squared difference between visual OT inputs and auditory ICX firing rates, the ideal quantity to be minimized for visually guided map formation. Unlike previous biophysical implementations of the delta rule (McLaren, 1989; Schultz & Dickinson, 2000), our implementation does not rely on an explicit neural representation of the error term. Rather, the error term is implicitly computed through the interplay of adaptation and STDP.

Our calculations showed that the emergence of the delta rule under SFA and STDP is remarkably robust. In conductance-based model neurons, the delta rule was well approximated irrespective of cellular parameters, provided that the visual drive arrived no later than τ_+ (potentiation window size) after offset of auditory responses, else there are no pre-post spike pairings that fall into the positive part of the STDP window. Also, for adaptation to give rise to an implicit error signal (Figure 2.2B), the adaptation time constant needed to be long enough to prevent recovery from adaptation before arrival of visual inputs, i.e. $\tau_K \gtrsim T_{lat}$. Even though in our analytical derivations we assumed (for simplicity) a fixed stimulus duration, a fixed auditory-visual latency and non-overlapping ICX auditory and visual responses, our findings (the delta rule) also applied to the general case in which stimulus durations and relative latencies are distributed. For example, map learning was also robust when we used a stimulus ensemble in the range of 75-200 ms, such that the ICX visual and auditory always overlapped.

Under special circumstances, when $\tau_- < \tau_+$, we found that the delta or perceptron rule can also be derived for neurons without SFA. However, because $\tau_- < \tau_+$ has not been reported experimentally, it remains to be seen whether this scenario is biologically relevant.

Another aspect of robustness that our model exhibits is its resilience when we artificially

"lesioned" a part of the ICC-to-ICX connectivity. When we clamped or removed some of the ICC-to-ICX synapses in a fully formed map, we found that the remaining plastic synapses readjusted in such a manner as to compensate for the loss of function of the clamped synapses. As a result, even though the relative strength of inputs is modified, little change in total synaptic weight occurs, the net synaptic input is conserved and output firing rates are stabilized (Figure 4.5). Such kind of a homeostatic mechanism in which inverse heterosynaptic modification compensates for homosynaptic potentiation or depression is found widely in the brain (Turrigiano, 1999), for example, in intercalated neurons of the amygdala, activity-dependent potentiation or depression of particular glutamatergic inputs leads to opposite changes in the strength of inputs ending at other dendritic sites (Royer & Pare, 2003).

5.4.1 STDP windows and nonlinear summation

The delta learning-rule in our model is rather robust to variations in the size of the STDP window (Figures B.4 and B.5). But would our model work with symmetric and other window types (Caporale & Dan, 2008) that are been observed in the brain? Strictly speaking, our network relies on a temporally asymmetric STDP window requiring (1) the positive leg of the STDP window extend to T_{lat} for synaptic potentiation to late visual error responses and (2) a negative leg of the STDP window that depresses strong synapses because the ICX response would then be short relative to the afferent drive. However, any window that can approximately satisfy these two requirements would suit itself for the implementation of perceptron learning rule. In this sense, a symmetric STDP window will be suitable for learning as long as the stimulus ensemble and latencies (in addition to an appropriate window size) somehow match up to the above mentioned requirements. Note, however, that it is possible to implement robust instructive learning with a symmetric STDP window which is less restrictive in terms of stimulus ensemble, latencies and window size if SFA is excluded from the model (Davison & Fregnac, 2006). In this case, the network can learn the map based on an correlated 'activity template scheme (but the perceptron learning rule will not be in operation).

Another assumption in our model w.r.t STDP is of the linear summation of synaptic changes of pre- and postsynaptic spike trains. Fortunately, this assumption does not turn

out to be a necessity and preliminary simulations where we included the effect of spike-triplets (which reduces the efficacy of STDP during bursting) show that the perceptron learning rule remains mostly unaffected by such non-linear plasticity rules Froemke & Dan (2002). The intuition as to why non-linear summation does not appear to affect our learning rule may be had by referring to a simple concept from feedback control systems theory: The STDP mechanism may be considered as a system with an infinite open-loop gain with spike-timing differences as inputs and synaptic weight changes as outputs. The open-loop gain is actually infinite because in our network, STDP makes additive changes to synapses with no regard to their absolute values (that is, if we did not clamp the weight to $g_{\max}$ or 0, the weights would explode to positive or negative infinity). Therefore, when we combine such an infinite gain open-loop system with a linear negative feedback system (thanks to SFA), the combined system also becomes linearized, a fact well known in the control systems theory.

We have not extensively explored the emergence of the delta learning-rule in networks with the 'multiplicative' version of STDP, where a synaptic strength change update is dependent on the current strength of the synapse. A problem with the multiplicative rule is that it intrinsically forces all the synaptic strengths towards a value of half the maximum synaptic strength (i.e. $0.5g_{\max}$), which competes with the delta rule which forces synapses towards either $g_{\max}$ or 0 depending on whether the presynaptic input is matched with the teacher input or not. This results in an equilibrium synaptic strengths distribution in which both the matched and unmatched synaptic input groups getting distributed near $0.5g_{\max}$ with only a minimal separation between the groups (Gutig et al., 2003; Davison & Fregnac, 2006).

5.5 Map stability in the absence of instructive inputs

During complete absence of instructive visual inputs (e.g. in the dark), synaptic weights in our model decayed down to zero, in agreement with the perceptron learning rule. A mechanism to counteract such undesirable synaptic decay could arise from the existence of an additional source of delayed input to ICX neurons, with function similar to the delayed visual inputs. For example, feedback loops between the ICX and OT (Reches & Gutfreund, 2008; Rodriguez-Contreras et al., 2005; Winkowski & Knudsen, 2007) could act as a delay line, giving rise to delayed auditory inputs with similar tuning as the preceding ICX auditory

responses, thereby promoting synaptic stability. Such a scenario could also apply to cortex, where SFA and STDP coexist (Ahmed et al., 1998; Fuhrmann et al., 2002; Meliza & Dan, 2006; Schuett et al., 2001) and where decay of feedforward connections could be prevented by delayed inputs arising from feedback loops via higher cortical areas (Johnson & Burkhalter, 1996; Douglas & Martin, 2004). Preliminary simulations performed to test this idea, showed that it was possible for the ICX map to maintain stability through delayed OT-ICX feedback loops. Moreover, we found that the feedback factor required to maintain stability is around a value of $\beta = 1.45$ implying that no special gain or amplification system is needed in the feedback-loop circuitry to produce such a signal.

We also demonstrated a second way to stabilize a learned map in total darkness. In this scheme the detrimental depression due to long duration auditory only stimuli is balanced out by potentiation to short duration auditory stimuli, with the net effect of zero decay of learned synaptic weights. Although it seems unlikely that the natural world stimulus ensemble would match the one required for stabilizing the auditory maps in complete darkness, our results nevertheless show that such a scheme may be applicable in other brain areas where there is a need for reconciling the apparently opposing requirements of plasticity and stability.

In both the schemes that we propose for stability when visual inputs are absent, the map slowly degrades over extended time periods of auditory only stimuli. Nevertheless, an animal could cope with some minor degradation overnight (that is, assuming a night rich in auditory stimuli) since, as we have shown, the time scale for readjustment, say, after day break, is an order of magnitude shorter than than the time scale of map degradation (Figures 4.7 and 4.8).

On a different note, there could also exist a mechanism of stimulus or plasticity gating that "turns off" plasticity when visual inputs are absent (Gutfreund et al., 2002; Winkowski & Knudsen, 2007; Crist et al., 2001; Stefan et al., 2004), and thus prevent undesired synaptic decay in complete darkness.

5.6 Barn owl midbrain findings that are not captured in our model

Our simplified model of the barn owl midbrain model does however sacrifice certain aspects of experimental findings. For example, because of the inherent delta learning rule, our ICX auditory map exhibits super fidelity irrespective of how and when it experiences shifted visual input. That is, our model ICX auditory map always faithfully realigns itself with the visual map from OT. By contrast, ICX auditory maps in barn owls do not exhibit unrestrained plasticity: Plasticity to large visual shifts declines with age, with juvenile owls being able to adapt completely and adult owls showing very limited ability to change (Brainard & Knudsen, 1998). But in adult owls, incremental training is able increase the plasticity of their ICX auditory maps and their auditory maps can eventually adapt to large visual shifts provided the visual field is shifted in a series of small incremental steps (Linkenhoker & Knudsen, 2002). Two previous models of auditory map formation were able to capture some aspects of this restrained plasticity in a mathematical model by setting a variable cost on neural rewiring (Kardar & Zee, 2002; Atwal, 2004). In these models, the assumption is that the cost of rewiring is low in the developing brains of juvenile owls and therefore the auditory maps are agile whereas in adult owls higher rewiring costs prevent a complete shift of the auditory map in the adaptive direction.

Another functional aspect not captured in our model and which may be considered for inclusion in a more biophysical midbrain model is the changing roles of inhibitory and NMDA synapses in the ICX, as explained in Section 5.3. Furthermore, our model of the midbrain is essentially a single layer perceptron network whereas in reality the owl's ICC, ICX and OT are made of several neuronal layers stacked together. Also, in our model the ICX is the only site of plasticity, whereas some limited plasticity in response to shifted visual inputs has also been observed in the superficial layers of the OT in adult owls (DeBello & Knudsen, 2004). We have not attempted in this thesis to model such layer-specific plasticity and functionalities in any detail.

5.7 Computational learning rules

Our work bridges a gap between the delta rule and simple neuron biophysics, and in more general terms, it strengthens the links between computational learning rules and adaptation and plasticity in biological systems. Many previous network models of synaptic learning have relied on the minimization of some suitable cost function without consideration of the biophysical plausibility of such learning rules. For example, the dynamics of receptive field remapping in the barn owl midbrain was shown to agree with optimality considerations derived using information theory (Atwal, 2004). Other examples include: minimization of image reconstruction errors using sparse priors, leading to linear filters reminiscent of simple cells receptive fields (Olshausen & Field, 1996; Karklin & Lewicki, 2005); minimization of sensory prediction errors that results in end-stop tuning as seen in cortical visual neurons (Rao & Ballard, 1999); and, minimization of retinal slip or amplified visual response errors that leads to emergence and maintenance of neural integrator networks (Robinson, 1989; Xie et al., 2002; Hahnloser, 2003).

In previous models of ICX map formation based on Hebbian plasticity (e.g., Friedel & van Hemmen, 2008; Witten et al., 2008), temporal correlations tied with response latencies are not considered, leaving out the potential significance of delayed inputs for instructive coding. By contrast, we interpret latency differences as a computational strategy of the brain (Meredith et al., 1987), agreeing with the notion that latency coding is very prominent in the visual system and can be found as early as in the retina (Gollisch & Meister, 2008).

In computational learning theories, STDP has been linked to temporal difference learning (Rao & Sejnowski, 2001; Roberts et al., 2008), maximization of mutual information (Toyoizumi et al., 2005) and to optimal information transmission (Hennequin et al., 2010). Here we extend this list of computational functions of STDP to include gradient-descent error minimization. By establishing a connection between the delta rule and simple neuron biophysics, our work strengthens the links between computational learning rules and adaptation and plasticity in biological systems. Along with similar efforts (Sprekeler et al., 2007) our work suggests that learning rules derived from computational insights may be more compatible with simple neuron biophysics than previously thought.

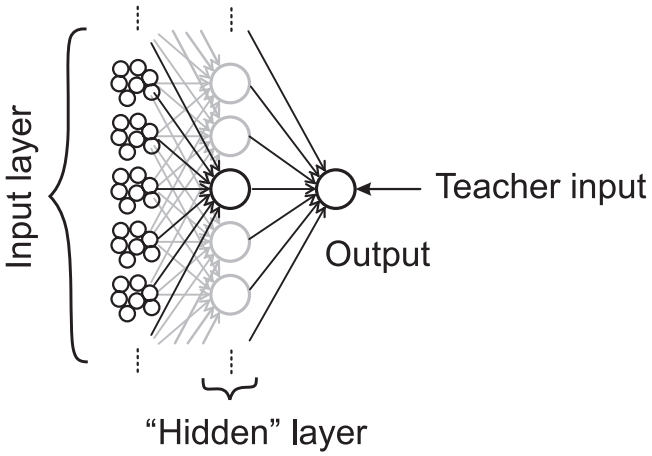

Figure 5.1: Schematic of a multilayer perceptron network. In this network, which is fully feed-forward, an intermediate layer of neurons called the "Hidden" layer sits in between the input neurons and the output neuron. All the left-to-right synapses (arrows) are plastic. The teacher input is provided only to the output neuron through a fixed synapse.

5.7.1 Multilayer perceptron network

The natural next step to our biophysical single-layer perceptron model with the error correcting learning would be the extension to a multilayer network. A limitation of single-layer perceptron well known in artificial neural networks theory that they can perform pattern classification only on linearly separable patterns. In contrast, a multilayer network contains one or more layers of *hidden neurons* that are not part of the input or the output of the network, see Figure 5.1. These hidden neurons enable the network to learn complex tasks by extracting more meaningful features from the input patterns. The main issue in such multilayer networks is how does one compute the synaptic weight updates of the intermediate layers based on the error measured at the output layer. In the artificial neural networks theory there is an elegant method, namely the backpropagation algorithm, which computes synaptic changes at all the layers based on the error (i.e. the difference between output and target signal) at the output layer (see, e.g., Haykin, 1994).

Would our SFA-STDP learning scenario be able to implement such an error backpropagation learning in a biological multilayer neuronal network? The answer to this question might rely on two key requirements. The first requirement is more of a "hardware" nature, that is, a need for (top-down) point-to-point error feedback connectivity. Indeed in the cortex, the midbrain and other brain areas, multilayer connectivity is the norm and the predominant organization principle, and this connectivity is frequently topographically

restricted and bi-directional, thus satisfying our first requirement. The second requirement is of a feedback delay mechanism to enable the computation through SFA of a local error gradient at the hidden layer neurons. The delayed feedback appears to be a harder problem to reconcile biologically because axodendritic delays in most neurons is on the order less than a few milliseconds, a delay that might be too less to compute error via SFA. Next, even if we assume that a delay mechanism may be somehow realizable, we still have to decipher how the error signal would be backpropagated, i.e., what would be the nature and content of the error signal. (For example, Rao & Ballard (1999) present a multilayer implementation of error-driven predictive coding in the visual cortex). A further problem that needs to be resolved is the self-consistency of the coding scenario: since SFA shortens the activity window of the postsynaptic neuron by some factor (relative to the presynaptic neurons), a downstream neuron would see only see input over, say 10 ms, for a 50 ms long presynaptic drive at the previous layer, and within this time window it is difficult to encode a firing rate. The instructive learning is therefore only possible along a few stages. We have not attempted in this thesis to answer these questions pertaining to the applicability of our SFA-STDP scheme to the multilayer network learning; and we relegate this task to a future investigator.

5.8 Conclusion

In this thesis we showed how the interplay between SFA and STDP leads to the delta learning rule and thus to the precise alignment of auditory-visual maps in model ICX neurons. The primary cues that spurred us into using these two cellular mechanisms in our model are, first, the clear experimental evidence for SFA in ICX leading to visual error responses (Gutfreund et al., 2002; Gutfreund & Knudsen, 2006), and second, the ever increasing evidence for the ubiquity of the STDP mechanism in various neural circuits over a wide spectrum of species, from insects to humans (Caporale & Dan, 2008). However, it is unknown at this point in time whether the STDP mechanism is in operation at the ICC-ICX synapses, and it remains to be seen what the outcome of such a future experiment would be. We have also not attempted in any way to incorporate the various functional roles played by inhibition in ICX map formation and the differential functional expression of NMDA/AMPA receptor currents in remapping (Zheng & Knudsen, 1999, 2001; Feldman & Knudsen, 1998b). On a

developmental level we have also entirely ignored the mechanisms for morphological changes at the cellular level that form the hardware substrate for remapping, for example, how axonogenesis and pathfinding could be triggered by an error signal.

Nevertheless, because of the mathematical generality of our findings, the inherent supervised learning rule in our network may have universal functional implications for adapting sensory systems in which both STDP and SFA have been found, such as in visual cortical networks (Schuett et al., 2001; Froemke & Dan, 2002; Meliza & Dan, 2006; Barkai et al., 1994; Schwindt et al., 1988; Ahmed et al., 1998; Fuhrmann et al., 2002), and many more.

Appendix A

Parameter values used in our simulations

	Parameter name	Symbol	Value/range	Unit
Integrate and fire neuron	Resting/Reset potential	E_{L}	-70	mV
	Threshold potential	E_θ	-50	mV
	Membrane capacitance	C_{m}	0.5	nF
	Leakage conductance	g_{L}	20	nS
SFA	Adaptation time constant	τ_{K}	110	ms
	Potassium reversal potential	E_{K}	-70	mV
	Adaptation conductance step	Δg_{K}	80	nS
STDP	Max potentiation per spike pair	$\mathcal{A}_+$	0.05	$\%g_{\max}$
	Area ratio	B	1.05	
	Max depression per spike pair	$\mathcal{A}_-$	$B\mathcal{A}_+\tau_+/\tau_-$	
	Potentiation window size	τ_+	50	ms
	Depression window size	τ_-	110	ms
ICC and OT afferents	OT input synaptic strength	g^V	3	nS
	ICC input synaptic strength	g^A	$0 - g_{\max}$	
	ICC input max synaptic strength	$g_{\max}$	1.25	nS
	Synaptic activation time constant	τ_{s}	10	ms
Input rates	Auditory-input firing rates	a	0-300	Hz
	Visual-input firing rates	v	0-250	Hz
Background input	Synapse strength	g_{b}	1	nS
	Firing rate		1000	Hz
Stimulus duration and latency*	Stimulus duration	T	15-200	ms
	Visual-input latency	T_{lat}	70	ms
	Auditory-input latency		r/c	
	Speed of sound in air	c	340	ms^{-1}
	Distance to stimulus	r	0-25	m
ICX map formation simulations*	ICC peak firing rate	a_{peak}	300	Hz
	ICC base firing rate	a_{base}	0	Hz
	ICC tuning width	σ^A	4	deg
	Receptive field separation $(\theta_j - \theta_{j+1})$	$\Delta\theta$	2.8	deg
	OT peak firing rate	v_{peak}	200	Hz
	OT base firing rate	v_{base}	0	Hz
	OT tuning width	σ^V	4-10	deg

Table A.1: Typical parameter values used in our simulations and numerical evaluations. *See the corresponding Methods for additional details.

Appendix B

Sensitivity of the learning rule to variation in model parameters

In the following plots we illustrate the effects of varying the different model parameters in our analytical model. Figure B.1 shows a comparison of the original (nonlinear) F-I curves versus the linearize F-I curves. Figures B.2 and B.3 show the effect of SFA on the neuronal firing rates. Figures B.4 and B.5 show the behaviour of the delta learning-rule to variation of model parameters.

All the plots presented here are based on the analytically derived equations in Chapter 2. Note that there will be some differences in the firing rates and equilibrium states between the simulation and analytical models because in our analytical derivations the input current, I_{s}, is a step function whereas in the simulations the synaptic input current rises and decays exponentially with a synaptic time constant of $\tau_{\mathrm{s}} = 10$ ms. Therefore, when predicting the simulation model behaviour from the following plots, there would be some deviation from analytical predictions for small values of time-constants such as τ_{K}, T, T_{lat}, etc. Nevertheless, in general, we have found the analytical derivations and the results from our simulations to be in good agreement.

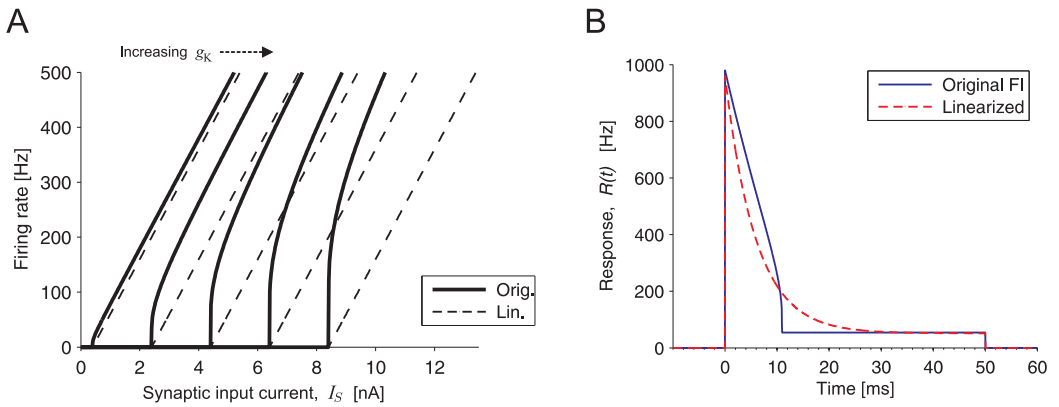

Figure B.1: Comparison of F-I curves and responses of the nonlinear and the linearized firing-rate functions. (**A**) F-I curves of a leaky integrate-and-fire neuron model for the original nonlinear function, Eq. (2.14) (solid lines) and of the threshold-linear approximation, Eq. (2.16) (dashed lines). The different curves correspond to different values of the adaptation conductance, g_K. (Left-to-right: $g_K = 0, 100, 200, 300, 400$ nS). (**B**) Response , $R(t)$, of a nonlinear and a linearized model neuron to a 50 ms step input current of amplitude 10 nA. Surprisingly, the response, $R(t)$, is nearly identical for both the nonlinear (solid line) and the linearized (dashed line) models even though the F-I curves of the nonlinear and linearized models do not match up in (A), a result attributable to the negative-feedback linearization of F-I curves by SFA (Ermentrout, 1998). The neuron's parameter values are as defined in Appendix A.

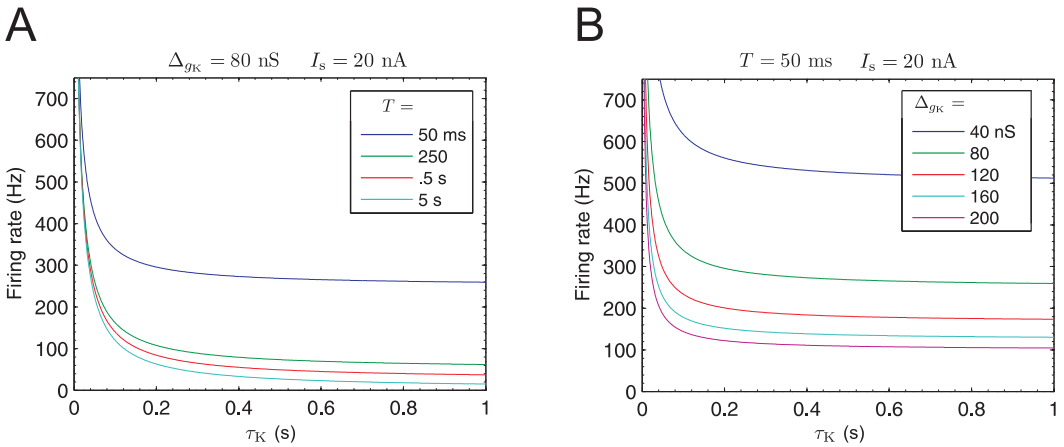

Figure B.2: Effect of the SFA parameters – τ_K and Δ_{g_K} – on the ICX neuron's firing rate. Shown are the plots of Eq. (2.20) illustrating the model ICX neuron's average firing rate as a function of the adaptation time constant τ_K for (**A**) different stimulus durations T and (**B**) for different adaptation conductance step Δ_{g_K}. The ICX neuron's firing rates are seen to be largely independent of τ_K and Δ_{g_K} for the range $\tau_K \gtrsim 140$ ms.

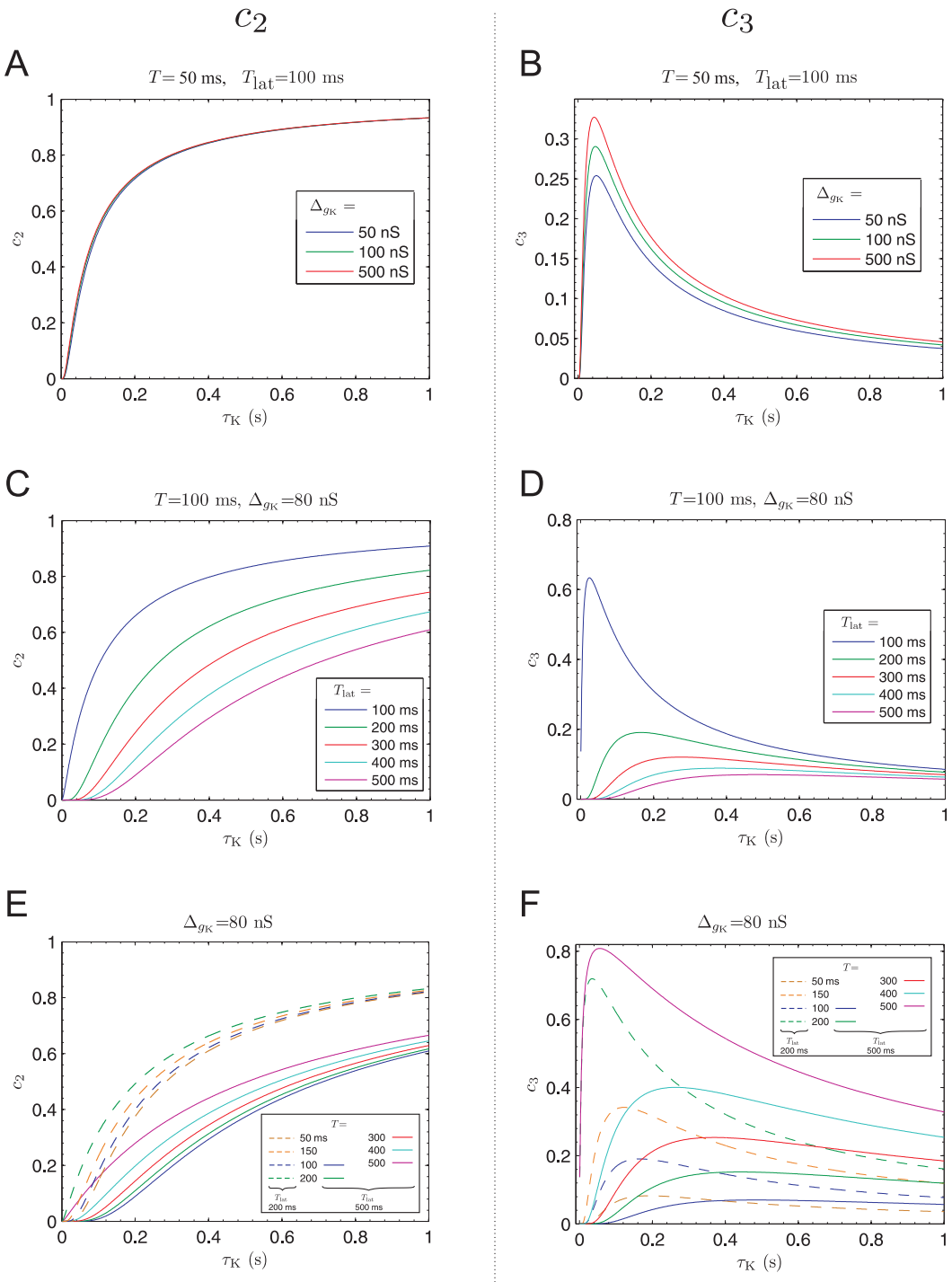

Figure B.3: Plots showing the effect of model and stimulation parameters on the linear relationship Eq. (2.24) (*left column*) and on the range of linear behaviour (Inequality (2.27))(*right column*). Shown is the dependence of constants c_2 and c_3 on different model and stimulation parameters. The constant c_2 describes the effect early ICX auditory responses A have on later ICX visual responses V, and the constant c_3 describes the range of linear behaviour, as depicted in Figure 2.2.

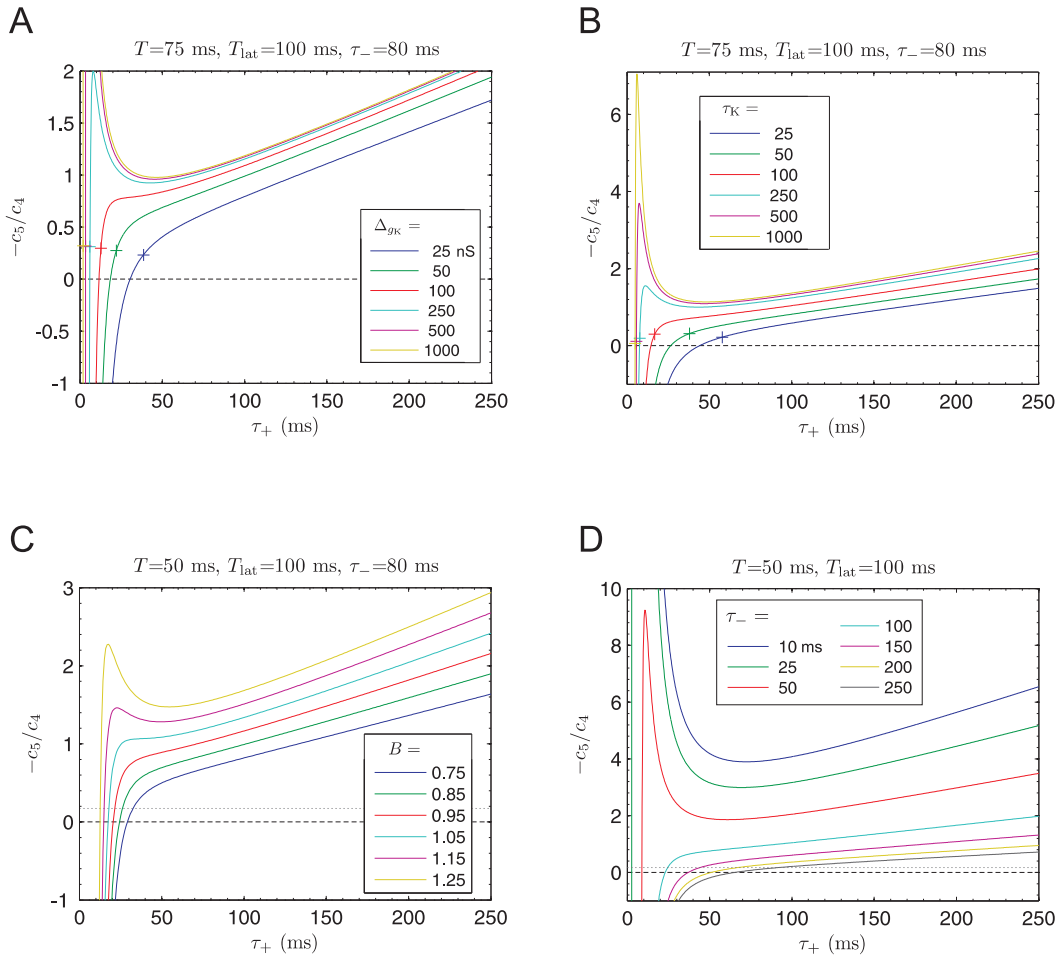

Figure B.4: The delta learning-rule is seen for a large range of model parameter values and is linear for a wide range of these parameters. Shown is the slope $-c_5/c_4$ of the equilibrium curve (Eqs. (2.5) and (2.30)) in Figure 2.3 as a function of the STDP window for potentiation, τ_+, for different values of (**A**) adaptation conductance step Δ_{g_K}, (**B**) adaptation time constant τ_K, (**C**) Ratio of the area of the half width of the STDP function, B, and (**D**) STDP window for depression τ_-. Also shown, by the '+' markers in plots (A) and (B), and dotted line in plots (C) and (D), is the slope c_3 of the line demarcating linear and non-linear regions in Figure 2.3 [see Inequality (2.27)]. The perceptron learning rule holds true whenever the slope is positive (i.e. in the region above the dashed line), and the linearity holds true whenever $-c_5/c_4$ is greater than c_3. The linearity range is the region above the dotted lines in (C) and (D), and to the right of the '+' markers in (A) and (B).

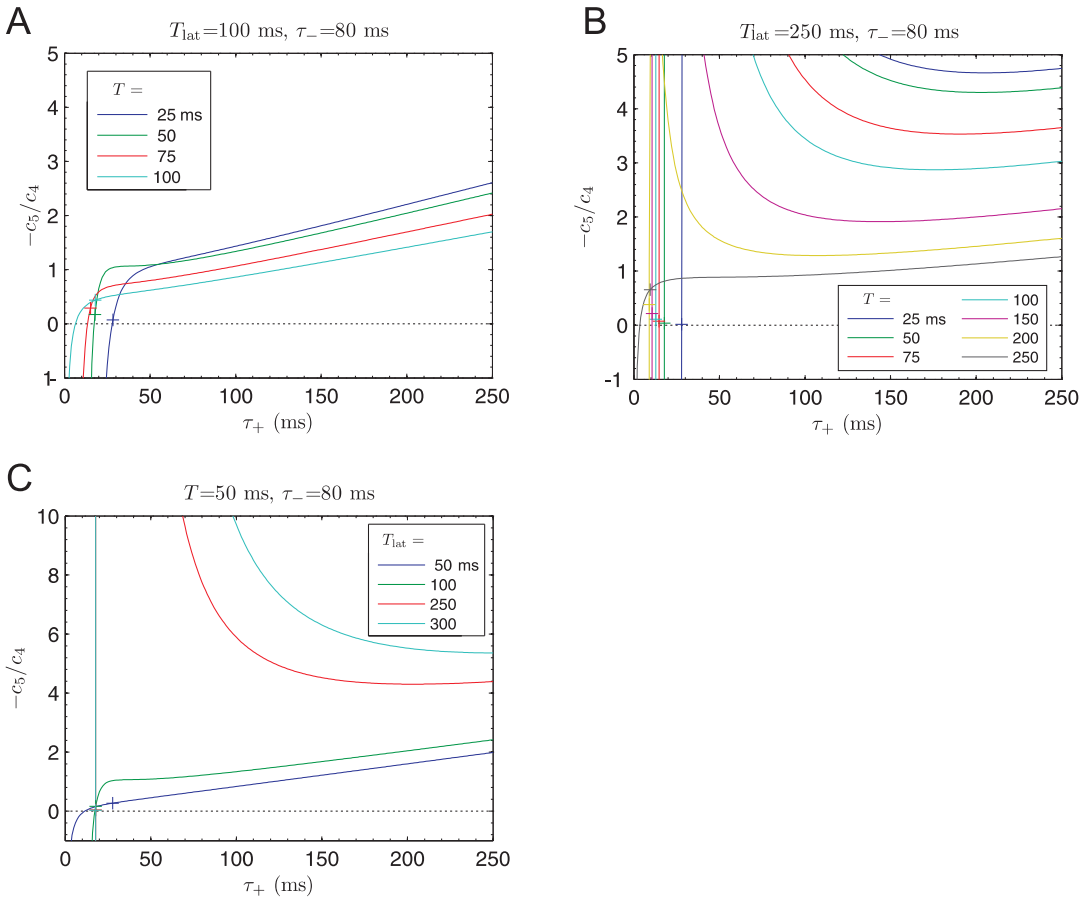

Figure B.5: The delta learning-rule is seen for a large range of stimulus durations and visual latencies and is linear for a wide range of these durations and latencies. Shown is the slope $-c_5/c_4$ of the equilibrium curve (Eqs. (2.5) and (2.30)) in Figure 2.3 as a function of the STDP window for potentiation, τ_+, for (**A**) different values of stimulus durations T with $T_{\rm lat}$ = 100 ms, (**B**) different values of stimulus durations T with $T_{\rm lat}$ = 250 ms, and (**C**) different values of visual latencies $T_{\rm lat}$ with T = 50 ms . Also shown, by the '+' markers, is the slope c_3 of the line demarcating linear and non-linear regions in Figure 2.3 [see Inequality (2.27)]. The perceptron learning rule holds true whenever the slope is positive (i.e. in the region above the dashed line), and the linearity holds true whenever $-c_5/c_4$ is greater than c_3. The linearity range is the region to the right of the '+' markers.

Appendix C

Demonstration of hysteresis in STDP-only learning

Simulation results demonstrating that in STDP-only learning, a fully formed spatial map can be insensitive and unable to shift in reaction to a displaced teacher signal in a network from Davison & Freǵnac (2006). In their paper, the authors report that robust map formation was possible provided the ratio of peak firing rates of the training population to the input population, $R_{\max}^{\text{Training}}/R_{\max}^{\text{Input}}$ (equivalent to $v_{\text{peak}}/a_{\text{peak}}$ in our model) is in the range of 0.6 to 1.4. They also show that the peak firing rate ratios in this range results in almost no discernible change in the learned weight pattern.
However, their network exhibits hysteresis and insensitivity to training inputs when this ratio is set to 0.45 or below, Figure C.1.

In contrast to these results, in our model a change in the ratio $v_{\text{peak}}/a_{\text{peak}}$ produces a proportional change in the learned ICC-to-ICX synaptic weights and of auditory response amplitude (Figure 3.6), and the responsiveness of our model is not restricted to any range of the firing rate ratios (Figure 2.3C, implied by the arrows driving the network into the same stable equilibrium irrespective of the initial state).

Methods: For the experiments described in Figure C.1, we used the same methods and parameters as implemented in Davison & Freǵnac (2006). Parameters are $\tau_+ = \tau_- = 20$ ms, $\tau_{\text{corr}} = 20$ ms, $A_+ = 0.01$, $R_{\max}^{\text{Input}} = 100$ Hz and $\sigma^{\text{In,Tr}} = 0.2$.

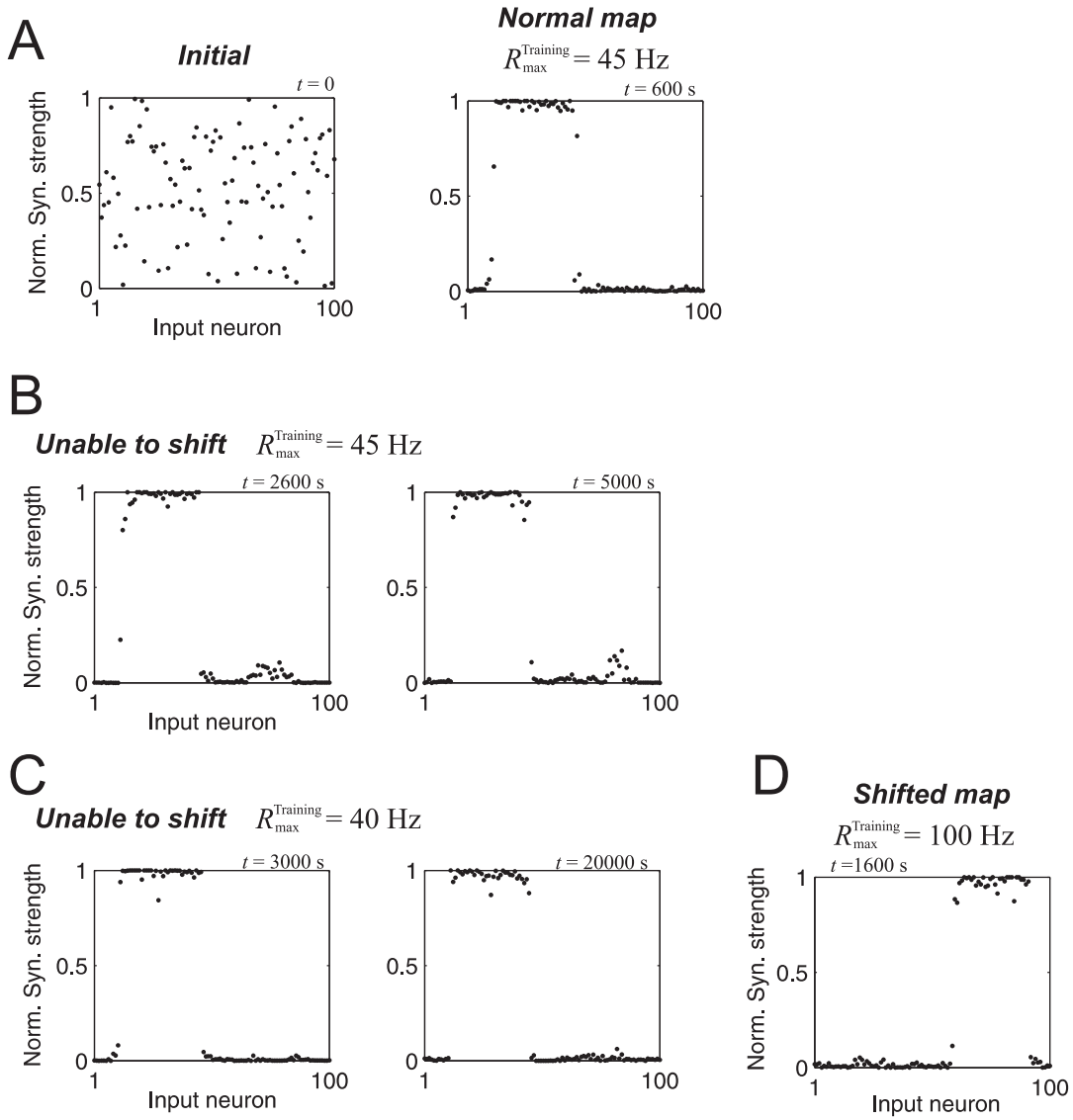

Figure C.1: Demonstration of locked modes (hysteresis) in STDP-only learning in a simulation of the network studied in Davison & Freǵnac (2006). The plots show afferent synaptic strengths (dots) converging on a single postsynaptic neuron under different visual input conditions. In each plot, the x-axis is index of the afferent synapses and the y-axis are the synaptic strengths, normalized to $g_{\max}$. (**A**)*Left*: Initial afferent synaptic strengths at time $t = 0$ are set to random values. *Right*: Under normal visual experience with $R_{\max}^{\text{Training}} = 45$ Hz, a stable map forms in about $t = 600$ s. The visual input center has been set to match input afferent #25. (**B**) When the visual input is shifted to match input afferent #75 at $t = 600$ s, the auditory map is unable to shift (*Left*: $t = 2600$ s, *Right*: $t = 5000$ s), although afferent synapses around index #75 appear to be trying to break through. (**C**) Same as (B), with a slightly reduced $R_{\max}^{\text{Training}} = 40$ Hz. *Left*: $t = 3000$ s, *Right*: $t = 20000$ s. (**D**) If the visual input peak firing rate is increased to $R_{\max}^{\text{Training}} = 100$ Hz, the map fully shifts and correctly matches the visual offset taking about 1000 s ($t = 1600$ s).

Appendix D

Computer simulation program

The main simulation program of our midbrain network model is a C program executable under MATLAB. The model and simulation parameters are stored and forwarded by MATLAB to the C program, which simulates the required number of time steps and returns command to MATLAB. Changing of the parameters and plotting the data are handled in MATLAB.

In MATLAB, the model and simulation parameters are contained in two structured arrays,

neuron:

```
neuron.E0 = -50e-3;       % Neuron firing Threshold
neuron.EL = -70e-3;       % Membrane resting/reset potential
neuron.gL = 20e-9;        % Membrane leakage conductance
neuron.Cm = 0.5e-9;       % Membrane capacitance

neuron.tauK = 110e-3;     % Adaptation time constant
neuron.EK = -70e-3;       % Potassium reversal potential (SFA)
neuron.DgK = 80e-9;       % Adaptation conductance step (SFA)

neuron.EX = 0e-3;         % Reversal potential of excitatory synapses

neuron.tauSO = 10e-3;     % Time constant of OT afferents
neuron.gV = 3e-9;         % OT synaptic strength

neuron.tauSC = 10e-3;     % Time constant of ICC afferents
neuron.gMAX = 1.25e-9;    % Max strength of ICC-to-ICX synapses

B = 1.06;
neuron.tau_plus = 50e-3;        % STDP potentiation window
neuron.tau_minus = 110e-3;      % STDP depression window
neuron.A_plus = 0.001;          % STDP max potentiation
```

```
neuron.A_minus = B*neuron.A_plus*neuron.tau_plus/neuron.tau_minus;
        % STDP max depression
```

and **simpar**:

```
simpar.Auditory_base = 5;          % Auditory (ICC) input properties
simpar.Auditory_peak = 300;        % peak rate (Hz)
simpar.rho_spon = 5;               % spontaneous activity (Hz)
simpar.Auditory_width = 10e-6;     % tuning width (secs ITD)
simpar.RF_separation = 7e-6;       % \Delta\Theta (secs ITD)

simpar.Visual_base = 5;            % Visual (OT) input properties
simpar.Visual_peak = 200;          % peak rate (Hz)
simpar.Visual_width = 4;           % tuning width (degrees)
simpar.Visual_shift = 0;           % Visual shift (degrees)
simpar.Visual_latency = 70e-3;     % OT input latency
```

After setting the neuronal and simulation parameters, the simulation program is executed in MATLAB as follows:

```
if ~exist('gj','var');
   gj = zeros(15,21);        % Initialize ICC-ICX synapses to zero
end                          % 21 ICC pools, 15 neurons per pool
N = uint32(2500);            % Number of time steps to simulate
                             % 1 time step h = 0.25 ms
%---- MAIN LOOP ----
for i = 1:1000;        % Number of stimulus presentations
    r = sns(neuron, simpar, gj, N);  % MEX solver
end
```

Each call to the C program (**sns**) simulates one auditory-visual stimulus presented at a random spatial location, and returns the variable **r** containing time-courses of some select model variables for this simulation run. The ICC-to-ICX synaptic weights are stored in the matrix **gj**.

All of the model's state variables such as $U(t)$, $g_{\mathrm{K}}(t)$, $s_j^{A,V}(t)$, etc. are saved between calls to the C program by defining them as "static" variables. Repeated calls to the C program therefore do not re-initialize these state variables and the simulations continue on from where they stopped at the end of the previous call.

The C program listed below is for the case where the stimulus duration and auditory latency varies from trial to trial. The code modifications for implementing a fixed stimulus duration, fixed auditory latency, and fixed visual stimulus location (to produce Figure 3.2D)

are straightforward and require only minor changes to the program. (These changes are not included in the program).

D.0.1 C source-code of the simulation program

```
/* ================================================================
 * Midbrain model with spiking neurons
 * PhD Thesis: Prashanth D'Souza
 * This is a MEX-file for MATLAB.
 * ================================================================ */

#include "mex.h"  /* Include necessary header files */
#include "math.h"

#define h 0.00025     /* Time step for numerical solving */

#define M 21        /* Total number of ICC pools */
#define Z 15        /* Number of ICC neurons in a pool */
#define Y 15        /* Number of OT neurons in the pool */

#define Wb   gMAX/1.25      /* Strength of background input synapse */
#define rho_b 1000          /* Background input firing rate */

void mexFunction(int nlhs, mxArray *plhs[], int nrhs,
   const mxArray *prhs[]) {          /* Main mex funtcion */

/* ---------------------- Define variables to use ---------------------- */
double *r;
double A_plus, A_minus, E0, EL, EK, EX, gMAX, gL, gV, DgK ;
double k1, k2, k41, k43, k5, k6;
bool xspk, icspk[M][Z], otspk[Y], bkspk;
unsigned int t1, t2, t4, t5;
unsigned int r1, r2[M], r3, rb;
unsigned int n, i, z, N;
double b, a, d, e, f, u1, u2, u3, u4;
double *gs_ptr;

/* Persistent variables (value is preserved between calls) */
static bool firstrun = true;
static double U, gK, s1[M][Z], s3[Y], g3[Y], sb;
static double D1, P1[M][Z];    /* Auxillary variables for STDP
                                  (see Song et al. (2000))   */
/*---------------------- Simulation parameters ----------------------*/
N = *((unsigned int*)mxGetPr(prhs[3]));/* Total number of time steps */
```

```
/*---------- Set up Input/Output pointers ----------*/
gs_ptr = mxGetPr(prhs[2]); /* ICC-to-ICX synaptic strengths matrix */

plhs[0] = mxCreateDoubleMatrix(N,11,mxREAL);
r = mxGetPr(plhs[0]);    /* Return variable 'r' (see end of program) */

/*---------- Load cellular and synaptic parameters ----------*/
A_plus = *mxGetPr(mxGetField(prhs[0], 0, "A_plus"));
A_minus = *mxGetPr(mxGetField(prhs[0], 0, "A_minus"));
E0 = *mxGetPr(mxGetField(prhs[0], 0, "E0"));
EL = *mxGetPr(mxGetField(prhs[0], 0, "EL"));
EK = *mxGetPr(mxGetField(prhs[0], 0, "EK"));
EX = *mxGetPr(mxGetField(prhs[0], 0, "EX"));
gMAX = *mxGetPr(mxGetField(prhs[0], 0, "gMAX"));
gL = *mxGetPr(mxGetField(prhs[0], 0, "gL"));
gV = *mxGetPr(mxGetField(prhs[0], 0, "gV"));
DgK = *mxGetPr(mxGetField(prhs[0], 0, "DgK"));

/*---------- Stimulus timing ----------*/
/* Uniformly distributed (15,100) ms stimulus durations */
i = (unsigned int)(15e-3/h + ((85e-3/h) *((double)rand())/RAND_MAX ));

/*t1 is Auditory stimulus onset, t2 is offset*/
t1 = (unsigned int)(0.075*rand()/RAND_MAX/h ); /* Stimulus distance
    uniformly distributed (0,25.5) m */
t2 = t1 + i;

/*t4 is Visual stimulus onset, t5 is offset*/
t4 = (unsigned int)(*mxGetPr(mxGetField(prhs[1], 0, "Visual_latency"))
    /h);
t5 = t4 + i;

/*---------- Auditory (ICC) stimulus ----------*/
/* (Note: All probabilities scaled to RAND_MAX)*/

b = *mxGetPr(mxGetField(prhs[1], 0, "Auditory_base"));
a = *mxGetPr(mxGetField(prhs[1], 0, "Auditory_peak")) - b;
d = *mxGetPr(mxGetField(prhs[1], 0, "Auditory_width"));
e = *mxGetPr(mxGetField(prhs[1], 0, "RF_separation"));

f = e*(((double)rand()/RAND_MAX)*(M+2)-1.5); /* Uniformly distributed
    stimulus spatial location */

for (i = 0; i < M; i++)    /* Firing probability for ICC pools */
```

```
    r2[i] = (unsigned int) ( RAND_MAX *  h * (b +
        exp(-(f-i*e)*(f-i*e)/(2*d*d)) * a) );

/*---------------------- Visual Stimulus (OT) ----------------------*/
b = *mxGetPr(mxGetField(prhs[1], 0, "Visual_base"));
a = *mxGetPr(mxGetField(prhs[1], 0, "Visual_peak")) - b;
d = *mxGetPr(mxGetField(prhs[1], 0, "Visual_width"));
e /= 2.5e-6;   /* Conversion of ITD in microsecs into visual degrees */

f = f/2.5e-6 + *mxGetPr(mxGetField(prhs[1], 0, "Visual_shift"));

/* Firing probability for OT pools */
r3 = (unsigned int) ( RAND_MAX *  h * (b +
    exp(-(f-10*e)*(f-10*e)/(2*d*d)) * a) );

/*---------------- Spontaneous background input ----------------------*/
r1 = (unsigned int)(RAND_MAX* h*
    *mxGetPr(mxGetField(prhs[1],0,"rho_spon")));
rb = (unsigned int) ( RAND_MAX *  h * rho_b);

/*-------- Initialize all state variables to zero first time -------*/
if (firstrun) {
   U = 0;
   gK = 0;
   D1 = 0;
   for (i = 0; i < M; i++)
      for (z = 0; z < Z; z++) {
         P1[i][z] = 0;
         s1[i][z] = 0;
         }
      for (z = 0; z < Y; z++)
         s3[z] = 0;
   firstrun = false;
   mexPrintf("First run\n");
   }

/* Set OT-ICX synaptic weights */
for (z = 0; z < Y; z++)
   g3[z] = gV;

/*--Pre-compute diff. eqn. time constants relative to time step 'h'--*/
k1 = h/ *mxGetPr(mxGetField(prhs[0], 0, "Cm"));
k2 = 1 - h/ *mxGetPr(mxGetField(prhs[0], 0, "tauK"));
k41 = 1 - h/ *mxGetPr(mxGetField(prhs[0], 0, "tauSC"));
k43 = 1 - h/ *mxGetPr(mxGetField(prhs[0], 0, "tauSO"));
```

```
k5 = 1 - h/ *mxGetPr(mxGetField(prhs[0], 0, "tau_minus"));
k6 = 1 - h/ *mxGetPr(mxGetField(prhs[0], 0, "tau_plus"));

/* ========================= MAIN TIME LOOP ========================= */

for (n = 0; n < N; n++) {
   d = 0;                          /* Net synaptic activation*/
   for (z = 0; z < Y; z++) {
      d += s3[z]* g3[z];    /* OT synaptic input */
      }
   for (i = 0; i < M; i++) {      /* ICC input... */
      for (z = 0; z<Z; z++) {
         d += s1[i][z]* *(gs_ptr + i*Z + z);
         }
      }
   d += sb*Wb; /* Background input */

   /* Runge-Kutta 4th order for mem. pot. U in Eq.(2.8) */
   u1 = k1*( -gL*(U-EL) - d*(U-EX) -gK*(U-EK) );
   u2 = k1*( -gL*((U+u1/2)-EL) - d*((U+u1/2)-EX) -gK*( (U+u1/2) -EK) );
   u3 = k1*( -gL*((U+u2/2)-EL) - d*((U+u2/2)-EX) -gK*( (U+u2/2) -EK) );
   u4 = k1*( -gL*((U+u3)-EL) - d*((U+u3)-EX) -gK*((U+u3)-EK) );

   /* If membrane potential reaches firing threshold*/
   if (( U += (u1+2*(u2+u3)+u4)/6 ) >= E0){
      U = EL;          /* Reset U */
      xspk = true;     /* Produce spike */
      }
   else
      xspk = false;       /* else, no spike */

   /* ICC inputs (Poissonian spikes generator) */
   if (n <= t1 || n > t2) {    /* ICC is inactive */
      for (i = M; i--;) {
         for (z = 0; z < Z; z++) {
            if (rand() < r1)          /* ICC spontaneously fires */
               icspk[i][z] = true;
            else
               icspk[i][z] = false;
            }
         }
      }
   else {                     /* ICC is active */
      for (i = M; i--;) {
         for (z = 0; z < Z; z++) {
```

```
            if (rand() < r2[i])      /* Produce spikes */
               icspk[i][z] = true;
            else
               icspk[i][z] = false;
            }
         }
      }

   /* OT inputs (Poissonian spikes generator) */
   if (n > t4 && n < t5) {     /* OT is active */
      for (z = 0; z < Y; z++) {
         if (rand() < r3)
            otspk[z] = true;
         else
            otspk[z] = false;
         }
      }
   else
      for (z = 0; z < Y; z++)
         otspk[z] = false;

   /* Background input (Poissonian spikes generator) */
   if (rand() < rb)
      bkspk = true;
   else
      bkspk = false;

   /* ========= STDP  ICC-to-ICX synapses ========= */
   for (i = 0; i < M; i++) {
      for (z = 0; z < Z; z++) {
         if (icspk[i][z]) {       /* If presynaptic ICC spikes then */
            if ((*(gs_ptr + i*Z + z) += gMAX*D1) < 0) /* depress */
               *(gs_ptr + i*Z + z) = 0;       /* Lower bound for g */
            }
         }
      }
   if (xspk){                    /* If postsynaptic ICX spikes then */
      for (i = 0; i < M; i++) {
         for (z = 0; z < Z; z++) {            /* potentiate */
            if ((*(gs_ptr + i*Z + z) += gMAX*P1[i][z]) > gMAX)
               *(gs_ptr + i*Z + z) = gMAX;    /* Upper bound for g */
            }
         }
      }
```

```
for (i = M; i--;)
   for (z = 0; z < Z; z++) {
      s1[i][z] *= k41;      /* ICC Synaptic activation decay */
      P1[i][z] *= k6;       /* STDP Potentiation trace decay */
      }
for (z = 0; z < Y; z++)
   s3[z] *= k43;          /* OT Synaptic activation decay */

sb *= k41;                /* Background Synaptic activation decay */
gK *= k2;                 /* Potassium conductance decay (SFA)*/
D1 *= k5;                 /* STDP Depression trace decay */

/* Set synaptic activations if there are ICC or OT spikes */
for (i = M; i--;) {
   for (z = 0; z < Z; z++) {
      if (icspk[i][z]) {
         s1[i][z] += 1;        /* ICC synaptic activations */
         P1[i][z] += A_plus;   /* Update STDP Potentiation trace */
         }
      }
   }
for (z = 0; z < Y; z++) {
   if (otspk[z])
      s3[z] += 1;             /* OT synaptic activations */
   }

if (bkspk)  /* Step synaptic activation of background synapse */
   sb += 1;

/* Update if there are ICX spikes */
if (xspk) {
   gK += DgK;          /* Step adaptation conductance */
   D1 -= A_minus;      /* Update STDP depression trace */
   }

/*============== RETURN VARIABLE 'r' ==============*/
r[n] = U;                 /* Membrane potential */
r[n+N] = s1[10][0];       /* ICC synapse activation (pool 10)*/
r[n+2*N] = gK;            /* Adaptation conductance */
r[n+3*N] = d;             /* Net synaptic activation */
r[n+4*N] = *(gs_ptr+10*Z+0);/* ICC-ICX synapse strength (pool 10) */
r[n+5*N] = s3[0];         /* OT synapse activation */
r[n+6*N] = P1[10][0];     /* P trace (STDP) (pool 10)*/
r[n+7*N] = D1;            /* D trace (STDP) */
r[n+8*N] = 0;             /* */
```

```
    r[n+9*N] = 0;              /* */
    r[n+10*N] = 0;             /* */
    }
}
```

Code modifications for delayed OT-ICX feedback simulations

To implement delayed OT-ICX feedback for the experiments shown in Figures 4.6 and 4.7, we modified the code as follows. During the ICX auditory response phase, we measured the ICX firing rate by counting the number of response spikes in the time interval n∈[t1, t2]. In the following visual (OT) input phase, n∈[t4, t5], we set the OT input firing probability, r3, to a value proportional to preceding ICX auditory firing rate times the feedback factor:

```
r3 = (unsigned int)( RAND_MAX * h * 1.45 *(double)(count)/50e-3 );
```

where variable 'count' is the number of preceding ICX response spikes and the feedback factor $\beta = 1.45$. Note that in these simulations the stimulus duration is held fixed at $T = 50$ ms.

Bibliography

Adolphs, R. (1993). Acetylcholinesterase staining differentiates functionally distinct auditory pathways in the barn owl. The Journal of Comparative Neurology, 329, 365–377.

Ahmed, B., Anderson, J. C., Douglas, R. J., Martin, K. A., & Whitteridge, D. (1998). Estimates of the net excitatory currents evoked by visual stimulation of identified neurons in cat visual cortex. Cerebral Cortex, 8, 462–476.

Atwal, G. S. (2004). Dynamic plasticity in coupled avian midbrain maps. Physical Review E, 70, 061904: 1–7.

Barkai, E., Bergman, R. E., Horwitz, G., & Hasselmo, M. E. (1994). Modulation of associative memory function in a biophysical simulation of rat piriform cortex. Journal of Neurophysiology, 72, 659–677.

Benda, J. & Herz, A. V. (2003). A universal model for spike-frequency adaptation. Neural Computation, 15, 2523–2564.

Benda, J., Longtin, A., & Maler, L. (2005). Spike-frequency adaptation separates transient communication signals from background oscillations. Journal of Neuroscience, 25, 2312–2321.

Bi, G. & Poo, M. (1998). Synaptic modification in cultured hippocampal neurons: dependence on spike timing, synaptic strength, and postsynaptic cell type. Journal of Neuroscience, 18, 10464–10472.

Brainard, M. S. & Knudsen, E. I. (1993). Experience-dependent plasticity in the inferior colliculus: a site for visual calibration of the neural representation of auditory space in the barn owl. Journal of Neuroscience, 13, 4589–4608.

Brainard, M. S. & Knudsen, E. I. (1995). Dynamics of visually guided auditory plasticity in the optic tectum of the barn owl. Journal of Neurophysiology, 73, 595–614.

Brainard, M. S. & Knudsen, E. I. (1998). Sensitive periods for visual calibration of the auditory space map in the barn owl optic tectum. Journal of Neuroscience, 18, 3929–3942.

Brody, C. D. & Hopfield, J. J. (2003). Simple networks for spike-timing-based computation, with application to olfactory processing. Neuron, 37, 843–852.

Brunel, N., Hakim, V., Isope, P., Nadal, J. P., & Barbour, B. (2004). Optimal information storage and the distribution of synaptic weights: perceptron versus Purkinje cell. Neuron, 43, 745–757.

Caporale, N. & Dan, Y. (2008). Spike timing-dependent plasticity: a Hebbian learning rule. Annual Review of Neuroscience, 31, 25–46.

Carr, C. E. & Boudreau, R. E. (1991). Central projections of auditory nerve fibers in the barn owl. The Journal of Comparative Neurology, 314, 306–318.

Crist, R. E., Li, W., & Gilbert, C. D. (2001). Learning to see: experience and attention in primary visual cortex. Nature Neuroscience, 4, 519–525.

Dan, Y. & Poo, M. M. (2004). Spike timing-dependent plasticity of neural circuits. Neuron, 44, 23–30.

Davison, A. P. & Fregnac, Y. (2006). Learning cross-modal spatial transformations through spike timing-dependent plasticity. Journal of Neuroscience, 26, 5604–5615.

DeBello, W. M., Feldman, D. E., & Knudsen, E. I. (2001). Adaptive axonal remodeling in the midbrain auditory space map. Journal of Neuroscience, 21, 3161–3174.

DeBello, W. M. & Knudsen, E. I. (2004). Multiple sites of adaptive plasticity in the owls auditory localization pathway. Journal of Neuroscience, 24, 6853–6861.

Diamond, M. E., Petersen, R. S., & Harris, J. A. (1999). Learning through maps: Functional significance of topographic organization in primary sensory cortex. Journal of Neurobiology, 41, 64–68.

Douglas, R. J. & Martin, K. A. (2004). Neuronal circuits of the neocortex. Annual Review of Neuroscience, 27, 419–451.

Drew, P. J. & Abbott, L. F. (2006). Extending the effects of spike-timing-dependent plasticity to behavioral timescales. Proceedings of the National Academy of Sciences (USA), 103, 8876–8881.

Ermentrout, B. (1994). Reduction of conductance-based models with slow synapses to neural nets. Neural Computation, 6, 679–695.

Ermentrout, B. (1998). Linearization of F-I curves by adaptation. Neural Computation, 10, 1721–1729.

Ermentrout, B., Pascal, M., & Gutkin, B. (2001). The effects of spike frequency adaptation and negative feedback on the synchronization of neural oscillators. Neural Computation, 13, 1285–1310.

Feldman, D. E. (2000). Timing-based LTP and LTD at vertical inputs to layer II/III pyramidal cells in rat barrel cortex. Neuron, 27, 45–56.

Feldman, D. E. & Knudsen, E. I. (1994). NMDA and non-NMDA glutamate receptors in auditory transmission in the barn owl inferior colliculus. Journal of Neuroscience, 14, 5939–5958.

Feldman, D. E. & Knudsen, E. I. (1997). An anatomical basis for visual calibration of the auditory space map in the barn owl's midbrain. Journal of Neuroscience, 17, 6820–6837.

Feldman, D. E. & Knudsen, E. I. (1998a). Experience-dependent plasticity and the maturation of glutamergic synapses. Neuron, 20, 1067–1071.

Feldman, D. E. & Knudsen, E. I. (1998b). Pharmacological specialization of learned auditory responses in the inferior colliculus of the barn owl. Journal of Neuroscience, 18, 3073–3087.

Fiete, I. R., Fee, M. S., & Seung, H. S. (2007). Model of birdsong learning based on gradient estimation by dynamic perturbation of neural conductances. Journal of Neurophysiology, 98, 2038–2057.

Franosch, J. P., Lingenheil, M., & van Hemmen, J. L. (2005). How a frog can learn what is where in the dark. Physical Review Letters, 95, 078106: 1–4.

Friedel, P. & van Hemmen, J. L. (2008). Inhibition, not excitation, is the key to multimodal sensory integration. Biological Cybernetics, 98, 597–618.

Froemke, R. C. & Dan, Y. (2002). Spike-timing-dependent synaptic modification induced by natural spike trains. Nature, 416, 433–438.

Fuhrmann, G., Markram, H., & Tsodyks, M. (2002). Spike frequency adaptation and neocortical rhythms. Journal of Neurophysiology, 88, 761–770.

Fujita, I. & Konishi, M. (1991). The role of GABAergic inhibition in processing of interaural time difference in the owl's auditory system. Journal of Neuroscience, 11, 722–739.

Gelfand, J., Pearson, J., Spence, C., & Sullivan, W. (1988). Multisensor integration in biological systems. In Proceedings IEEE International Symposium on Intelligent Control 1988, pp. 147–153.

Gollisch, T. & Meister, M. (2008). Rapid neural coding in the retina with relative spike latencies. Science, 319, 1108–1111.

Gutfreund, Y. & Knudsen, E. I. (2006). Adaptation in the auditory space map of the barn owl. Journal of Neurophysiology, 96, 813–825.

Gutfreund, Y., Zheng, W., & Knudsen, E. I. (2002). Gated visual input to the central auditory system. Science, 297, 1556–1559.

Gutig, R., Aharonov, R., Rotter, S., & Sompolinsky, H. (2003). Learning input correlations through nonlinear temporally asymmetric Hebbian plasticity. Journal of Neuroscience, 23, 3697–3714.

Haessly, A., Sirosh, J., & Miikkulainen, R. (1995). A model of visually guided plasticity of the auditory spatial map in the barn owl. In Proceedings of the Seventeenth Annual Meeting of the Cognitive Science Society (COGSCI-95), pp. 154–158.

Hahnloser, R. H. R. (2003). Emergence of neural integration in the head-direction system by visual supervision. Neuroscience, 120, 877–891.

Haykin, S. (1994). Neural Networks: A Comprehensive Foundation. (Macmillan).

Hennequin, G., Gerstner, W., & Pfister, J.-P. (2010). STDP in adaptive neurons gives close-to-optimal information transmission. Frontiers in Computational Neuroscience, 4.

Hyde, P. S. & Knudsen, E. I. (2000). Topographic projection from the optic tectum to the auditory space map in the inferior colliculus of the barn owl. Journal of Comparative Neurology, 421, 146–160.

Hyde, P. S. & Knudsen, E. I. (2001). A topographic instructive signal guides the adjustment of the auditory space map in the optic tectum. Journal of Neuroscience, 21, 8586–8593.

Hyde, P. S. & Knudsen, E. I. (2002). The optic tectum controls visually guided adaptive plasticity in the owl's auditory space map. Nature, 415, 73–76.

Joachim, M. & Eric, I. K. (1993). Early monaural occlusion alters the neural map of interaural level differences in the inferior colliculus of the barn owl. Brain Research, 619, 29–38.

Johnson, R. R. & Burkhalter, A. (1996). Microcircuitry of forward and feedback connections within rat visual cortex. Journal of Comparative Neurology, 368, 383–398.

Kardar, M. & Zee, A. (2002). Information optimization in coupled audio-visual cortical maps. Proceedings of the National Academy of Sciences (USA), 99, 15894–15897.

Karklin, Y. & Lewicki, M. S. (2005). A hierarchical Bayesian model for learning nonlinear statistical regularities in nonstationary natural signals. Neural Computation, 17, 397–423.

Kempter, R., Gerstner, M., & van Hemmen, J. L. (1999). Hebbian learning and spiking neurons. Physical Review E, 59, 4498–4514.

Kempter, R., Gerstner, W., & van Hemmen, J. L. (2001). Intrinsic stabilization of output rates by spike-based Hebbian learning. Neural Computation, 13, 2709–2741.

Knudsen, E. (1983). Subdivisions of the inferior colliculus in the barn owl (Tyto alba). The Journal of Comparative Neurology, 218, 174–186.

Knudsen, E., Konishi, M., & Pettigrew, J. (1977). Receptive fields of auditory neurons in the owl. Science, 198, 1278–1280.

Knudsen, E. I. (1982). Auditory and visual maps of space in the optic tectum of the owl. Journal of Neuroscience, 2, 1177–1194.

Knudsen, E. I. (1994). Supervised learning in the brain. Journal of Neuroscience, 14, 3985–3997.

Knudsen, E. I. (2002). Instructed learning in the auditory localization pathway of the barn owl. Nature, 417, 322–328.

Knudsen, E. I. & Brainard, M. S. (1991). Visual instruction of the neural map of auditory space in the developing optic tectum. Science, 253, 85–87.

Knudsen, E. I., Zheng, W., & DeBello, W. M. (2000). Traces of learning in the auditory localization pathway. Proceedings of the National Academy of Sciences (USA), 97, 11815–11820.

Köppl, C., Gleich, O., & Manley, G. A. (1993). An auditory fovea in the barn owl cochlea. Journal of Comparative Physiology A, 171, 695–704.

Kuznetsova, M. S., Higgs, M. H., & Spain, W. J. (2008). Adaptation of firing rate and spike timing precision in the avian cochlear nucleus. Journal of Neuroscience, 28, 11906–11915.

Legenstein, R., Naeger, C., & Maass, W. (2005). What can a neuron learn with spike-timing-dependent plasticity? Neural Computation, 17, 2337–2382.

Linkenhoker, B. A. & Knudsen, E. I. (2002). Incremental training increases the plasticity of the auditory space maps in adult barn owls. Nature, 419, 293–296.

Liu, Y. H. & Wang, X. J. (2001). Spike-frequency adaptation of a generalized leaky integrate-and-fire model neuron. Journal of Computational Neuroscience, 10, 25–45.

Luksch, H., Gauger, B., & Wagner, H. (2000). A candidate pathway for a visual instructional signal to the barn owl's auditory system. Journal of Neuroscience, 20, RC70.

Madison, D. V. & Nicoll, R. A. (1984). Control of the repetitive discharge of rat CA 1 pyramidal neurones in vitro. Journal of Physiology, 354, 319–331.

Markram, H., Lübke, J., Frotscher, M., & Sakmann, B. (1997). Regulation of synaptic efficacy by coincidence of postsynaptic APs and EPSPs. Science, 275, 213–215.

McLaren, I. (1989). The computational unit as an assembly of neurones: An implementation of an error correcting learning algorithm. In The Computing Neuron, R. Durbin, C. Miall, & G. Mitchison, eds. (Boston, MA: Addison-Wesley Longman Publishing Co., Inc.), pp. 160–179.

Meliza, C. D. & Dan, Y. (2006). Receptive-field modification in rat visual cortex induced by paired visual stimulation and single-cell spiking. Neuron, 49, 183–189.

Meredith, M. A., Nemitz, J. W., & Stein, B. E. (1987). Determinants of multisensory integration in the superior colliculus neurons. 1. Temporal factors. Journal of Neuroscience, 7, 3215–3229.

Michaelis, B. & Chaplain, R. A. (1975). Ion conductance changes associated with spike adaptation in the rapidly adapting stretch receptor of the crayfish. European Journal of Physiology, 354, 367–377.

Olshausen, B. A. & Field, D. J. (1996). Emergence of simple-cell receptive field properties by learning a sparse code for natural images. Nature, 381, 607–609.

Peron, S. & Gabbiani, F. (2009). Role of spike-frequency adaptation in shaping neuronal response to dynamic stimuli. Biological Cybernetics, 100, 505–520.

Pouget, A., Zhang, K., Deneve, S., & Latham, P. E. (1998). Statistically efficient estimation using population coding. Neural Computation, 10, 373–401.

Prechtl, J. C., Cohen, L. B., Pesaran, B., Mitra, P. P., & Kleinfeld, D. (1997). Visual stimuli induce waves of electrical activity in turtle cortex. Proceedings of the National Academy of Sciences (USA), 94, 7621–7626.

Rao, R. P. N. & Ballard, D. H. (1999). Predictive coding in the visual cortex: a functional interpretation of some extra-classical receptive-field effects. Nature Neuroscience, 2, 79–87.

Rao, R. P. N. & Sejnowski, T. J. (2001). Spike-timing-dependent Hebbian plasticity as temporal difference learning. Neural Computation, 13, 2221–2237.

Reches, A. & Gutfreund, Y. (2008). Stimulus-specific adaptations in the gaze control system of the barn owl. Journal of Neuroscience, 28, 1523–1533.

Roberts, P. D., Santiago, R. A., & Lafferriere, G. (2008). An implementation of reinforcement learning based on spike timing dependent plasticity. Biological Cybernetics, 99, 517–523.

Robinson, D. A. (1989). Integrating with neurons. Annual Review of Neuroscience, 12, 33–45.

Rodriguez-Contreras, A., Liu, X. B., & DeBello, W. M. (2005). Axodendritic contacts onto calcium/calmodulin-dependent protein kinase type II-expressing neurons in the barn owl auditory space map. Journal of Neuroscience, 25, 5611–5622.

Rosen, D. J., Rumelhart, D. E., & Knudsen, E. I. (1993). A connectionist model of the owl's sound localization system. In NIPS, J. D. Cowan, G. Tesauro, & J. Alspector, eds., pp. 606–613. (Morgan Kaufmann).

Rosenblatt, F. (1958). The perceptron: A probabilistic model for information storage and organization in the brain. Psychological Review, 65, 386–408.

Rothman, J. S., Cathala, L., Steuber, V., & Silver, R. A. (2009). Synaptic depression enables neuronal gain control. Nature, 457, 1015–1018.

Royer, S. & Pare, D. (2003). Conservation of total synaptic weight through balanced synaptic depression and potentiation. Nature, 422, 518–522.

Rubin, J., Lee, D. D., & Sompolinsky, H. (2001). Equilibrium properties of temporally asymmetric Hebbian plasticity. Physical Review Letters, 86, 364–367.

Rucci, M., Tononi, G., & Edelman, G. M. (1997). Registration of neural maps through value-dependent learning: Modeling the alignment of auditory and visual maps in the barn owl's optic tectum. Journal of Neuroscience, 17, 334–352.

Schuett, S., Bonhoeffer, T., & Huebener, M. (2001). Pairing-induced changes of orientation maps in cat visual cortex. Neuron, 32, 325–337.

Schultz, W. & Dickinson, A. (2000). Neuronal coding of prediction errors. Annual Review of Neuroscience, 23, 473–500.

Schwindt, P. C., Spain, W. J., Foehring, R. C., Chubb, M. C., & Crill, W. E. (1988). Slow conductances in neurons from cat sensorimotor cortex in vitro and their role in slow excitability changes. Journal of Neurophysiology, 59, 450–467.

Seriès, P., Latham, P. E., & Pouget, A. (2004). Tuning curve sharpening for orientation selectivity: coding efficiency and the impact of correlations. Nature Neuroscience, 7, 1129–1135.

Seung, H. S. & Sompolinsky, H. (1993). Simple models for reading neuronal population codes. Proceedings of the National Academy of Sciences (USA), 90, 10749–10753.

Shriki, O., Hansel, D., & Sompolinsky, H. (2003). Rate models for conductance-based cortical neuronal networks. Neural Computation, 15, 1809–1841.

Smith, R. L. (1977). Short-term adaptation in single auditory nerve fibers: some poststimulatory effects. Journal of Neurophysiology, 40, 1098–1111.

Song, S. & Abbott, L. F. (2001). Cortical development and remapping through spike timing-dependent plasticity. Neuron, 32, 339–350.

Song, S., Miller, K. D., & Abbott, L. F. (2000). Competitive Hebbian learning through spike-timing-dependent synaptic plasticity. Nature Neuroscience, 3, 919–926.

Sprekeler, H., Michaelis, C., & Wiskott, L. (2007). Slowness: An objective for spike–timing-dependent plasticity? PLoS Computational Biology, 3, 1136–1148.

Stefan, K., Wycislo, M., & Classen, J. (2004). Modulation of associative human motor cortical plasticity by attention. Journal of Neurophysiology, 92, 66–72.

Sullivan, W. E. & Konishi, M. (1984). Segregation of stimulus phase and intensity coding in the cochlear nucleus of the barn owl. Journal of Neuroscience, 4, 1787–1799.

Takahashi, T. T. & Konishi, M. (1986). Selectivity for interaural time difference in the owls midbrain. Journal of Neuroscience, 6, 3413–3422.

Takahashi, T. T. & Konishi, M. (1988a). Projections of nucleus angularis and nucleus laminaris to the lateral lemniscal nuclear complex of the barn owl. The Journal of Comparative Neurology, 274, 212–238.

Takahashi, T. T. & Konishi, M. (1988b). Projections of the cochlear nuclei and nucleus laminaris to the inferior colliculus of the barn owl. The Journal of Comparative Neurology, 274, 190–211.

Toyoizumi, T., Pfister, J. P., Aihara, K., & Gerstner, W. (2005). Generalized Bienenstock-Cooper-Munro rule for spiking neurons that maximizes information transmission. Proceedings of the National Academy of Sciences (USA), 102, 5239–5244.

Turrigiano, G. G. (1999). Homeostatic plasticity in neuronal networks: the more things change, the more they stay the same. Trends in Neurosciences, 22, 221–227.

Wagner, H. (1990). Receptive fields of neurons in the owl's auditory brainstem change dynamically. European Journal of Neuroscience, 2, 949–959.

Wagner, H., Mazer, J. A., & von Campenhausen, M. (2002). Response properties of neurons in the core of the central nucleus of the inferior colliculus of the barn owl. European Journal of Neuroscience, 15, 1343–1352.

Wagner, H., Takahashi, T. T., & Konishi, M. (1987). Representation of interaural time differences in the central nucleus of the barn owls inferior colliculus. Journal of Neuroscience, 7, 3105–3116.

Wang, X. J. (1998). Calcium coding and adaptive temporal computation in cortical pyramidal neurons. Journal of Neurophysiology, 79, 1549–1566.

Wang, X.-J., Liu, Y., Sanchez-Vives, M. V., & McCormick, D. A. (2003). Adaptation and temporal decorrelation by single neurons in the primary visual cortex. Journal of Neurophysiology, 89, 3279–3293.

Widrow, B. & Hoff, M. E. (1960). Adaptive switching circuits. In IRE WESCON Convention Record. (New York: Institute of Radio Engineers), pp. 96–104.

Winkowski, D. E. & Knudsen, E. I. (2007). Top-down control of multimodal sensitivity in the barn owl optic tectum. Journal of Neuroscience, 27, 13279–13291.

Witten, I. B., Bergan, J. F., & Knudsen, E. I. (2006). Dynamic shifts in the owl's auditory space map predict moving sound location. Nature Neuroscience, 9, 1439–1445.

Witten, I. B., Knudsen, E. I., & H., S. (2008). A Hebbian learning rule mediates asymmetric plasticity in aligning sensory representations. Journal of Neurophysiology, 100, 1067–1079.

Wong, R. O., Meister, M., & Shatz, C. J. (1993). Transient period of correlated bursting activity during development of the mammalian retina. Neuron, 11, 923–938.

Xie, X., Hahnloser, R. H. R., & Seung, S. H. (2002). Selectively grouping neurons in recurrent networks of lateral inhibition. Neural Computation, 14, 2627–2646.

Zheng, W. & Knudsen, E. I. (1999). Functional selection of adaptive auditory space map by GABA A-mediated inhibition. Science, 284, 962–965.

Zheng, W. & Knudsen, E. I. (2001). GABAergic inhibition antagonizes adaptive adjustment of the owl's auditory space map during the initial phase of plasticity. Journal of Neuroscience, 21, 4356–4365.

Acknowledgments

I'd like to express my immense thanks to my supervisors Shih-Chii and Richard for their mentoring, motivation and kindness throughout my thesis time. They have spent countless hours sitting through our meetings, discussing simulation results, developing new ideas, and writing and proof-reading our paper. Thanks too for the money. It was a pleasure working with you guys.

I also want to thank the founders of our institute, Professors Rodney J. Douglas and Kevan A. Martin, for this wonderful neuroscience lab that they have created and managed. The people, the facilities and the environment at this lab have made my time here both intellectually nurturing and enjoyable. Also, my special thanks are to Rodney for accepting to be on my thesis committee.

Finally, I would like to thank the Zentrum fuer Neurowissenschaften of the University of Zurich and ETH Zurich for the funding to pursue this research.

Curriculum Vitae

Name: **D'SOUZA, Prashanth**

Date of birth: **24.01.1976**

Nationality: **Indian**

EDUCATION

College/University	Major Subjects	Period	Degree	Year
St. Joseph's Indian High School, Bangalore	Languages, Mathematics, Science, Social Studies	1989-92	SSLC	1992
St. Joseph's Pre-University College, Bangalore	Physics, Mathematics, Chemistry, Electronics	1992-94	PUC	1994
St. Joseph's College, Bangalore University	Physics, Mathematics, Electronics	1994-97	B. Sc	1998
University of Oldenburg, Germany	Engineering Physics	2000-04	M. Eng	2004

Master thesis title: **Development of data analysis techniques for classification of oculomotor behaviour for use in cognitive neuroscientific research.**

Doctoral Student at University of Zurich since April 2005.

PAPERS PUBLISHED DURING DOCTORAL STUDIES

D'Souza P, Liu S-C, Hahnloser RHR **Perceptron learning rule derived from spike-frequency adaptation and spike-time-dependent plasticity.** PNAS USA (March, 2010).

GRANTS

3-year Ph.D. grant from the Zentrum fuer Neurowissensch aften Zuerich (2006-2008).
